

The Pennsylvania State University

The Graduate School

College of Engineering

**PREDICTIVE GAIT SIMULATIONS FOR INVESTIGATION OF
MUSCULOSKELETAL STRUCTURE AND LOCOMOTOR FUNCTION**

A Dissertation in

Mechanical Engineering

by

Huseyin Celik

©2014 Huseyin Celik

Submitted in Partial Fulfillment
of the Requirements
for the Degree of

Doctor of Philosophy

August 2014

The dissertation of Huseyin Celik was reviewed and approved* by the following:

Stephen J. Piazza

Associate Professor of Kinesiology, Mechanical & Nuclear Engineering and Orthopaedics and Rehabilitation

Dissertation Advisor

Chair of Committee

Ashok Belegundu

Professor of Mechanical Engineering

Joseph P. Cusumano

Professor of Engineering Science & Mechanics

H. Joseph Sommer III

Professor of Mechanical Engineering

Daniel C. Haworth

Professor of Mechanical Engineering

Professor-In-Charge of MNE Graduate Programs

*Signatures are on file in the Graduate School.

ABSTRACT

Human locomotion is often assumed to be governed by optimality principles. To the extent that this is true, it should be possible to reproduce various human gaits (walking, running, sprinting) with a predictive approach employing some sort of optimality criterion in an optimization framework. While there are many instances of humans using aperiodic gaits in everyday life and sporting activities, previous simulations of bipedal locomotion have focused almost exclusively on periodic gaits. The main purpose of this dissertation is to implement model-based optimal controls approaches to create novel bipedal gait simulations that are both periodic and aperiodic. Those simulations are used to investigate new optimality criteria for normal human walking and to characterize relationships between musculoskeletal architecture and human sprinting performance.

In our first study, a novel computational model and a simulation framework were developed to create the first simulation of aperiodic sprinting from rest. The model used was a modified spring-loaded inverted pendulum (SLIP) biped driven by torque actuators at the hip and force actuators on retracting legs. The direct multiple shooting method was used to formulate the optimization problem in which the time to traverse 20 m from rest was minimized. The initial guess to the simulation was a “jogging” simulation obtained using a proportional-derivative feedback to control trunk attitude, swing leg angle, and leg retraction and extension. Although the model was very simple, it exhibited a number of features characteristic of human sprinters, such as forward trunk lean at the start, straightening of the trunk during acceleration, and a dive at the finish.

In our second study, a muscle driven computational model was developed to create simulations of normal bipedal walking using the direct multiple shooting method and evaluation

of optimality criteria. We implemented a set of optimality measures derived from muscle activation, mechanical energy expenditure, or metabolic energy expenditure to represent effort; and trunk angle as well as vertical ground reaction force (GRF). Initial guesses to the optimizations were generated using a feedforward control that relied on muscle reflex loops. The simulations converged to distinct gait cycles for different optimality criteria. The additional trunk angle and vertical GRF terms helped to alleviate some undesired behaviors observed in predictive simulations of normal walking such as spikes in GRF and excessive trunk excursion.

In our third study, maximum speed sprinting simulations were created with a muscle-actuated bipedal model and the direct multiple shooting method. The simulation framework and model successfully reproduced salient features of human sprinting once maximum speed has been attained. We perturbed several musculoskeletal architecture parameters of the plantarflexors in isolation (maximum isometric force, optimal fiber length, tendon stiffness, and moment arm) to investigate how variations in musculotendon architecture affect maximum speed bipedal sprinting performance. We found that increases in each parameter analyzed in the study enhanced maximum speed bipedal sprinting performance.

In our fourth study, we used the computational model and simulation framework developed in the third study to investigate how variations in the maximum isometric force parameter of each major muscle group affect sprinting performance. The maximum isometric force parameter of each musculotendon actuator in the model was perturbed in isolation. The results showed that increasing each muscle's force-generating capacity enhanced sprinting performance, but hip flexors and quadriceps were found to have the most and least potential, respectively, to increase sprinting speed. The model employed mechanisms similar to those

observed in human sprinters to attain higher speeds. Additional plantarflexor and hip flexor force increased speed primarily by enhancing stride length and stride frequency, respectively.

In conclusion, this dissertation is the first study to create an aperiodic bipedal sprinting simulation from rest. We demonstrated that additional optimality criteria, vertical GRF and trunk angle, have the potential to eliminate some undesired behaviors and increase fidelity of predictive walking simulations. Contrary to the experimental findings showing that sprinters have smaller plantarflexor moment arms, we found that larger plantarflexor moment arms favor sprinting performance in the maximum speed sprinting phase. The results suggest that special attention should be given to strengthening hip flexor and plantarflexor muscles to increase maximum sprinting speed. The models and simulation frameworks described in this thesis can be used to simulate other bipedal gaits with only minor modifications.

TABLE OF CONTENTS

List of Figures.....	x
Acknowledgements	xvii
Chapter 1 Introduction.....	1
1.1 Background	1
1.2 Purpose of the dissertation	3
1.3 Specific aims	3
1.4 Organization of the dissertation	4
Chapter 2 Literature Review	5
2.1 Computer simulation of bipedal locomotion	5
2.1.1 Formulations of optimization problem	5
2.1.2 Simulations of walking	7
2.1.3 Simulations of running.....	13
2.2 Determinants of sprinting performance	14
2.2.1 Mechanics of human sprinting.....	14
2.2.2 Musculoskeletal architecture of elite sprinters	16
2.3 Use of simulation to identify muscle roles	21
Chapter 3 Simulation of aperiodic bipedal sprinting	23
3.1 Introduction.....	23
3.2 Methods.....	25

3.2.1 The biped model	25
3.2.2 The foot-floor contact model	27
3.2.3 Optimal control problem formulation.....	28
3.2.4 Discretization of the optimal control problem.....	29
3.2.5 Initial guess for the first iteration.....	31
3.2.6 Solution of the NLP problem.....	31
3.3 Results.....	33
3.4 Discussion.....	35
Chapter 4 A hybrid dynamic walking simulation with evaluation of optimality criteria....	49
4.1 Introduction.....	49
4.2 Methods.....	52
4.2.1 The musculoskeletal biped model.....	52
4.2.2 The foot-ground contact model.....	52
4.2.3 Optimization framework.....	53
4.2.4 Objective functions and simulations.....	54
4.3 Results.....	57
4.4 Discussion.....	60
Chapter 5 Sensitivity of maximum simulated sprinting speed to plantarflexor muscle parameters.....	74
5.1 Introduction.....	74

5.2 Methods.....	77
5.2.1 Musculoskeletal biped model	77
5.2.2 Foot-ground contact model	79
5.2.3 Optimal control problem formulation.....	81
5.2.4 Discretization of the optimal control problem.....	81
5.2.5 Initial guess for the first iteration.....	82
5.2.6 Solution of the NLP Problem.....	83
5.2.7 Sensitivity analysis simulations	84
5.3 Results.....	85
5.4 Discussion.....	87
Chapter 6 Sensitivity of maximum simulated sprinting speed to the maximum force- generating capacity of individual muscles	100
6.1 Introduction.....	100
6.2 Methods.....	102
6.3 Results.....	105
6.4 Discussion.....	106
Chapter 7 Discussion	117
7.1 Summary.....	117
7.2 Limitations and future work.....	120
7.3 Conclusion	123

Appendix A	Simple biped properties and parameters	124
Appendix B	Musculoskeletal biped properties and parameters.....	126
References	132

LIST OF FIGURES

- Figure 3-1 The simple biped model used to simulate sprinting. Body segment inertial properties shown in the figure are defined in the text, as are the generalized coordinates of the model, hip actuator torques, and leg actuator forces. The right and left legs of the model were identical; labeling of the left leg inertial properties, generalized coordinates, and actuator forces and torques are omitted here for purposes of clarity. The left hip flexion angle θ_L is positive when the hip is flexed..... 41
- Figure 3-2 Stick-figure trajectories for the model (top) completing the 20 m course under PD control that produced a “jog” with duration of 6.64 s; and (middle) sprinting following optimization for which the course was covered in 2.79 s. The sprinting simulation begins with the trunk flexed forward, straightens as the race progresses, and dives forward at the finish. The first 5 meters of the sprinting simulation are also shown in detail (bottom). The time between frames represented in these illustrations are 125 ms (top) and 53 ms (middle and bottom). 42
- Figure 3-3 Forward velocity of the hip in for the initial guess “jog” (*gray*) and sprinting (*black*) simulations. Both simulations began from rest. The feedback-controlled “jog” slowly approached a steady forward velocity of approximately 4 m s^{-1} . The sprinting simulation gains speed quickly over the first few steps, then reaches a steady speed of about 8 m s^{-1} for much of the race, before diving forward at the end. 43
- Figure 3-4 The horizontal (continuous lines) and vertical (broken lines) ground reaction forces of the initial guess “jog” simulation (top) and the sprinting simulation (bottom). Ground reaction forces for the left and right feet are shown in gray and black, respectively. 44

Figure 3-5 The net horizontal impulses of the ground reaction force (GRF) for each step during the initial guess “jog” simulation (unfilled markers) and the sprinting simulation (filled markers). Impulses for GRFs applied to both the right (diamonds) and left (squares) feet are shown. Large forward impulses were generated in the first few steps of the sprinting simulation and again in the last two steps to generate the terminal dive..... 45

Figure 3-6 The angular position of the trunk in the sprinting simulation. The trunk angle was defined such that negative values of θ_t corresponded to forward flexion (Figure 3-1). The negation of that angle is plotted here, with 90° corresponding to the trunk parallel to the ground and 0° indicating an upright posture..... 46

Figure 3-7 Temporal foot contact pattern for the initial guess “jog” simulation (gray) and the sprinting simulation (black). Both simulations resulted in alternating gaits. While the foot contacts in the initial guess simulation were fairly constant in duration, in the sprinting simulation contact times were larger at the start during the acceleration phase and became much shorter for the remainder of the simulation..... 47

Figure 3-8 Flexion of the right hip plotted versus time for the sprinting simulation. Right foot contact (circles), consistently occurred as the hip was beginning to extend following maximum flexion. This “leg retraction” behavior was not present in the initial guess “jog” simulation, for which foot contact always coincided with maximum hip flexion..... 48

Figure 4-1 The stride length (SL) and stride frequency (SF) values observed in the walking simulations. The diamond, plus sign, and square markers indicated muscle activation, mechanical energy expenditure, and metabolic energy expenditure simulations respectively. Cyan, red, blue, and green colors were used for weighting factors (1,0,0), (1,0,1), (1,1,0),

and (1,1,1) respectively. The black lines with the filled circular marker showed average experimental values for SL and SF derived from Chao et al., 1983. 66

Figure 4-2 The joint angles, joint moments, and GRFs of the muscle activation simulations for one full walking cycle from left foot heel strike to left foot heel strike. Cyan, red, blue, and green colors were used for weighting factors (1,0,0), (1,0,1), (1,1,0), and (1,1,1) respectively. The shaded gray areas in the ankle, knee, and hip angles and moments were reproduced from Kadaba et al., 1989; which are enclosed by one plus and minus standard deviations' of a representative subjects' nine trials (three cycles x three days). According to the sign convention, plantarflexion, knee flexion, and hip extension were negative. The shaded gray area in the trunk angle enclosed by ± 1 degree (Winter, 1995). The shaded gray areas in GRFs were reproduced from Chao et al., 1983; which are enclosed by one plus and minus standard deviations' of the general pattern of 26 normal subjects. 67

Figure 4-3 The muscle activations for one full walking cycle from left foot heel strike to left foot heel strike for the muscle activation simulations. Cyan, red, blue, and green colors were used for weighting factors (1,0,0), (1,0,1), (1,1,0), and (1,1,1) respectively. The gray lines were reproduced from Kadaba et al., 1989; and represent the mean value of EMG envelopes of a representative subjects' nine trials (three cycles x three days). 68

Figure 4-4 The joint angles, joint moments, and GRFs of the mechanical energy expenditure simulations for one full walking cycle from left foot heel strike to left foot heel strike. Cyan, red, blue, and green colors were used for weighting factors (1,0,0), (1,0,1), (1,1,0), and (1,1,1) respectively. The shaded gray areas in the ankle, knee, and hip angles and moments were reproduced from Kadaba et al., 1989; which are enclosed by one plus and minus standard deviations' of a representative subjects' nine trials (three cycles x three days).

According to the sign convention, plantarflexion, knee flexion, and hip extension were negative. The shaded gray area in the trunk angle enclosed by ± 1 degree (Winter, 1995).

The shaded gray areas in GRFs were reproduced from Chao et al., 1983; which are enclosed by one plus and minus standard deviations' of the general pattern of 26 normal subjects... 69

Figure 4-5 The muscle activations for one full walking cycle from left foot heel strike to left foot heel strike for the mechanical energy expenditure simulations. Cyan, red, blue, and green colors were used for weighting factors (1,0,0), (1,0,1), (1,1,0), and (1,1,1) respectively. The gray lines were reproduced from Kadaba et al., 1989; and represent the mean value of EMG envelopes of a representative subjects' nine trials (three cycles x three days)..... 70

Figure 4-6 The joint angles, joint moments, and GRFs of the metabolic energy expenditure simulations for one full walking cycle from left foot heel strike to left foot heel strike. Cyan, red, blue, and green colors were used for weighting factors (1,0,0), (1,0,1), (1,1,0), and (1,1,1) respectively. The shaded gray areas in the ankle, knee, and hip angles and moments were reproduced from Kadaba et al., 1989; which are enclosed by one plus and minus standard deviations' of a representative subjects' nine trials (three cycles x three days).

According to the sign convention, plantarflexion, knee flexion, and hip extension were negative. The shaded gray area in the trunk angle enclosed by ± 1 degree (Winter, 1995).

The shaded gray areas in GRFs were reproduced from Chao et al., 1983; which are enclosed by one plus and minus standard deviations' of the general pattern of 26 normal subjects... 71

Figure 4-7 The muscle activations for one full walking cycle from left foot heel strike to left foot heel strike for the metabolic energy expenditure simulations. Cyan, red, blue, and green colors were used for weighting factors (1,0,0), (1,0,1), (1,1,0), and (1,1,1) respectively. The

gray lines were reproduced from Kadaba et al., 1989; and represent the mean value of EMG envelopes of a representative subjects' nine trials (three cycles x three days). 72

Figure 4-8 Average metabolic energy expenditure rate for muscle activation, mechanical energy expenditure, and metabolic energy expenditure simulations. Cyan, red, blue, and green colors were used for weighting factors (1,0,0), (1,0,1), (1,1,0), and (1,1,1) respectively. The black horizontal dashed line indicated the experimental value, 4.7 W/kg (Burdett et al., 1983) 73

Figure 5-1 The joint angles, joint moments, and GRFs for one full sprinting cycle from left foot heel strike to left foot heel strike for the maximum speed sprinting simulation with nominal parameter values. The shaded gray areas in the joint angles and GRFs plots were reproduced from Miller et al., 2012; which are enclosed by two plus and minus between twelve women subjects' standard deviations around the mean (mean speed 6.42 ± 0.61 m/s). The blue and red lines in the joint moment plots were reproduced from Schache et al., 2011; and represent mean joint moments of eight subjects running at 5.02 m/s (red) and 6.97 m/s (blue). The dashed vertical gray lines indicate the time of toe-off. 94

Figure 5-2 The muscle activations for one full sprint cycle from left foot heel strike to left foot heel strike for the maximum speed sprinting simulation with nominal parameter values. The cyan lines were reproduced from Miller et al., 2012; and represent EMG linear envelopes. The dashed vertical gray lines indicate the time of toe-off..... 95

Figure 5-3 The changes in the mechanical energy and the joint powers of ankle, knee, and hip for one full sprint cycle from left foot heel strike to left foot heel strike for the maximum speed sprinting simulation with nominal parameter values. The shaded gray area is enclosed by the start and the end of the propulsive phase of support. The blue and red lines in the joint

power plots were reproduced from Schache et al., 2011; and represent mean joint power of eight subjects running at 5.02 m/s (red) and 6.97 m/s (blue)..... 96

Figure 5-4 The alterations in top sprint speed, stride length, and stride frequency for -2 SD, -1 SD, +1 SD, and +2 SD perturbations of plantarflexor muscles parameters, namely, maximum isometric force (FM), optimal fiber length (FL), tendon stiffness (TS), and moment arm (MA) normalized with values from the maximum speed sprinting simulation with nominal parameter values (NOM). 97

Figure 5-5 The alterations in swing time, contact time, and effective impulse of GRF_y for -2 SD, -1 SD, +1 SD, and +2 SD perturbations of plantarflexor muscles parameters, namely, maximum isometric force (FM), optimal fiber length (FL), tendon stiffness (TS), and moment arm (MA) normalized with values from the maximum speed sprinting simulation with nominal parameter values (NOM). 98

Figure 5-6 The alterations in average ground force of GRF_y, work done in the propulsive phase of support, and peak ankle power for -2 SD, -1 SD, +1 SD, and +2 SD perturbations of plantarflexor muscles parameters, namely, maximum isometric force (FM), optimal fiber length (FL), tendon stiffness (TS), and moment arm (MA) normalized with values from the maximum speed sprinting simulation with nominal parameter values (NOM)..... 99

Figure 6-1 Percent change in maximum sprinting velocity over the nominal simulation for isolated positive (black bar) and negative (gray bar) perturbations of each muscle group. 111

Figure 6-2 Percent change in stride length (SL) over the nominal simulation for isolated positive perturbation of each muscle group..... 112

Figure 6-3 Percent change in stride frequency (SF) over the nominal simulation for isolated positive perturbation of each muscle group. 113

Figure 6-4 Percent change in stride length (SL) over the nominal simulation for isolated negative perturbation of each muscle group..... 114

Figure 6-5 Percent change in stride frequency (SF) over the nominal simulation for isolated negative perturbation of each muscle group. 115

Figure 6-6 Percent change in maximum sprinting velocity scaled with the magnitude of the perturbation over the nominal simulation for isolated positive (black bar) and negative (gray bar) perturbations of each muscle group..... 116

ACKNOWLEDGMENTS

I would like to thank my advisor Dr. Steve Piazza sincerely for his guidance, wisdom, and support during my graduate studies at Penn State. This dissertation would not have been possible without his guidance and support.

I would also like to thank my dissertation committee of Dr. Belegundu, Dr. Cusumano, and Dr. Sommer for their time and effort.

I would especially like to thank my fellow graduate students without whom I would not have learned nearly as much: Herman, Tony, Becky, Mike, and Josh.

I am grateful to Amanda and Nicole for their help with making digital approximations of the graphs taken from published papers, and to Pinar for her help with making figures depicting the models.

My parents Müfit and Müslüme and brothers Bahadır and Emre, who always showed their support and love.

Last but not least, I thank my love Serap who has been by my side throughout this PhD, living every single minute of it, and without whom I would not have had the courage to embark on this journey in the first place. For everything you have done for me, I thank you.

This dissertation is dedicated to my love Serap and sweet son Jan

Chapter 1

Introduction

1.1 Background

Bipedal locomotion is accomplished using a variety of gaits and the study of gait mechanics often assumes that some optimality criterion is being satisfied for each different gait. For instance, by using the cost of transport as the optimality criterion, Alexander (1980 and 1992) simulated bipedal and quadruped gaits with simple planar models, while Anderson and Pandy (2001a) simulated normal human walking with a complex musculoskeletal model. Indeed, there are experimental (Ralston, 1976) and computational modeling studies (Srinivasan and Ruina, 2006) demonstrating that humans walk at speeds that use the least energy and energetic economy is a commonly understood goal for distance running. For these reasons, energy expenditure has been used frequently as an optimality criterion in dynamic simulations of walking and running. However, estimating energy expenditure or effort in a muscle-actuated computational model requires somewhat complex calculations of energy consumption by individual muscles, and so alternative optimality criteria have been implemented. The most commonly used such alternative is muscle activation, which is already a state in most dynamic simulations. Nevertheless, while there is experimental evidence indicating that humans prefer to walk with minimum effort, previous simulations using such an optimality criterion have not been able to reproduce several important features of human walking.

Computer modeling of human walking and running typically has focused on simulations in which periodic strides are constrained to occur. The periodic nature of steady-state gait justifies simulation of a single stride in which the initial conditions are equivalent to the terminal

conditions (or simulation of a half of a stride if right/left symmetry is also assumed). Gaits appropriate for simulation using this approach include steady-state walking (Ackermann and van den Bogert, 2010) and running (Schultz and Mombaur, 2010), and sprinting (Miller et al., 2012a) that occurs once top speed has been reached and maintained. There are, however, gaits which are necessarily aperiodic such as sprinting from rest or initiation of a walking gait before a steady state motion is reached. Simulation of aperiodic gaits has received little attention from previous researchers but is nonetheless important because the mechanics of some gaits are quite different in periodic and aperiodic phases of motion. Such aperiodic gait simulations would allow better evaluation of how the musculoskeletal system contributes to aspects of performance, understanding of factors limiting the ability to reach steady state, and assessment of asymmetry.

Simulations of locomotion may be developed by “tracking” movements previously measured in the motion laboratory or by predicting movements that represent optimal performance. Generally, in a tracking simulation, the muscle excitation histories are searched that would minimize the deviations from the experimentally measured joint angles and the ground reaction forces or they are treated as constraints that must be satisfied within a prescribed tolerance (Pandy, 2001). The tracking approach has several advantages: the motions and forces measured in an experiment are often reproduced with great accuracy; once a simulation has been developed, the modeler has the ability to estimate variables that cannot be measured in the laboratory; and the information available from such a simulation may be useful in investigating cause-effect relationships (for example, simulation-based estimates of joint and tendon loads may be related to injury mechanisms). The tracking approach has been used to perform muscle-induced acceleration analyses that estimate the contributions of individual muscles to propulsion and support during locomotion. On the other hand, a predictive approach is necessary under the

following conditions (Anderson and Pandy, 2001b): when accurate experimental data is not available or is not easy to collect experimental data with current techniques (e.g., for walking in other planets); when the optimality criteria is a time-dependent performance metric (e.g., maximum-height in jumping or minimum time in sprinting); or there is a need for creating novel simulations (e.g., for sensitivity analysis). Therefore, predictive simulations have the potential to be used to study the roles of muscles in maximum-performance tasks or in the absence of accurate experimental data in ways that would go beyond muscle-induced acceleration analysis in a tracking simulation. It can be quite challenging to create predictive simulations, however, due to problems in convergence to a solution and high computational demands.

1.2 Purpose of the dissertation

The general purpose of this dissertation is to make use of an optimal controls approach to develop novel simulations of bipedal gait. These simulations are used to investigate new optimality criteria and explore the functional roles of muscles in sprinting. Another purpose is to demonstrate how an approach of adding feedback and feedforward control loops to the model may be useful to obtain initial guesses to the optimization problems and to demonstrate abilities of computer models employed in the study. The last main purpose of this dissertation is to show how variations in architecture of musculoskeletal system influence sprinting performance with a simulation approach.

1.3 Specific aims

The dissertation had three proposed specific aims:

- i) To create a simulation framework with a simple bipedal torque-driven model and synthesize optimal sprinting from rest by minimizing the locomotion time for a prescribed distance.

- ii) To use the same simulation framework developed above as the basis for more complex muscle-driven models.
- iii) To use the model developed in 'ii' to
 - a. Analyze sensitivity of sprint performance to musculoskeletal architecture parameters of plantarflexor muscles
 - b. Analyze sensitivity of sprint performance to maximum isometric force capacity of ankle, knee, and hip muscles
 - c. Investigate and compare commonly used optimality measures for normal walking

1.4 Organization of the dissertation

In the following chapters, four research studies along with a review of the relevant literature and a final discussion will be presented. The literature review is presented in Chapter 2. Chapter 3 presents a novel aperiodic sprinting simulation. Chapter 4 describes a musculoskeletal model and a hybrid approach to create predictive simulations of normal walking and evaluate optimality criteria. In Chapter 5, a maximum sprinting simulation is developed to explore how variations in architecture of plantarflexors influence sprinting performance. In Chapter 6, the same model and simulation framework are used to study sensitivity of maximum simulated sprinting speed to the maximum force-generating capacity of individual muscles. The closing chapter, Chapter 7, includes a summary of four studies and conclusion of the dissertation.

Chapter 2

Literature Review

2.1 Computer simulation of bipedal locomotion

2.1.1 Formulations of optimization problem

The human locomotor system is a redundant system in that the number of muscle actuators in the human body is larger than the number of degrees of freedom at the joint level. This redundancy makes the human locomotor system an indeterminate system, for which the same motor output could be generated by a theoretically infinite number of distinct combinations of muscle excitations.

The classic conjecture is that human sensorimotor system favors optimality while performing motor tasks (Todorov, 2004). Thus, when previous researchers have tried to reproduce human gaits using computer simulation, they usually have used an optimization framework that minimizes or maximizes some optimality criterion such as muscle force or muscle energy expenditure, or some combination of criteria. Two main techniques, ‘static optimization’ and ‘dynamic optimization’ have been used to solve this optimization problem. In static optimization (e.g., Seireg and Arvikar, 1975; Crowninshield and Brand, 1981), intrinsic muscle dynamics are mostly neglected, and muscle forces are estimated in a series of postural configurations assuming static equilibrium and minimal muscular effort in an optimization framework. As its name suggests, dynamic optimization accounts for the time-dependent dynamics of the muscles and the body segments. Dynamic simulations usually are created by either tracking movements and external forces previously measured in the gait laboratory or by predicting movements that represent optimal behavior without tracking.

Dynamic simulations are usually treated as optimal controls or trajectory optimization problems. Methods for solving such problems are generally classified as direct or indirect (please refer to Betts 1998 and 2010 for detailed descriptions and formulations of direct and indirect methods). A direct method seeks a minimum of the objective function for the discretized form of the problem while an indirect method attempts to find a root of the necessary conditions for optimality with explicit derivation of the necessary conditions for the original problem. However, due to major difficulties in the application of indirect methods (Betts, 2010), they are not often preferred for creating computer simulations of bipedal simulation.

In direct methods, the optimal controls problems are transcribed into nonlinear programming (NLP) problems. A NLP problem requires locating a finite number of variables such that an objective function is optimized without violating a set of linear or nonlinear constraints and simple bounds (Betts, 2010). For the transcription of the problem, the following three methods have been used widely: (1) direct single shooting, (2) direct collocation, and (3) direct multiple shooting. Direct single shooting is the most extensively used of these methods, perhaps because it describes the NLP with a relatively small number of optimization variables (a subset of initial and final conditions, control histories, and parameters such as final time) and because the implementation of single shooting is generally straightforward. In dynamic simulations of human gait, direct single shooting is most commonly used to search for muscle control histories that minimize an optimality measure while trying to satisfy periodicity constraints on initial and final states (e.g. Anderson and Pandy, 2001a). Direct collocation, a method heavily used for optimization of aircraft trajectories, has been implemented to create gait simulations (e.g., Ackermann and van den Bogert, 2010) in which muscle controls along with state trajectories are searched to minimize an objective function subjected to algebraic

constraints originated from the governing equations of the system, and any other constraints such as periodicity. Direct multiple shooting (e.g., Diehl et al., 2006) combines features of direct single shooting and direct collocation. In this method, the original problem is discretized at n -many nodes, thus the total time span of the simulation is divided into several short integration intervals ($m = n-1$), each of which has a set of initial states and controls. An optimality measure is minimized subject to constraints requiring that the terminal values for the states at the end of each integration interval are equal to the initial values for the next interval along with any other constraints of the simulation. Direct multiple shooting is a robust method that avoids some shortcomings of other methods. For example, accumulation of nonlinearity on the terminal conditions and numerical instability during forward integration are the major issues in direct single shooting because changes early in the trajectory propagate to the end of the trajectory (Betts, 1998). Direct collection eliminates forward integration, but error between discretizations must be estimated with re-gridding i.e., the optimal controls problem must be solved repeatedly progressively finer meshes. This process generally requires implementations of complex meshing algorithms, but has not properly addressed in most simulations (Diehl et al., 2006).

2.1.2 Simulations of walking

Human locomotion has been simulated with a wide variety of models that range from simple torque-driven models to highly complex muscle-driven models. Several simulation approaches, from passive walking to inverse dynamics based numerical optimization, have been implemented to explore bipedal locomotion.

Passive walkers have been used to gain insight into the underlying passive mechanics of bipedal gait. McGeer (1990) built an extremely simple walking model without actuators that can effectively walk down a shallow ramp with a gait that is comparable to human gait. The energy

lost in the inelastic foot strikes are compensated for by gravity, and the resulting walking motion is periodic in nature. Garcia et al. (1998) developed an irreducibly simple passive dynamic walking model with a point mass at the hip, two rigid massless legs hinged at the hip, and infinitesimal point masses at the feet. Collins et al. (2001) increased the number of kinematic degrees of freedom (dof) by building the first three-dimensional passive dynamical walker with knees. Kuo (2002) introduced the idea of a minimally actuated biped by powering Garcia et al.'s simplest walking model for level walking by applying an impulse immediately before the toe-off and a torque applied on the stance leg. Wisse et al. (2004) added a passive upper body to the simplest walking model which improves the resistance to disturbances. Gomes and Ruina (2011) showed with a three-link walking model that level walking is possible with zero energy input into the system provided that the foot collision occurs at zero velocity.

The simulations created with torque and/or force driven models enabled to investigate locomotor function in the joint level with ideal actuators. Chow and Jacobson (1971) were the first to study human locomotion with optimal controls (indirect single shooting) with minimization of mechanical energy expenditure of a torque-driven planar computational model. Although they had a multi-link model including ankle, knee, and hip joints, they actually performed optimization on the swing leg by introducing several simplifications to the problem. The main reason for the simplifications was the limited computational power available at the time. Onyshko and Winter (1980) developed a seven segment walking model driven by torques at each joint. They changed the manually derived governing equations of motion from phase to phase by changing the topology of the model. The model was actuated by joint moment histories evaluated by inverse kinematic analysis of experimentally obtained human walking data. To compensate for differences between model and subjects, they made manual adjustment on initial

states and joint moment histories to able to create gait cycles. Pandy and Berme (1988) used open and closed kinematic chains to simulate human walking in single and double support phases of walking respectively. The authors used experimentally obtained initial states and obtained estimates of the joint moments through trial and error. The improvement of that model study was that it offered an alternative to manually deriving the equations defining a mathematical model for human gait. Gilchrist and Winter (1997) improved the model of Onyshko and Winter (1980) by extending it to three dimensions and increasing the number of segments to nine. The authors equipped the model with torsional and linear springs and dampers to ensure a smooth motion. The joint moments obtained from an inverse dynamics analysis were used to drive the model, along with controls on the trunk and physiological range of motion of joints. By using optimal controls, Srinivasan and Ruina (2006) simulated possible gaits of a minimal biped actuated by force actuators, and the model discovered walking at low speeds and running at higher speeds to minimize energy expenditure. In an another predictive dynamic simulation, Ren et al. (2007) simulated normal bipedal walking at 1.5 m/s by minimizing mechanical energy expenditure in an inverse dynamics optimization framework. Several gait patterns emerged with varying levels of energy cost, but the best gait pattern in terms of reproducing natural human walking was the one with lowest energy cost. However, there were still significant deviations from natural human walking such as relatively large trunk excursions and non-smooth ground reaction forces. Xiang, Arora, and Abdel-Malek (2011) used inverse dynamics in an optimization framework to simulate asymmetric human gait with a torque-driven 38-dof 3D model. The sum of the joint torques squared used as the optimality measure. The joint angle histories were discretized using B-spline interpolation, then joint torques and ground

reaction forces were solved using inverse dynamics. The simulation framework was able to generate gaits with different left and right step lengths.

Tracking simulations obtained through dynamic optimization of muscle-driven models have been used to reproduce experimentally measured motion and muscle activation trajectories with high accuracy and to assess muscle function during gait. Davy and Audu (1987) used dynamic optimization to predict muscle forces in the swing phase of walking by using an optimality measure combination of tracking error and metabolic energy consumption. They used a three-dof lower limb model driven by nine muscle groups. The authors compared muscle forces obtained by dynamic optimization with forces estimated through static optimization, and pointed that the former ones are generally larger and latter. Yamaguchi and Zajac (1990) used a 3D eight-dof model with a compliant contact model to simulate functional neuromuscular stimulation assisted walking by minimizing an objective functions consisted of deviations from the nominal trajectory and the sum of cubed muscle stresses. The simulation results suggested using an ankle-foot orthosis would help to stabilize the stance leg. Piazza and Delp (1996) simulated swing phase of gait with a five-segment leg model actuated by 12 muscle groups. The authors did not minimize the deviation error from experimental measurements; instead they used averaged experimental trajectories and muscle controls directly. The simulation demonstrated that removal of rectus femoris action causes knee hyperflexion. Neptune, Kautz, and Zajac (2001) created a normal walking simulation with a muscle (15 muscle actuators per leg) driven model of a trunk, right and left legs (thigh, shank, patella and foot) to evaluate contributions of ankle plantarflexors to support, forward progression and swing initiation. The objective function was solely tracking error. The authors extended the capabilities of the tracking simulation by adding muscle induced acceleration analysis. The muscle-induced accelerations were determined

by applying estimated individual muscle forces at a time in a series of snapshots of postural configurations. The simulation results suggested that both plantarflexor muscles provide vertical support in the single support phase of walking, yet only gastrocnemius contributes to swing initiation. Sasaki and Neptune (2006) used a planar model to create another tracking-based dynamic simulation of normal walking and running at the walk-run transition speed to investigate differences in muscle function during walking and running at the same speed. Authors reported that muscle function is different between two gaits at the same speed, and extensor muscles produced greater power output. The efficiency of tracking simulations was improved using the “Computed Muscle Control” method (Thelen and Anderson, 2006) in which not tracking error but the sum of volume scaled second power of muscle activations were minimized. The optimization converges to a solution when the error between experimentally obtained accelerations and model accelerations driven by optimized muscle activation profiles falls below a threshold value. The error is controlled with a feedback controller and fed to the optimization process. Authors reported that they were able to reproduce joint motions in a walking step with high accuracy (mean root-mean-squared errors generally less than 1 degree) in 30 minutes. Researchers from our laboratory (Hast and Piazza, 2013) exploited a similar approach to reproduce knee motion and muscle activity with high accuracy. Such a simulation could be used to estimate contact forces in knee that are otherwise not measureable without an invasive technique.

The predictive dynamics simulations with muscle-driven models facilitate creating gait cycles without relying experimentally obtained gait data, discovering novel gaits, and estimating muscle forces guided by some optimality criteria. This approach also enables to synthesize gait cycles on altered or different conditions to make sensitivity studies. Probably the most famous

predictive dynamic simulation was created by Anderson and Pandy (2001a). Those authors used a 3D model with 23 kinematics dof and 54 muscle actuators to simulate normal human walking. Their objective function was to minimize metabolic energy expenditure per unit distance traveled, i.e., cost of transport. Although the simulation reproduced significant features of normal gait, the problem never satisfied the terminal conditions even after 10,000 hours of CPU time in parallel machines. Further, the simulation overestimated metabolic energy expenditure by 47 percent. To evaluate their newly developed human muscle energy expenditure model, Umberger, Gerritsen, and Martin (2003) created a simulation of one full step of walking of a planar model. The simulation searched for switching times and excitation amplitudes while minimizing cost of transport. The model estimated whole-body rate of energy expenditure as 4.4 W/kg which was very close experimental value (4.0 - 4.3 W/kg) at the pre-specified walking speed and inertial properties. By using a family of objective functions based on muscle activation integrals and direct collocation method, Ackermann and van den Bogert (2010) simulated normal bipedal walking at 1.1 m/s with a seven-segment planar model actuated by eight muscles on each leg. The objective functions were classified as either cost or fatigue-like depending upon weighting factors and exponents. It was demonstrated that different cost functions lead to substantially distinct gait simulations. For instance, effort-like cost functions converged to straight-legged pattern in the stance phase; on the other hand, fatigue-like cost functions illustrated stance phase knee flexion. Same authors used the same simulation framework to simulate gait in Mars ($g_{\text{Mars}} = 3.72 \text{ m/s}^2$) and Moon ($g_{\text{Moon}} = 1.63 \text{ m/s}^2$) (Ackermann and van den Bogert, 2012) at a speed 1.1 m/s and 2.0 m/s. The simulation results suggested that skipping gait is more efficient in terms of effort and less fatiguing than walking or running under low gravity.

2.1.3 Simulations of running

Running is simulated by using various models such as passive running, actively controlled and torque driven, optimality introduced, and muscle driven models. Tad McGeer is a pioneer researcher not only in passive dynamic walking but also in passive dynamic running. He simulated human-like level running with a model consisting of two telescoping legs with linear springs, connected by a hip joint with a torsional spring that make the legs swing in a scissor action (McGeer, 1990b). The stride frequency of the model was very close to the natural frequency of the scissoring oscillations of the legs (McGeer, 1990b; Alexander, 1995). Prior to that Blickhan (1989) developed a simple massless spring-mass model for running and hopping; even the simplicity of the model, it predicted the mass specific energy fluctuations of the center of mass per distance to be similar for animals of various size. The ground reaction forces produced by these models, however, were smooth curves with a single maximum which do not resemble the initial peak force at the foot contact. In addition, these models were passive models running in a periodic motion with no viscous damping and without any control input to the system. On the other hand, running was also simulated by actively observing and controlling the motion of the models. For instance, Raibert (1985) developed physical and computer models of hoppers, bipeds, and quadrupeds that run by observing and controlling its hopping height, forward speed, and body attitude. Neptune, Wright, and van den Bogert (2000) used a tracking approach to simulate stance phase of running, and the simulation framework was able to reproduce subjects' limb motion and ground contact forces within two standard deviations. Schultz and Mombaur (2010) simulated running of a torque-driven 3D running model which has 25 kinematic dof. The torques drive the model was estimated by minimizing a cost function composed by addition elements of weighted torques squared and variations in torques squared

vectors. They did not validate their cost function, but the model imitated the maximal sprinting of Griffith-Joyner, who is the world record holder in 100-m women. Van den Bogert and Ackermann (2009) simulated maximum speed sprinting with a seven-segment muscle-driven model using direct collocation. The simulation converged to solution with a maximal sprint velocity of 7.45 m/s at a stride frequency of 1.90 Hz. When the moment arm parameter of the gluteal muscle group was perturbed, larger moment arms increased the maximum sprint velocity. Miller et al. (2012c) simulated human running using a predictive approach and a planar bipedal model, and demonstrated that even there is experimental evidence to indicate humans run at speeds that would minimize cost of transport, the simulation in which muscle activation integrals used as the optimality criteria agreed most with the experimental kinetic, kinematic, and EMG data collected from human runners. Miller et al. (2012 a, b) made two sprinting simulations using the same simulation framework. Miller et al. (2012a) perturbed the characteristic parameters of the muscle force-velocity relationship, and showed that maximum sprinting speed is most sensitive to maximum shortening velocity parameter. Miller et al. (2012b) removed muscle mechanical properties in isolation to quantify their influence on maximum sprinting speed, and illustrated that muscle force-velocity relationship is the most influential property of in terms of limiting maximum sprinting speed.

2.2 Determinants of sprinting performance

2.2.1 Mechanics of human sprinting

Sprinting is a gait that enables one to traverse a distance in the minimum time which may lead to catching prey, avoiding a predator, or winning a trophy. Unlike walking and running, sprinting is an explosive motion and non-periodic in nature with a rapid acceleration phase at the start. In a dash race, sprinter gives his or her maximum effort to accelerate in the first strides, reaches the

maximum speed after a couple of strides, and then tries to keep the pace until the end of the race. The characteristics of the first strides of a sprinter are different from those of the strides that follow due to the transient system dynamics, rapid acceleration phase, postural configuration, and demand from the musculoskeletal system. Indeed, these first strides have the utmost importance, since they are the ones that differentiate an elite sprint performance from a merely good one (Baumann, 1976; Hunter et al., 2005).

The sprint start from starting blocks and the accelerations in the first steps are the most important phases of a sprint race in terms of their contribution to the final result. Athletes accelerate rapidly (approximately $10 \text{ m}\cdot\text{s}^{-2}$) in the first few meters to reach maximum speed as quickly as possible. Coh et al. (1998) found that the kinetic parameters such as maximal force, maximal force gradient, force impulse, and time to maximal force; and kinematic parameters such as horizontal start velocity of center of gravity and the ankle angle in the front starting block are correlated with the sprint start acceleration. Harland et al. (1997) suggested such a postural configuration at the block that front and rear knee angles are 90 and 130 degrees respectively, with the hips held moderately high to develop the maximum force for the minimum block clearance time, the maximum block leaving velocity, and the maximum block leaving acceleration. Slawinski et al. (2010) studied kinetics and kinematics of sprint start and two subsequent steps on elite and well-trained athletes. They indicated that impulsive forces (276.2 N·s vs 215.4 N·s) and average speed (start, 3.48 m/s vs 3.24 m/s; steps, 4.06 m/s vs 3.87 m/s) of elite athletes are significantly greater than well-trained ones in the sprint start and two subsequent steps. Eriksen et al. (2008) studied the running of the fastest man in the world, Usain Bolt, who traversed 100-meter in 9.69 seconds, reached to the top speed 12.2 m/s, had a speed of

9.05 m/s at 10-meter, and used only 40 strides to finish the race (four less than any of the other athletes in the field) in the 2008 Beijing Olympic Games.

2.2.2 Musculoskeletal architecture of elite sprinters

Muscles are the actuators of the locomotor system. As with many systems in the nature, muscle is a nonlinear system and force development in muscle depend on both nonlinear force-length and force-velocity properties. A.V. Hill conducted a series of experiments on isolated muscle fibers and proposed an empirical relation which today is known as Hill's Equation. The equation specifies that the lower a muscles shortening velocity, the higher the force in the muscle (McMahon, 1984). The force length property specifies that there is an optimal length for muscle to produce the maximum isometric force, and this optimal length is around the sarcomere rest length (Rassier et al., 1999). Muscle does not produce passive force unless it is lengthened more than its rest length.

According to the cross-bridge theory (Huxley, 1957), the sliding motion in sarcomere is enabled by the physical attachment of myosin protein heads to actin protein helix. The force-length and force-velocity relationships of muscle are influenced by the interactions of these proteins (Bodine et al., 1982). Shortening velocity of sarcomere is dependent on the attachment and detachments rates of the myosin and the actin proteins (McMahon, 1984). Slow-twitch and fast-twitch fibers have different shortening velocity characteristics, and this affect specific tensions of fibers (Powell et al, 1984). For fast-twitch mammalian muscle fiber, the specific tension value is 22.5 N/cm^2 , but it is less for slow-twitch fiber (Lieber et al., 2000).

Physiological cross sectional area (PCSA), muscle fiber length, and pennation angle are other factors affecting force producing properties of muscle (Lieber et al., 2000). Higher PCSA means more parallel muscle fibers, so more tension in the muscle. Longer fiber length is also

conducive to force production, since longer fibers are able to maintain near maximal muscle tension for fast and large joint excursions. Higher pennation angles, however reduce the amount of force and excursion transferred to the tendon, but increases the PCSA.

Hildebrand and Goslow (1995) discussed rigorously the morphology of various animals that surpass other species in running, jumping, digging, etc., and their functional needs to survive. Although, the morphology-function relationship seems to be well stated across species, this does not seem to be the case within species. The best animal sprinters, such as the cheetah and the greyhound, have long forefoot and short heel bones (Hudson et al., 2011 a, b) which suggest higher gear ratio, the ratio of the ground reaction force (GRF) moment arm to the muscle moment arm (Hildebrand, 1960). Higher gear ratio favors reduces ankle extensor muscles shortening velocity and thus increases muscle force. Carrier et al. (1994) stated that human feet and toes provide a mechanism for changing the gear ratio of the ankle extensor, and this variable gear ratio could allow muscle contractile properties to remain optimized despite rapid changes in running speed as experienced in the first phase of sprinting (Hudson et al., 2011 a, b). Although some musculoskeletal architecture parameters such as smaller muscle moment arm and larger PCSA of muscle may be a sign of better sprinting ability, there are some other factors that affect performance. For instance, the greyhound is slower than cheetah, even though greyhounds seem to have smaller moment arms and larger musculature than those of the cheetah (Hudson et al., 2011 a, b). On the other hand, cheetah has longer heavier hindlimb and higher duty factor which promote longer strides and ground contact times respectively.

There are also significant variations within the human beings, and those variations have been linked with sprinting ability. Healthy young people mostly walk at a similar pace (around 1.3 m/s), but when they sprint, the pace would significantly differ from person to person. Is there

are a relation between observed variations in human and sprinting performance? It has been mentioned that reaction time, technique, electromyographic (EMG) activity, force production, neural factors, and muscle structure are the significant factors of sprinting performance (Mero et al., 1981, 1990, and 1992). The authors suggested that running velocity is positively correlated with fast twitch fibers, stride rate, upward speed strength, forward speed strength, and maximal isometric force; and to optimize starting action it is desirable to activate muscles before any force detected against the blocks.

The leg muscles of elite sprinters have longer muscle fascicles than non-sprinter. Longer muscle fascicles enhance force generation in fibers because longer fibers would operate in more favorable ranges (i.e., nearer to isometric) on the force-length curve. Abe et al. (2000) compared fascicle length of leg muscles of elite sprinters (100 m time, 10.0-10.9 s), elite distance runners, and untrained subjects. The vastus lateralis and gastrocnemius medialis and lateralis muscles' fascicle lengths were estimated from images obtained via ultrasound imaging. The authors found that fascicle length of leg muscles is significantly greater in sprinters than distance runners. On the other hand, they did not find a similar significant difference between distance runners and untrained subjects. Kumagai et al. (2000) and Abe et al. (2001) investigated the relationship between sprint performance and fascicle length, and showed that fascicle length is positively correlated with sprinting performance.

Previous experimental studies showed that sizes of certain muscles of sprinters are larger when compared to non-sprinters. Muscle size is usually quantified as muscle's physiological cross sectional area (PCSA) (Powell et al., 1984), and greater PCSA indicates higher muscle strength. Maughan et al. (1983) measured knee extensor muscle cross sectional areas of sprinters, distance runners, and untrained subjects using computed tomography. In the same experiment,

maximum isometric voluntary isometric force exerted by the knee extensor muscles was also measured using an isometric chair. The authors found the knee extensor muscle cross sectional areas of sprinters to be larger than those of distance runners and untrained subjects. They also reported that maximum isometric voluntary isometric force of sprinters were significantly more than endurance runners but not more than untrained subjects. In the same study mentioned above, Abe et al. (2000) also reported that the thickness of the knee extensors and plantarflexors were greater among sprinters than for distance runners and untrained subjects. Kubo et al. (2011) showed that plantarflexor and medial side knee extensor muscle thickness was larger for sprinters when compared to non-sprinters. Furthermore, a significant correlation between 100m sprint time and muscle thickness at the medial side of knee extensor was estimated in the same study. To date, there is no study that related size of hip flexor and sprinting performance.

Experimental studies showed that sprinters' have stiffer Achilles' tendon compared to non-sprinters. Arampatzis et al. (2007) took images of distal aponeuroses of the gastrocnemius muscle of sprinters, distance runners, and non-trained adults using ultrasound imaging technique during the MVC to estimate tendon stiffness. They also recorded isometric maximal voluntary plantar flexion contractions (MVC) on a dynamometer. The results of the study indicated that sprinters have higher normalized stiffness (relationship between tendon force and tendon strain) than the distance runners and non-trained subjects. Authors also reported significant correlations between tendon stiffness and maximal tendon force achieved during the MVC. However, they did not relate tendon with sprinting performance. Kubo et al. (2000) studied the relationship between tendon stiffness of leg muscles and sprinting performance. Authors used ultrasound imaging to measure elongation of tendon of vastus lateralis and medial gastrocnemius muscles of sprinters and non-trained subjects during isometric knee extension and planter flexion

respectively. The results of the study illustrated that there is no significant differences on tendon stiffness between sprinters and non-sprinters, yet the tendon of vastus lateralis was more compliant for sprinters. Kubo et al. (2011) studied tendon stiffness in another study and came up with results similar as previously reported. The authors also did not find any significant correlation between tendon stiffness of leg muscles and sprinting performance. Indeed, there is no study reporting such a relationship yet.

Previous work in our laboratory (Lee and Piazza, 2009; Baxter et al, 2012) showed that human sprinters have shorter moment arms and longer toes than height-matched non-sprinters by using imaging instruments and measurement tools. Furthermore, Baxter et al. (2012) linked shorter moment arms of sprinters with differences in the location of the center of rotation rather than differences in the path of the Achilles tendon. Muscle force is transferred to tendon, and it converts force to torques and excursions around the joint rotation center by a moment arm. Although higher moment arm seems to favor higher torque around the joint rotation center, it is not the case since the muscle force is a nonlinear function of muscle length and shortening velocity as mentioned above. A larger moment arm increases muscle fiber shortening and rate of shortening, which decrease the tension in the muscle (Nagano et al., 2003). Hence, the increased moment produced by having a longer moment arm may not compensate for the loss in muscle tension that is also required for torque generation. This reasoning was used by Lee and Piazza (2009) and Baxter and Piazza (2012) to explain what advantage human runner sprinters may have by having shorter plantarflexor moment arms than non-sprinters of similar size. However, Karamanidis et al. (2011) could not find the correlations between musculoskeletal architecture parameters and sprint performance among elite sprinters. All these suggest that musculoskeletal architecture affects sprinting ability in complex ways.

2.3 Use of simulation to identify muscle roles

Commonly used computational methods in biomechanics such as forward and inverse dynamics cannot be used to relate individual actuator contribution to the tasks in locomotion such as for propulsion, support, and braking of the body. Because, the locomotion tasks are at different coordinate systems and time scales than the actuators have. A methodological approach known as muscle induced acceleration (MIA) analysis is capable of solving this problem (Zajac and Gordon, 1989). Anderson and Pandy (2003) used MIA analysis to quantify individual muscle contribution to support the body during normal gait. Authors demonstrated that plantarflexors support body almost solely in late stance phase and cause second bump in the vertical ground-reaction curves. Neptune et al. (2004) showed that muscle force redistributes segmental power for forward progression of trunk and legs during walking by using MIA analysis. In a two-part review article, Zajac, Neptune, and Kautz (2002 and 2003) presented a broad review on individual muscle contribution to trunk support and forward progression in normal walking by analysis of MIA and segmental powers.

In a study of running and sprinting, Hamner et al. (2010) employed MIA analysis to assess individual muscle contribution to braking, propulsion, and support of body during running steady state at 3.96 m/s. They found that ankle plantarflexors, the soleus and gastrocnemius make the greatest contribution to propulsion and support of body during the second half of the stance phase. Hamner et al. (2013) extended their original work by analyzing MIA over a range of running speeds (2.0, 3.0, 4.0, and 5.0 m/s). The results of the analysis indicated that the plantarflexor soleus generates the greatest upward mass center acceleration at all running speeds. Dorn et al. (2012) used MIA analysis to investigate muscle contributions to running (at 3.5, 5.0, and 7.0 m/s) and sprinting (>8.0 m/s). The results of the analysis illustrated that plantarflexors

contribute to vertical support forces most significantly speeds up to 7 m/s. After that speed, hip muscles accelerated hip and knee joints more vigorously.

Chapter 3

Simulation of aperiodic bipedal sprinting

3.1 Introduction

The mathematical models used to simulate human walking and running have generally taken one of two forms: (1) complex models that incorporate many degrees of freedom (DOF), joints with realistic kinematics, and dozens of muscle-tendon actuators; or (2) simple models that have many fewer DOF and minimal actuation. Complex musculoskeletal models are needed to understand the roles played by individual muscles when the movements under consideration involve multiple joints and are governed by coupled dynamic equations of motion (e.g., Anderson and Pandy, 2001a). Analysis of simple models has also yielded valuable insights that have changed our understanding of the dynamics of locomotion. For example, the knowledge gained from simple dynamic models has informed the design of legged robots (e.g., Collins et al., 2005) and artificial limbs (e.g., Hansen et al., 2006).

Examples of simple models of bipedal locomotion include the three-segment ballistic walking model of Mochon and McMahon (1980), which led to the development of passive dynamic walking simulations and robots (McGeer, 1990). These studies demonstrated that stable downhill walking patterns comparable to human walking could be realized without active control or actuation of the joints. Garcia et al. (1998) extended this approach by developing an irreducibly simple passive dynamic walking model with a point mass at the hip, two rigid massless legs, and infinitesimally small point masses at the feet. Alexander (1992) presented a model with force-actuated telescoping legs and torque-actuated revolute-joint hips. The model could be made to walk or run depending on how the work performed by the actuators is minimized. Srinivasan and Ruina (2006) used a minimal biped model with telescoping legs that

“discovered” walking at low speeds and running at higher speeds as it attempted to minimize energy expenditure.

Common to nearly all previous simulations of walking and running is the constraint that the motion be periodic. Application of this constraint enhances computational tractability because it permits simulation of a single stride (or a half-stride if symmetric gait is assumed). The assumption of periodicity is a sensible one for steady-state walking or running because such gaits are generally considered to repeat after several transient cycles associated with gait initiation. There are, however, necessarily aperiodic gaits such as sprinting from rest and the initiation of walking that have received less attention from previous investigators. Several aperiodic non-locomotor activities have been simulated with numerical optimization, including: maximum-height human jumping (Pandy et al., 1990); rising from a chair (Pandy et al., 1995); optimal high dives (Albro et al., 2000); and vaulting (Cheng et al., 2009).

Sprinting has unique qualities that separate it from other bipedal gaits. The initiation of running at the start of a long distance race is not important to the outcome of the race, but the rapid acceleration at the start of a sprint race is critical to performance (Baumann, 1976; Hunter et al., 2005). During this period the muscles work to increase the forward velocity of the body’s center of mass and it is unlikely that this acceleration is accomplished with the same concern for energetic efficiency that we commonly attach to walking and distance running. Similar to maximal height jumping, sprinting has an unambiguous objective: to traverse a given distance in the shortest time possible.

Bipedal sprinting has been simulated using models of varying complexity. Vaughan (1983) simulated a sprinter using a mass subject to ground reaction forces and drag forces. Ward-Smith (1985) used a mathematical model based on the first law of thermodynamics to

explain why peak velocity is not achieved until the middle stages of a 100 m race. Putnam et al. (1987) described a sensitivity study in which joint moments were systematically changed to elucidate joint mechanics during recovery action in sprinting. Thelen et al. (2005) used a 31-dof muscle actuated model to simulate the swing phase of sprinting to investigate muscle and tendon injury mechanisms. Lee and Piazza (2009) simulated push-off a sprinter with a three-link muscle-driven model, and demonstrated why longer toes and shorter plantarflexor moment arms might enhance the generation of forward impulse. Van den Bogert et al. (2009) simulated periodic maximal sprinting with a seven-segment 9-dof muscle-driven model by discretizing the system dynamics into a set of algebraic equations and solving for the maximum forward speed. Schultz and Mombaur (2010) simulated contact and flight phases of periodic sprinting using a torque-driven three-dimensional model with 25 dof. The joint torque controls were estimated by minimizing a cost function that was a weighted sum of torque magnitudes and torque variations while satisfying a forward velocity matching constraint.

To our knowledge, there are no previous reports of simulated sprinting from rest in which a biped model takes multiple discrete and aperiodic steps. The purpose of this study was to create a dynamic simulation of a seven-DOF planar biped model that begins from rest and traverses 20 m with time-optimal control without the imposition of a periodicity constraint. The results of the optimization were examined in order to identify features in common with human sprinting.

3.2 Methods

3.2.1 The biped model

We sought to create a planar biped model that was at once simple enough to facilitate control yet complex enough to reproduce recognizable features of human sprinting. The modified spring loaded inverted pendulum (SLIP) biped model (Figure 3-1) employed in the present study had

seven degrees of freedom controlled by four actuators and was based on models previously used in successful simulations of locomotion (e.g., Alexander, 1992; Abdallah et al., 2008; Raibert, 1986). The model was composed of telescoping legs that were fitted with springs, dampers, and axial actuators, point-feet (with mass m_f), and a rigid trunk segment (with mass m_t and moment of inertia I_t). The upper portion of each leg had mass (m_{leg}) and moment of inertia (I_{leg}). Each leg was connected to the trunk by a revolute hip joint. Flexion/extension torques T_1 and T_2 were applied at each hip joint and the leg actuators applied forces F_1 , and F_2 that extended or retracted the lower part of each leg with respect to the upper part. Thus, the controls were:

$$\mathbf{u} = [T_R, T_L, F_R, F_L] \quad (3.1)$$

The model had seven generalized position variables: the horizontal and vertical positions of hip (x, y); the lengths of legs (l_1, l_2); the angle between the trunk and the vertical (θ_t); and the hip angles between the legs and the vertical (θ_R, θ_L):

$$\mathbf{p} = [x, y, l_R, l_L, \theta_t, \theta_R, \theta_L] \quad (3.2)$$

The dynamics of the system was described by the nonlinear second order system

$$\mathbf{M}(\mathbf{p})\ddot{\mathbf{p}} = \mathbf{f}(\dot{\mathbf{p}}, \mathbf{p}, \mathbf{u}) \quad (3.3)$$

in which $\mathbf{M}(\mathbf{p})$ was 7x7 positive definite symmetric mass matrix, and \mathbf{f} was 7x1 vector of functions encompassing Coriolis, centrifugal, gravitational, and contact forces that depended on positions and velocities

$$\mathbf{v} = [\dot{x}, \dot{y}, \dot{l}_R, \dot{l}_L, \dot{\theta}_t, \dot{\theta}_R, \dot{\theta}_L] \quad (3.4)$$

and the control forces and torques given by \mathbf{u} . The explicit form of the Equation 3.3 was given in the Appendix A. The model had also seven generalized speed variables which were the

derivatives of the generalized position variables, i.e., $\mathbf{v}=\dot{\mathbf{p}}$. Then, the dynamics of the system was described by first order differential equations:

$$\dot{\mathbf{p}} = \mathbf{v} \quad (3.5)$$

$$\mathbf{M}(\mathbf{p})\dot{\mathbf{v}} = \mathbf{f}(\mathbf{v}, \mathbf{p}, \mathbf{u}) \quad (3.6)$$

The mass matrix was inverted using a symbolic manipulator package (MATLAB Symbolic Math Toolbox v5.5) in order to obtain first-order differential equations of motion in the form:

$$\dot{\mathbf{p}} = \mathbf{v} \quad (3.7)$$

$$\dot{\mathbf{v}} = \mathbf{M}^{-1}(\mathbf{p})\mathbf{f}(\mathbf{v}, \mathbf{p}, \mathbf{u}) \quad (3.8)$$

3.2.2 The foot-floor contact model

A modified version of the model developed by Marhefka and Orin (1999) was used to simulate foot-floor contact. According to this model, the floor applies point forces to one foot or both feet that depend on the penetration depth of each contacting foot into the floor and the velocity of the foot with respect to the floor. The formulation of the model eliminates discontinuous impact forces and sticky tensile forces. The vertical component of the point force

$$GRF_y = a\delta^3(1+b\dot{\delta}) \quad (3.9)$$

was a nonlinear function of vertical penetration of the foot (δ) into the ground and the velocity of the vertical penetration ($d\delta/dt$), and the constants ‘ a ’ and ‘ b ’ were vertical stiffness and damping parameters respectively. The vertical penetration

$$\delta = -y_f \tilde{\mathbf{H}}(-y_f) \quad (3.10)$$

was a function of the height of the foot above the floor (y_f) and an approximation of the Heaviside step function $\tilde{\mathbf{H}}$. Similarly, the vertical penetration velocity

$$\dot{\delta} = -\dot{y}_f \tilde{\mathbf{H}}(-y_f) \quad (3.11)$$

was a function of vertical foot velocity and the approximate Heaviside step function. The discontinuous Heaviside step function was approximated with a smooth function

$$\tilde{H}(z) = \frac{1}{2} + \frac{1}{2} \tanh \frac{z}{s} \quad (3.12)$$

to guarantee differentiability. The horizontal component of the foot-floor contact force (i.e., the frictional force) was a combination of Coulomb and viscous friction:

$$GRF_x = \mu GRF_y \tanh \frac{z}{s} + c \dot{x}_f \tilde{H}(-y_f) \quad (3.13)$$

The Coulomb component was also modeled with the approximate Heaviside step function to ensure differentiability. The viscous friction component was included to decrease sliding of the foot relative to the floor. The constants μ and c were Coulomb and viscous friction parameters respectively. All parameter values defining the foot-floor contact model are given in the Appendix A.

3.2.3 Optimal control problem formulation

The problem was formulated to find the time-optimal solution

$$\min t_f \quad (3.14)$$

that satisfies the constraints based on system dynamics,

$$\dot{\mathbf{p}}(t) = \mathbf{v}(t) \quad (3.15)$$

$$\dot{\mathbf{v}}(t) = \mathbf{M}^{-1}(\mathbf{p}(t))\mathbf{f}(\mathbf{v}(t), \mathbf{p}(t), \mathbf{u}(t)) \quad (3.16)$$

simple bounds

$$\mathbf{r}^{lower} \leq \mathbf{r} \leq \mathbf{r}^{upper} \quad (3.17)$$

on all optimization problem variables,

$$\mathbf{r} = [t_f; \mathbf{p}(t); \mathbf{v}(t); \mathbf{u}(t)] \quad (3.18)$$

and boundary conditions such as the initial and final configurations and initial (zero) velocity of the model:

$$\mathbf{b}(t = 0) - \mathbf{b}_b = 0 \quad (3.19)$$

$$\mathbf{b}(t = t_f) - \mathbf{b}_f = 0 \quad (3.20)$$

3.2.4 Discretization of the optimal control problem

The optimal control problem described above with generalized states and controls that were continuous functions of time is of infinite dimension. We chose to reduce the dimensionality and nonlinearity of this problem by first discretizing the problem. This approach of first discretizing then optimizing, also called the “direct method” (Betts, 2010), results in the optimal control problem being transformed into one of nonlinear programming (NLP).

A “multiple shooting” approach was used to formulate the optimal control problem. Multiple shooting, a method for solving boundary value problems (BVP), may be used to transcribe a BVP into a NLP problem (Betts, 2010; Diehl et al., 2006). Following this transcription, zeros of functions in the BVP domain would enforce continuity of the state trajectories and constraints corresponding to the boundary conditions in the NLP domain. Direct multiple shooting offers advantages of both collocation, which transcribes the original problem into piecewise sub-problems, and single shooting, which enables the use of adaptive, error controlled ODE solvers (Betts, 2010; Diehl et al., 2006). Multiple shooting was implemented in this case to benefit from these advantages, and also in order to avoid both the accumulation of nonlinearity on the boundary conditions and the numerical instability that occurs with single shooting.

In direct multiple shooting (Betts, 2010; Diehl et al., 2006), the time domain was broken into $n-1$ intervals at n nodes

$$t_b = t_1 < t_2 < \dots < t_n = t_f \quad (3.21)$$

and the control functions $\mathbf{u}(t)$ were discretized with piecewise zero-order polynomials

$$\mathbf{u}(t) = \mathbf{z}_i, \quad i = 1 \dots n, \quad t \in [t_i, t_{i+1}) \quad (3.22)$$

Each generalized time-continuous position and velocity function was transformed into artificial initial conditions (\mathbf{p}_i and \mathbf{v}_i , $i=1 \dots n$) on discrete time nodes for multiple intervals forward integration scheme. For each interval, the system dynamics equations (Equations 3.15 and 3.16) were forward integrated with an error-controlled and adaptive Adams-Bashforth-Moulton PECE solver (Shampine and Gordon, 1975) in MATLAB. The relative and absolute error tolerances were both set to 10^{-12} . The integrated generalized positions and velocities from t_i to t_{i+1} were denoted by $\hat{\mathbf{p}}_i$ and $\hat{\mathbf{v}}_i$ respectively which were used to define m -many continuity constraints ($m=n-1$) for each generalized state (Equations 3.24 and 3.25). Also, simple bounds (Equation 3.26) and boundary conditions (Equations 3.27 and 3.28) were also transformed into discrete forms. The discretized NLP problem was as follows:

$$\min_q t_f \quad \text{subject to} \quad (3.23)$$

$$\mathbf{p}_{j+1} - \hat{\mathbf{p}}_j = 0, \quad j = 1 \dots m \quad (3.24)$$

$$\mathbf{v}_{j+1} - \hat{\mathbf{v}}_j = 0, \quad j = 1 \dots m \quad (3.25)$$

$$\mathbf{q}^{lower} \leq \mathbf{q} = [t_f; \mathbf{p}_i; \mathbf{v}_i; \mathbf{z}_i] \leq \mathbf{q}^{upper}, \quad i = 1 \dots n \quad (3.26)$$

$$\mathbf{b}(t_1) - \mathbf{b}_b = 0 \quad (3.27)$$

$$\mathbf{b}(t_n) - \mathbf{b}_f = 0 \quad (3.28)$$

3.2.5 Initial guess for the first iteration

Successful solution of the NLP problem requires a good initial point from which to begin the iterative solution process. For our purposes, we sought an initial set of controls that caused the model to run 20 m with an alternating gait. To obtain this initial guess, an event-based forward simulation was performed by integrating the system differential equations defined in Equation 3.15 and 3.16. Each event triggered a transition to another state of the model, and then the system differential equations were numerically integrated forward in time by using error-controlled and adaptive time steps until the subsequent event occurs. Integration was stopped when the model traverses the prescribed distance and the control and state trajectories were then re-sampled at n -number of nodes and used as the initial guess for the optimization process. A three-phase proportional-derivative (*PD*) control scheme similar to that described by Raibert (1986) was implemented to control the model during this forward simulation: (i) servo the upper body to $\theta_t = 0$ when the model is at single stance posture, (ii) servo the swing leg to the prescribed desired angular position, (iii) sweep the contact leg for push-off or landing, and contract the swing leg for foot clearance.

3.2.6 Solution of the NLP problem

The NLP problem was solved iteratively by using a sequential quadratic programming (SQP) method. In SQP, the original nonlinearly constrained problem is solved using a sequence of quadratic programming (QP) sub-problems with linearized constraints. SNOPT (via MATLAB executable, *mex*, interface from TOMLAB), an SQP-based optimizer described by Gill et al. (2005) was used to solve the optimization problem.

The linear objective function, $f(\mathbf{q})=t_f$, was also the first variable in the optimization problem. For this reason, the gradient of the objective function with respect to the optimization problem variables \mathbf{q} was:

$$g(q) \equiv \frac{\partial f}{\partial q} = \begin{bmatrix} 1 \\ 0 \\ \vdots \\ 0 \end{bmatrix} \quad (3.29)$$

The Jacobian of the nonlinear equality constraints (Equation 3.24 and 3.25) was obtained using an external sparse finite difference technique. Each column of the Jacobian matrix was obtained by perturbing each optimization problem variable with fixed perturbation size, $e=10^{-8}$. The sparsity pattern was provided to the solver, allowing the solver to perturb more than one variable at a time, and thus estimate the Jacobian in fewer than $k+1$ function evaluations for a system with k -many NLP variables. Specifically, this problem had $18 \cdot n+1$ NLP variables and each nonlinear equality constraint depended on NLP variables at only two time nodes so the Jacobian could be estimated with approximately $18 \cdot 2 = 36$ function evaluations. The tolerance for the nonlinear equality constraints of the NLP problem (Eqs. 3.24, 3.25, 3.27, and 3.28) was set to 10^{-6} .

All NLP variables except t_f were scaled using the bounds (Eq. 3.26) to place them in the interval $[-0.5 \ 0.5]$ ($[0 \ 1]$ for t_f). The bounds on the controls were the maximum force or torque capacity of the actuators. For the generalized coordinate variables, the bounds were derived from the geometry of the model. The bounds originated from actuators and geometry were active at some time nodes. The bounds on the generalized speed variables were used only for purposes of scaling, however, and were set wide enough such that none of these bounds was active on the solution of the optimization problem. The initial velocities and initial leg lengths (at $t=0$) were

effectively eliminated from the optimization problem by setting both the lower and upper bounds on these equal to zero (for the initial hip and leg extension velocities) and setting both bounds on initial leg length to a nominal value of 1.0 m. The initial trunk and hip angles, however, were included in the optimization problem. The boundary conditions were that the mass center of the trunk was located at $x = 0$ m at $t=0$ and was located at $x = 20$ m at $t=t_f$. The bounds on the actuators and generalized coordinate variables are found in the Appendix A.

The *PD*-controlled simulation for producing the initial guess required 30 seconds on an Intel Xeon E53442 CPU. In this initial guess simulation, the model traversed the 20 meters in 6.64 seconds. The positions, velocities, and control trajectories were then re-sampled using 40 nodes for each second (*i.e.*, 40 *Hz*), giving a total of $n = 265$ discrete nodes for each state and control variable. Next, the initial guess for NLP was created by collecting all discrete state and control nodes and the final time, a total of 4771 ($265 \cdot 14 + 265 \cdot 4 + 1$) variables. SNOPT was then used to solve the optimal control problem, which required 3.6 hours to converge on the same processor.

3.3 Results

The optimization converged to a solution that represented a substantial improvement over the initial guess provided to the solver (Figure 3-2). The *PD*-controlled initial guess simulation traversed 20 m in 6.64 seconds; following optimization, this time was reduced to 2.79 s. For both the initial guess and the optimized sprint, the model accelerated at the start and reached a maximum speed (Figure 3-3), but the acceleration was accomplished more quickly (1.2 s versus 4.3 s) and resulted in a much higher steady-state top speed (8.5 ms^{-1} versus 4.3 ms^{-1}) in the optimized simulation.

Ground reaction force (GRF) (Figure 3-4) was the only external force acting on the model aside from gravity, and the optimization produced a faster sprint by causing the model to generate ground reaction forces more favorable to forward propulsion. During the fourth step of the sprint, which occurs during the critical initial acceleration phase when the speed of the model increases from zero to its maximum value, the propulsive impulse of the GRF was 0.167 BW s in the optimized simulation, increased from 0.043 BW s in the initial guess simulation. The net horizontal impulses of the GRF were 1.011 BW s and 0.447 BW s (summed over all steps and both legs) for the time optimal and *PD*-controlled initial guess simulations, respectively, with greater forward impulses occurring for the first six steps and the final two steps for the optimized simulation (Figure 3-5).

Several gait features acquired by the simulation during optimization correspond to behaviors known to be associated with human sprinting. Most obvious among these is forward lean of the trunk. The *PD*-controlled initial guess simulation began with an upright trunk that was controlled to remain upright throughout the simulation, but optimization produced a trunk that leaned forward to the maximum extent allowed, such that it was parallel to the ground with $\theta_t = 90^\circ$ at $t = 0.0$ s (Figure 3-6). Following the start, the trunk of the optimized sprint model straightened, reaching a minimum forward lean of $\theta_t = 35^\circ$ at $t = 1.97$ s, but then began to tilt forward again in preparation for a forward dive that was executed as the model crossed the 20 m mark (Figure 3-2).

There were also differences in the timing of the footfalls that appeared following optimization. The initial guess simulation exhibited footfalls that were of relatively long duration (lasting 0.210 s on average throughout the simulation), but the optimized sprint model used shorter contact times (0.065 s on average). At the start of the optimized sprint the model

employed longer contact times that facilitated greater propulsive impulses but later in the race, after top speed had been attained, the model used contact times of very short duration (Figure 3-7). Prior to optimization, initial foot contact occurred with the ipsilateral hip in peak flexion but following optimization this timing was altered such that the hip was beginning to flex at the time of foot contact (Figure 3-8). This behavior was exhibited for every foot contact in the optimized simulation.

3.4 Discussion

The sprinting of a simple biped model was simulated successfully. Distinct from most previous simulations of walking and running, the gait was not constrained to be periodic. To our knowledge, the present study represents the first simulation of multistep aperiodic sprinting with optimal controls. While the model was simple, the optimized sprint simulation exhibited several features in common with the sprinting of humans. These included: reaching a steady-state forward velocity after a rapid acceleration from rest; use of longer duration foot contacts during the acceleration phase and short contacts later in the race; making contact with the ground while the foot is being drawn backward relative to the body; maximizing forward impulse of the GRF during the acceleration phase; beginning the race with the trunk pitched forward followed by gradual trunk straightening; and, finally, a forward dive at the end that ensured the trunk center of mass crossed the finish line first. It should be noted that none of these behaviors was specified explicitly by the constraints of the optimization problem; each was “discovered” by the optimizer as it attempted to minimize the objective function, which was simply the time at which the trunk center of mass reached $x = 20$ m.

Human sprinters are well known to benefit from a forward leaning posture during the initial acceleration phase followed by a period during which the trunk becomes more upright

(Slawinski et al., 2010). The model in the optimized simulation took on a forward-leaning trunk posture (Figures 3-2 and 3-6) similar to that employed by human sprinters in the starting blocks. This posture decreases the acute angle between the body and ground, permitting the linear actuators in the leg to generate higher forward impulse. Another benefit of leaning forward at the start is to place the trunk center of mass close to the line of action of the GRF, thus preventing the body from tipping backward when large forward impulsive forces are applied to the feet. Both human sprinters (Mann, 2011) and the model in the optimized simulation (Figures 3-2 and 3-6) rotate their trunk toward an upright position as acceleration progresses and a steady-state forward velocity is reached.

Patterns of foot striking in elite human sprinters are similar to those discovered by the optimized simulation. Optimization reduced foot-floor contact times from the values used in the *PD*-controlled initial guess simulation, but the presence of longer-duration contacts early in the race persisted in the optimized simulation (Figure 3-7). Similar contact time patterns are observed in elite human sprinters, whose contact times during the initial steps are substantially greater than those employed later in the race (Mann, 2011). The optimized simulation also featured extension of the swing leg hip just prior to foot contact (Figure 3-8), behavior observed in human sprinters that has been hypothesized by other researchers to reduce the braking impulse of GRF by minimizing the horizontal velocity of the foot relative to the ground just before the impact (Hunter et al., 2005; Hay, 1994). Seyfarth et al. (2003) used a simple model with a feed-forward controller to demonstrate that the stability of running animals is enhanced by leg retraction, the increase in angle of attack between the leading leg and the ground before contact. Such changes in the angle of attack follow from the hip extensions just prior to every foot contact in the optimized simulation of the present study.

Perhaps the most remarkable feature of the optimized sprinting simulation is the dive forward that the model makes at the end of the simulation. This dive is a complex behavior accomplished by a sequence of actions taken over the final several steps of the sprint. At the conclusion of a sprint race, it is common to see the runners lunge forward at the tape. One suggested technique has the sprinter cross the finish line “with the head lowered and both arms thrust backward to create a forward falling action” (Rogers, 2000). The model in the optimized simulation performs a similar maneuver as it pitches the trunk forward to generate forward falling. The behavior of the model might be considered to be an exaggerated version of the falling forward strategy that risks injury, but injury risk was not incorporated into the optimizer’s objective function. It is interesting to note that in exceptionally close races it is not unusual to see sprinters actually dive at the finish line; this notably occurred recently in the 100 m T37 disability classification final at the 2012 London Paralympic Games, when Fanie van der Merwe of South Africa dived across the finish line to win a gold medal and set a world record.

Previous simulations of sprinting have made use of periodicity constraints. Van den Bogert et al. (2009) simulated a full step of maximal sprinting with a more complex seven-segment muscle-driven model. The direct collocation (DC) method was used to solve the optimal control problem with constraints representing Newton’s laws, periodicity, and an objective function that maximized the forward velocity. The optimization generated movement similar to that of a human runner. For the formulation of the optimal control problem used in the present study, however, DC method often produced infeasible or sub-optimal solutions. In another sprinting simulation, Schultz et al. (2010) simulated one step of sprinting with a torque-driven three-dimensional model. As in the present study, direct multiple shooting was used to solve the optimal control problem but with the addition of periodicity constraints, a fixed average forward

speed, and minimization of torques and torque variation. The optimization process produced a realistic simulation of maximal sprinting which provided insight into the internal forces and torques required to produce natural human running.

Previous authors have used an optimal controls approach to cause a simulation to “discover” gaits. Anderson and Pandy (2001) used a 23 DOF model actuated by 54 muscles that discovered human walking following solution of an optimal control problem that minimized muscle metabolic energy consumed per unit distance traveled by the model. The resulting simulation reproduced many features of normal human walking. In another study, Srinivasan and Ruina (2006) used a much simpler model to perform a similar optimization, and their minimal biped model discovered walking at low speeds and running at higher speeds when energy expenditure was minimized. In the present study several features of human sprinting were reproduced, but without attempting to minimize energy consumption or cost. For sprinting, the optimization would have attempted instead to maximize the useful expenditure of energy in order to reach top speed as quickly as possible so that the final time would be minimized.

Certain limitations affected our study. The model is a simple one with few degrees of freedom and as such it is not capable of reproducing features of sprinting associated with joints it does not have. It does not, for example, possess ankle or knee joints and the function of these joints is known to be critical to human sprint performance. In addition, the model was actuated by leg forces and hip torques rather than muscle forces. This choice of actuation prevented consideration of several factors known to affect performance, including muscle composition and architecture and neural function.

While the optimized sprint simulation represents a substantial reduction in time to run 20 m, we cannot know for certain that it represents a global optimum. We did perturb the optimal

solution by restarting the optimizer following addition of uniform random noise to the solution vector. This perturbation did not cause the solution to migrate to a lower objective function value. It is interesting to note that, while the contact times changed as the optimal solution was reached, the number of steps taken by the model in the optimized and *PD*-controlled initial guess simulation was nearly the same: 22 for the initial and 21 for the optimized simulations. It may be that the optimal control scheme could not find solutions that differed by much in terms of the number of steps taken.

Several design choices made during creation of the sprinting simulation require further explanation. One such choice was the selection of $x = 20$ m for the sprinting distance. This distance was selected because it allowed the model to reach a steady-state velocity, although 20 m is shorter than the 30 m to 40 m distance required by elite human sprinters (Mann, 2011) to accomplish the same task. Using $x = 20$ m rather than a greater distance also reduced the dimensionality of the problem and thus enhanced the numerical tractability. It was possible to create longer or shorter simulations using the same methods; a simulation with a final distance of $x = 15$ m was created for which an optimal solution was found in which the locomotion time was reduced from 5.43 s to 2.23 s and this simulation exhibited the same behaviors noted for the 20 m simulation, except for a shorter steady-state velocity phase. Another design choice was the inclusion of spring and damper elements along with active actuators in the model's legs. We chose to base our model on ones previously used to successfully simulate locomotion (e.g., Alexander, 1992; Abdallah et al., 2008; and Raibert, 1986). The spring and damping elements in our model's legs may have facilitated control by generating forces when active actuator bounds were exceeded, but it is also possible that spring/damper elements are not essential to simulating aperiodic sprinting if the actuator bounds were adjusted accordingly.

To investigate the effects of actuator bound selection, we made two additional simulations with the bounds on the controls increased and decreased by 10%. The time required to traverse the 20 m was reduced from 2.79 s to 2.65 s when the bounds were increased, and increased to 2.93 s when the bounds were made smaller. Aside from this small difference in final time, the human-like sprinting behaviors in these simulations were much the same as in the original simulation, although early simulations attempted with much tighter restrictions on the controls resulted in a non-alternating gait similar to skipping. There are actuator properties other than these bounds that we would expect to affect sprint performance, such as force-velocity properties and excitation-activation dynamics of muscles (e.g., van Soest et al., 2000; Rankin et al., 2008), yet were not represented in this model. We are currently at work adding such properties to a muscle-actuated model of sprinting.

Recent experimental studies suggest that there are differences in musculoskeletal architecture between trained sprinters and non-sprinters (Lee and Piazza, 2009; Kubo et al., 2011; and Baxter et al., 2012), and the methods employed in this study could be extended to study the relationship between muscle and joint structure and optimal performance. Such an extension of the model would require the addition of musculotendon actuators and the inclusion of additional of joints, such as the ankles. It is hoped that such an approach will enhance our understanding of the musculoskeletal characteristics that determine gait speed in pathological populations as well as in elite athletes. In addition, the results of this study could aid in the identification of essential elements of effective sprinting that could be helpful to the creation of controllers for sprinting robots.

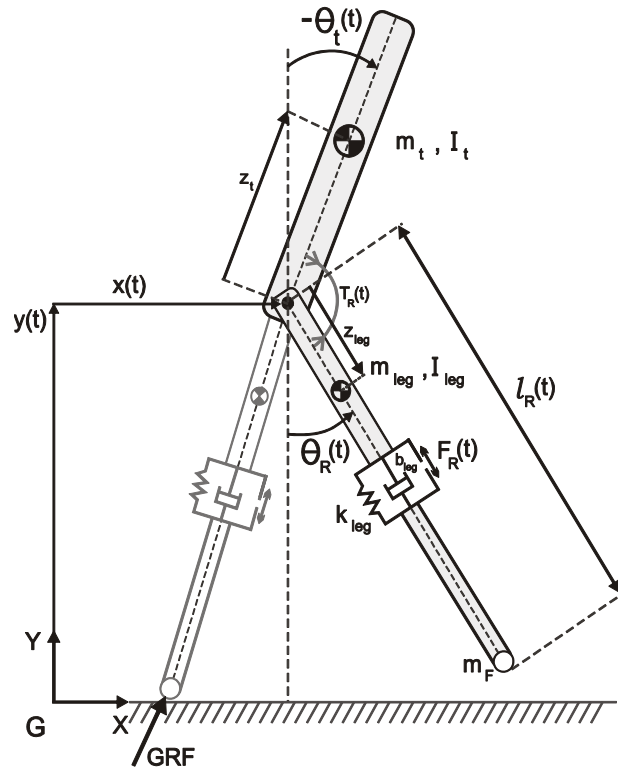


Figure 3-1 The simple biped model used to simulate sprinting. Body segment inertial properties shown in the figure are defined in the text, as are the generalized coordinates of the model, hip actuator torques, and leg actuator forces. The right and left legs of the model were identical; labeling of the left leg inertial properties, generalized coordinates, and actuator forces and torques are omitted here for purposes of clarity. The left hip flexion angle θ_L is positive when the hip is flexed.

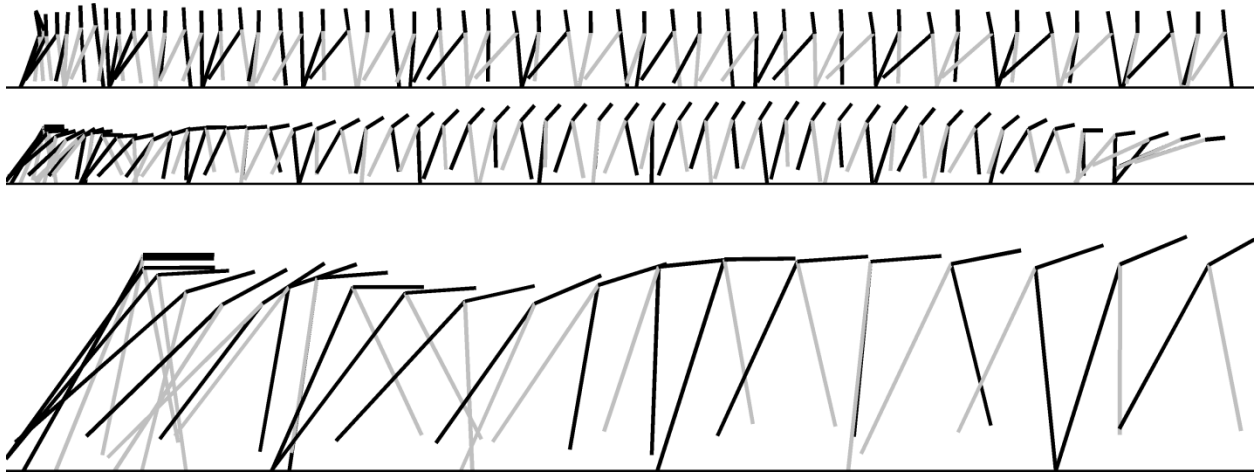


Figure 3-2 Stick-figure trajectories for the model (top) completing the 20 m course under PD control that produced a “jog” with duration of 6.64 s; and (middle) sprinting following optimization for which the course was covered in 2.79 s. The sprinting simulation begins with the trunk flexed forward, straightens as the race progresses, and dives forward at the finish. The first 5 meters of the sprinting simulation are also shown in detail (bottom). The time between frames represented in these illustrations are 125 ms (top) and 53 ms (middle and bottom).

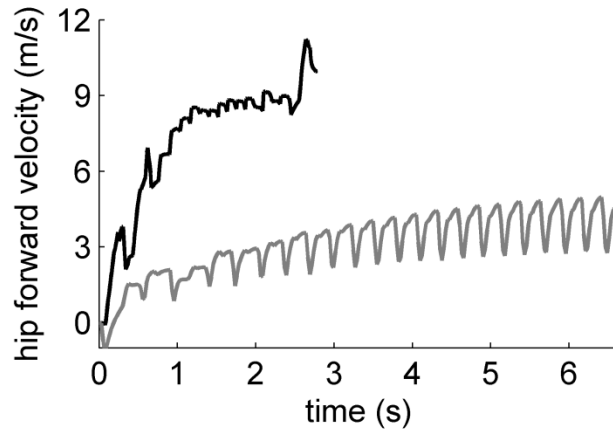


Figure 3-3 Forward velocity of the hip in for the initial guess “jog” (*gray*) and sprinting (*black*) simulations. Both simulations began from rest. The feedback-controlled “jog” slowly approached a steady forward velocity of approximately 4 m s^{-1} . The sprinting simulation gains speed quickly over the first few steps, then reaches a steady speed of about 8 m s^{-1} for much of the race, before diving forward at the end.

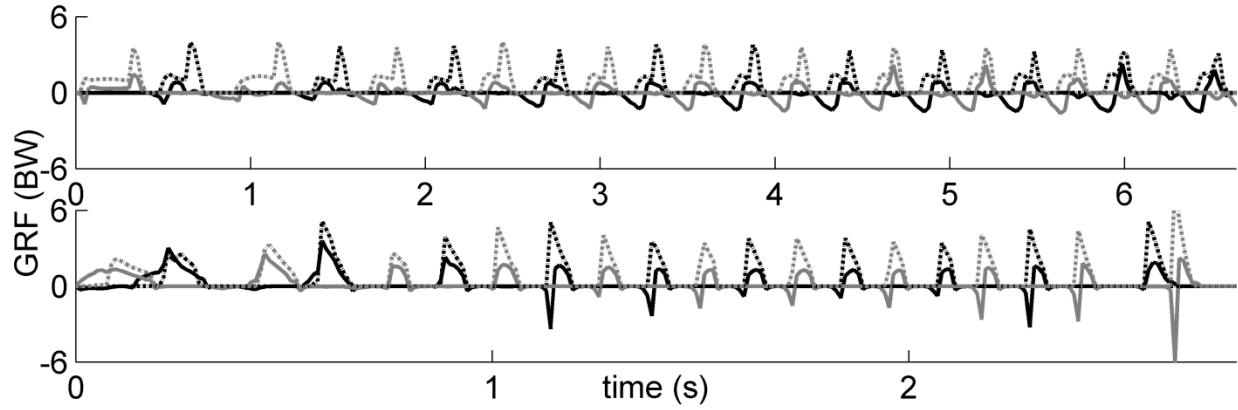


Figure 3-4 The horizontal (continuous lines) and vertical (broken lines) ground reaction forces of the initial guess “jog” simulation (top) and the sprinting simulation (bottom). Ground reaction forces for the left and right feet are shown in gray and black, respectively.

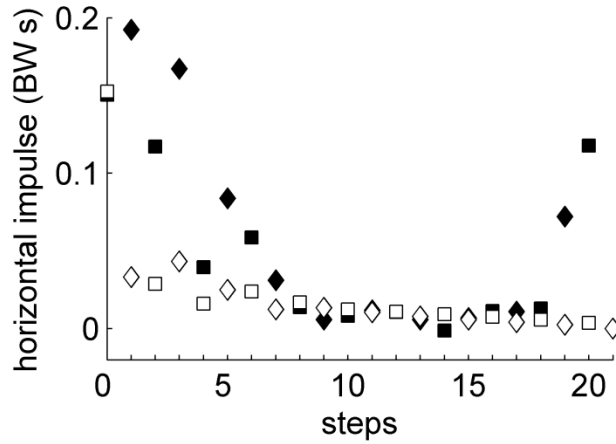


Figure 3-5 The net horizontal impulses of the ground reaction force (GRF) for each step during the initial guess “jog” simulation (unfilled markers) and the sprinting simulation (filled markers). Impulses for GRFs applied to both the right (diamonds) and left (squares) feet are shown. Large forward impulses were generated in the first few steps of the sprinting simulation and again in the last two steps to generate the terminal dive.

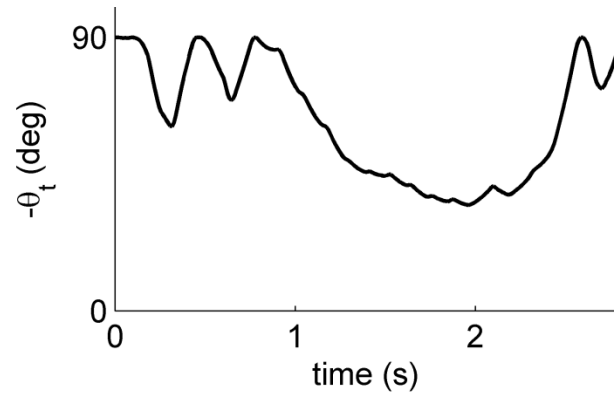


Figure 3-6 The angular position of the trunk in the sprinting simulation. The trunk angle was defined such that negative values of θ_t corresponded to forward flexion (Figure 3-1). The negation of that angle is plotted here, with 90° corresponding to the trunk parallel to the ground and 0° indicating an upright posture.

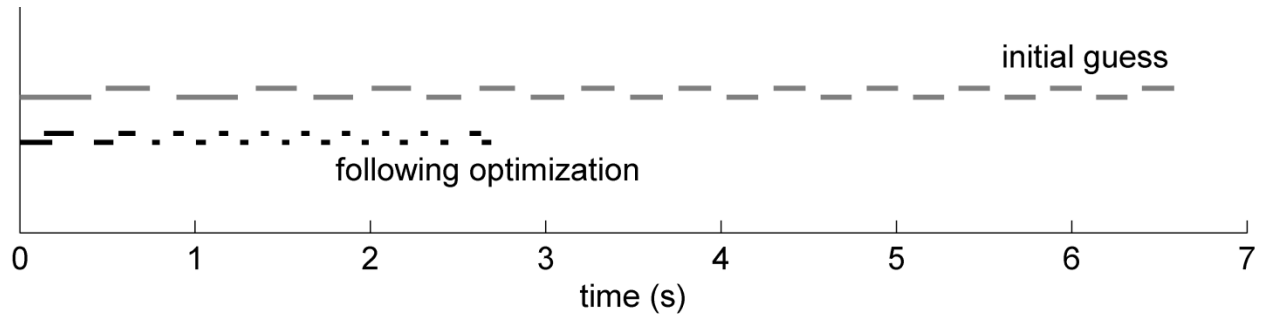


Figure 3-7 Temporal foot contact pattern for the initial guess “jog” simulation (gray) and the sprinting simulation (black). Both simulations resulted in alternating gaits. While the foot contacts in the initial guess simulation were fairly constant in duration, in the sprinting simulation contact times were larger at the start during the acceleration phase and became much shorter for the remainder of the simulation.

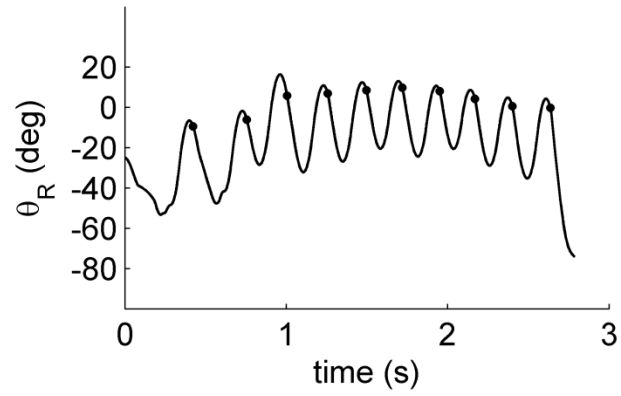


Figure 3-8 Flexion of the right hip plotted versus time for the sprinting simulation. Right foot contact (circles), consistently occurred as the hip was beginning to extend following maximum flexion. This “leg retraction” behavior was not present in the initial guess “jog” simulation, for which foot contact always coincided with maximum hip flexion.

Chapter 4

A hybrid dynamic walking simulation with evaluation of optimality criteria

4.1 Introduction

There are two main approaches used to create dynamic gait simulations. One commonly used approach is to track experimentally measured joint angles and ground reaction forces (GRFs) by minimizing the deviations from the experimental measurements in an optimization framework (Zajac et al., 2003). This approach produces a simulation that reproduces what happened in the motion capture experiment and permits estimation of variables that cannot be measured (or are not convenient to measure) in an *in vivo* experiment, such as muscle forces. The second approach is to generate predictive dynamic simulations that rely on some optimality criterion (or combination of criteria) in an optimization framework to *predict* joint angles, GRFs, muscle forces, and etc. This approach permits synthesis and analysis of gaits under altered conditions. While the predictive power of such simulations exceeds what is possible with a tracking simulation, creating predictive dynamic simulations can be quite challenging due to the highly nonlinear nature of the problem and the complex gait machinery. Another challenge in creating predictive simulations of locomotion using optimal controls is to identify optimality measures with the potential to predict important features of the specific gait under investigation.

Predictive simulations are generally created by transcribing the optimal control problem into a nonlinear programming (NLP) problem using one of the following three methods: (1) direct single shooting, (2) direct collocation, and (3) direct multiple shooting (Figure B-2 in Appendix B). While direct methods discretize the control problem and apply NLP procedures; indirect methods search a solution for the necessary conditions of optimality without discretization. Direct single shooting (e.g., Anderson and Pandy, 2001) is the most commonly

used method and searches for only muscle control histories that minimize an optimality measure while trying to satisfy periodicity constraints on initial and final states. Direct collocation (DC) is a method borrowed from physics-based computer graphics that has recently been employed to muscle-driven gait simulations (e.g., Ackermann and van den Bogert, 2010) in which muscle control along with state trajectories are searched to minimize an optimality measure subjected to algebraic constraints originated from the governing equations of the system, as well as any other constraints such as periodicity (Betts, 2010). Direct multiple shooting (e.g., Diehl et al., 2006) is another method in which the total time span of the simulation is divided into several short integration intervals, each of which has a set of initial states and controls. An optimality measure is minimized subjected to constraints requiring that the terminal values for the states at the end of each integration interval are equal to the initial values for the next interval along with any other constraints of the simulation. Each integration interval is independent from the other integration intervals and forward integration time spans are relatively shorter, thus possible integration errors are distributed through intervals, in other words, propagation of error from initial to final states are attenuated. Another advantage is that direct multiple shooting suits better to parallelization paradigm due to independency of integration intervals.

A good initial guess is required regardless of the choice of transcription method. A randomly chosen initial guess may be problematic since shooting methods require integration of state equations, and a random initial guess for initial states may lead integration errors, so the fail of the optimization process. Multiple shooting, however, has the potential to tolerate a poor initial guess, because that guess may be integrable in each of the shorter integration intervals. Multiple shooting still requires an initial guess for the states and controls that gives initial constraint violations small enough that a feasible solution is possible. One method for

determination of the initial guess is to collect experimental gait data and solve for states and controls using inverse dynamics and static optimization. Another method is to generate an approximation of the desired gait using forward dynamics and a feedback controller (Celik and Piazza, 2013). A third approach might make use of state-dependent muscle reflex loops to synthesize walking (Geyer and Herr, 2010); an approach that has been extended to walking and running at different velocities by incorporating estimation of control parameters and initial states while maximizing an optimality measure (Wang et al., 2012).

While there is no consensus on the best optimality measure for dynamic simulation of walking measures based on the following have been proposed: mechanical energy (e.g., Ren et al., 2007), metabolic energy (e.g., Anderson and Pandy, 2001), and muscle force (Pedotti et al., 1978), muscle activation (e.g., Ackermann and van den Bogert, 2010). Stability (e.g., Townsend and Seireg, 1972) and trunk attitude and altitude (Gubina et al., 1974) have been used with controllers that to synthesize bipedal locomotion. Selection of proper optimality criteria is critical to creating a predictive simulations, because simulation behavior at the level of muscle force may be sensitive to this choice even when the overall output motion is not (Ackermann and van den Bogert, 2010).

The purposes of this study were: (i) to create predictive dynamic simulation of a complete one full periodic walking cycle with direct multiple shooting method; and (ii) to evaluate a set of optimality measures derived from muscle activation, or mechanical energy expenditure, or metabolic energy expenditure to represent ‘effort’, as well as trunk angle and vertical GRF in order to reproduce salient features of human walking. Initial guesses for the optimizations were obtained using a simulation of bipedal walking that relied on muscle reflex loops (Geyer and Herr, 2010).

4.2 Methods

4.2.1 *The musculoskeletal biped model*

The musculoskeletal model (Figure B-1 in Appendix B) used in the simulations was planar and had seven body segments: a trunk and right and left thighs, shanks, and feet. The body segments were connected with revolute joints at ankle, knee, and hip and a planar joint connected the trunk to the ground. The model was driven by sixteen (eight on each leg) Hill-type musculotendon actuators representing eight muscles or muscle groups on each side of the body: soleus (SOL), tibialis anterior (TA), gastrocnemius (GAS), vasti (VAS), hamstrings (HAM), rectus femoris (RF), glutei (GLU), and hip flexors (HFL).

The model had nine kinematic degrees of freedom (dof), each of which was associated with two generalized states (position and velocity). Each musculotendon (MT) actuator also had two states, a muscle fiber length and a muscle activation. Each MT actuator had a muscle control variable, so the model had fifty states in all and sixteen muscle controls. The joint moments were sums of products of MT force and moment arm, and passive joint moments, which were included to model mechanical effects of other tissues than MT. Further details of the model can be found in the Appendix B.

4.2.2 *The foot-ground contact model*

The foot-ground interaction was modelled with a compliant contact model with nonlinear damping (Marhefka et al., 1999; van den Bogert et al., 2009). The model applies point forces in horizontal and vertical directions which depend on penetration and penetration velocity of the contact points with respect to the ground. To be able to eliminate discontinuity in the vertical contact forces, a relatively small linear force was applied to the contact points when the leg was

in the swing phase. The formula of the ground reaction force in vertical direction (GRF_y) is as follows:

$$GRF_y = \begin{cases} -k_1 y_{cp} (1 - b\dot{y}_{cp}) & \text{if } y_{cp} \geq 0 \\ (-k_1 y_{cp} - k_2 y_{cp}^3)(1 - b\dot{y}_{cp}) & \text{if } y_{cp} < 0 \end{cases} \quad (4.1)$$

A differentiable Coulomb friction model was used for the horizontal, i.e., friction forces with the aid of a tangent hyperbolic function. The formula of the friction force is as follows:

$$GRF_x = -\mu GRF_y \tanh(c\dot{x}_{cp}) \quad (4.2)$$

There were eleven equidistant contact points between the ball of the foot and the heel. The constants in Equations 4.1 and 4.2 and the coordinates of the contact points were given in the Appendix B.

4.2.3 Optimization framework

The direct multiple shooting method (Diehl et al., 2006; Betts, 2010) was used to formulate the optimization problem. Each continuous state trajectory was discretized at n -many discrete nodes, and constant muscle controls were used between those discrete nodes. Then, the system dynamics equations were integrated not in a single shot but in multiple shots, where each discrete state value at discretization node was used as an initial state in m -many integration intervals ($n = m - 1$). The continuity violations were modelled as nonlinear constraints which were the differences between the terminal values for the states at the end of each integration interval and the initial values for the next interval (Figure B-2 in Appendix B). Another nonlinear constraint was derived from the locomotion velocity of the bipedal model. Bilateral symmetry was imposed, so that only one step of walking was simulated, with the right-side terminal conditions constrained to match the left-side initial conditions and vice-versa. These periodicity constraints were implemented as linear equality constraints. In addition to the linear and nonlinear

constraints, simple bounds were set for every state and muscle control of the model. The bounds on generalized position states were based on natural joint limits of human ankle, knee, and hip joints as well as the geometry of the model. The bounds on generalized velocity and muscle fiber length states were arbitrary values, and never active in the solution. They were implemented solely to scale the optimization problem. The muscle activations and controls were bounded between 0.01 and 1. The optimization variables were discrete values of states at discretization nodes ($50 \cdot n$) and constant controls ($16 \cdot n$) between two subsequent discretization nodes, and the final or step time (t_f). Fifty discretization nodes ($n=50$) were used for each state variable and muscle control. A scalar objective function (see next sub-section) was minimized subject to those constraints and simple bounds. The above described NLP problem was solved with a SQP solver, specifically SNOPT (Gill et al., 2005). Initial guess of the NLP problem was generated by re-sampling state and control trajectories of a complete one full walking cycle which was obtained by using muscle reflex loops previously described by Geyer and Herr (2010) to control the model.

4.2.4 Objective functions and simulations

Three optimality measures representing effort were tried, including terms based on muscle activation (ε_1), mechanical energy expenditure (ε_2), or metabolic energy expenditure (ε_3). These effort terms were augmented with additional terms based on trunk angle and vertical GRF to stabilize the trunk and avoid GRF spikes resulting from foot slapping as

$$J = w_1 \varepsilon_{1|2|3} + w_2 \frac{1}{n} \sum_{i=1}^n \hat{\theta}_{t_i}^2 + w_3 \frac{1}{2n} \sum_{i=1}^n \hat{GRF}_{y_{rfi}}^4 \quad (4.3)$$

where $w_1, w_2,$ and w_3 are weighting factors (either zero or one); $\hat{\theta}_i$ is the trunk angle in degrees with respect to the vertical at the discrete nodes; $\hat{GRF}_{y_{if}}$ ground reaction force (in BW) in vertical direction for right and left foot at the discrete nodes.

When an objective function which only represents effort is used, the bipedal model might just try to traverse some distance with the prescribed average forward speed, that is, 1.306 m/s in all simulations (Kadaba et al., 1989); and would not “feel” an urge to keep the trunk upright. Normally, balancing the trunk segment in humans is a complex motor task with the involvement of multiple sensory receptors, reflex loops, and muscles. The trunk orientation in the sagittal plane fluctuates about ± 1 degrees over a stride, and with relatively small accelerations of head, human balance and postural system provides a stable base for visual and vestibular systems (Winter, 1995). Our model does not rely on information from such sources for control of its movements, as it utilizes optimal controls. Improved control of the trunk may enhance the ability of the simulation in terms of reproducing more realistic walking cycles, so a term derived from the trunk angle was incorporated into the optimality criteria, and its influence on the simulations was tested.

Although it is possible for the foot of the swing leg to slap the ground with minimal neuromuscular control (and minimal effort), in reality the body actively controls preparation for stance by activating hip and knee extensors, along with dorsiflexors. While slapping the foot on the ground would minimize activation and effort, the attendant repeated impulsive forces would be implicated in fatigue accumulation which may lead to tissue failure, thus mitigating such forces at heel strike is highly important to musculoskeletal tissue health (Collins et al., 1989; Whittle, 1999; Warner et al., 2013). An objective function composed of only an effort term may

thus be inadequate to promote such a control on stance preparation, and a term derived from vertical GRF was incorporated and its effect was tested in the simulations.

Almost all simulations of walking utilizing an optimization framework include an effort term as one of the optimality criteria (or the sole criterion). Such measures derived from muscle stress (e.g., Glitsch and Baumann, 1997) or muscle activations (e.g., Ackermann and van den Bogert, 2010) with various exponents and weighting factors were often implemented not only their ability to reproduce salient features of gait but also their convenience in application, since they are readily available variables in simulations, thus they do not require additional modeling effort. The first effort term we implemented in this study was

$$\varepsilon_1 = \frac{1}{h \sum V_{m_i}} \sum_{i=1}^{n_m} V_{m_i} \int_0^{t_f} a_i^2 dt \quad (4.4)$$

where V_m is muscle volume; n_m is number of muscles; a is muscle activation, and h is duration of integration in each multiple shooting interval. For torque driven simulations, a sensible choice is minimizing mechanical energy expenditure over a complete gait cycle (e.g., Ren et al., 2007). In this study we used a muscle actuated model and included an effort term based on mechanical energy expenditure on ankle, knee, and hip joints per unit distance traveled to make comparisons with other effort terms.

$$\varepsilon_2 = \frac{1}{m_{body} s_L} \sum_{i=1}^6 \int_0^{t_f} |\tau_{j_i} v_{j_i}| dt \quad (4.5)$$

where m_{body} is total body mass, s_L is walking step length, τ_j is joint moment, and v_j is joint angular velocity. Another effort term used in predictive dynamic simulations of walking is minimizing metabolic energy expenditure per unit distance traveled (e.g., Anderson and Pandy, 2001), as it has been shown with human experiments that people prefer to walk at speeds which would minimize cost of transportation (Ralston, 1976). The muscle energy expenditure rate (

\dot{E}_{muscle}) was presented sum of four terms, namely, activation heat rate (\dot{h}_A), the maintenance heat rate (\dot{h}_M), the shortening/lengthening heat rate (\dot{h}_{SL}), and the mechanical work rate of the contractile element (\dot{w}_{CE}) (Umberger et al., 2003 and Umberger, 2010 for the detailed description of the model)

$$\dot{E}_{muscle} = \dot{h}_A + \dot{h}_M + \dot{h}_{SL} + \dot{w}_{CE} \quad (4.6)$$

The last effort term used in the simulations was

$$\varepsilon_3 = \frac{1}{m_{body} S_L} \left(m_{nonmuscle} \int_0^{t_f} \dot{E}_{nonmuscle} dt + \sum_{i=1}^{n_m} m_{muscle_i} \int_0^{t_f} \dot{E}_{muscle_i} dt \right) \quad (4.7)$$

where $m_{nonmuscle}$ is mass of tissue in the body other than muscle; $\dot{E}_{nonmuscle}$ is the rate metabolic energy expenditure of nonmuscle tissue (was set to 1.2 W/kg, which is the normal energy rate for standing (Umberger et al., 2003; Waters et al., 1999)); m_{muscle} is the muscle mass of each muscle modelled in the study. The integrals in Equation 4.5 and 4.7 were estimated with numerical integration, but the integral in Equation 4.4 was calculated analytically as the explicit form of it was available and integrable. Four simulations were created for each effort term by setting such weighting factors as $(w_1, w_2, w_3) = (1, 0, 0)$, $(w_1, w_2, w_3) = (1, 0, 1)$, $(w_1, w_2, w_3) = (1, 1, 0)$, and $(w_1, w_2, w_3) = (1, 1, 1)$ in Equation 4.3. Hereafter, independent of weighting factors combination, the simulations used effort term ε_1 , ε_2 , and ε_3 were named as muscle activation effort term, mechanical energy expenditure effort term, and metabolic energy expenditure effort term simulations.

4.3 Results

The initial guess for each optimization was a walking cycle; following optimization, the simulations always converged to different walking cycles with substantially lower effort. For

instance, the effort objective was decreased 65.7% for the muscle activation effort term simulation with only effort term (i.e., $(w_1, w_2, w_3) = (1, 0, 0)$). The optimization located feasible and optimal periodic walking simulations for muscle activation effort term and metabolic energy expenditure effort term simulations. The optimality tolerance for the mechanical energy expenditure effort term simulations, however, were never satisfied even the solutions were feasible. The wall-clock times to create simulations showed variation among effort terms. For example, the solutions were obtained approximately in an hour for muscle activation effort term simulations while the other simulations took between 1.5 and 26 hours.

The model's SL and SF were very close to the experimental values as 1.35 m at 0.97 Hz when mechanical energy expenditure based objective functions with such weighting factors as $(w_1, w_2, w_3) = (1, 1, 0)$ and $(w_1, w_2, w_3) = (1, 1, 1)$ were used. The model took relatively smaller steps (1.15 - 1.26 m) with higher cycling frequencies (1.04 - 1.14 Hz) in muscle activation effort term simulations (Figure 4-1). The locomotion velocity was fixed as 1.306 m/s in all simulations, but the stride length (SL) and stride frequency (SF) were free to vary. SL and SF values of the simulations were compared with the average experimental values derived from Kadaba et al., 1989 (SL: 1.361 m, SF: 0.9596 Hz) in Figure 4-1.

When compared to the experimental data, the joints generally followed similar extension/flexion patterns (Figure 4-2, 4-4, and 4-6). Peak values for joint angles, however, did show some discrepancies. For example, only the simulation with the mechanical energy effort criterion (Figure 4-4) was able to produce knee flexion during stance phase that was similar to that observed during normal human walking. In terms of joint moments, the simulations did not perform well to reproduce human-like trajectories (Figure 4-2, 4-4, and 4-6). The model's joint moments did not exhibit smooth trajectories especially for hip moment in metabolic energy

expenditure effort term simulations, and for knee and hip moments in mechanical energy expenditure effort term simulations.

When an effort term was used as the only optimality criterion, the peak vertical GRFs were larger than 4 BW (Figure 4-2, 4-4, and 4-6). When a vertical GRF term was added to the objective function, the peak vertical contact forces at the heelstrike were reduced to 1.22 BW (muscle activation effort term), 1.34 BW (mechanical energy expenditure effort term), and 1.13 BW (metabolic energy expenditure effort term); when vertical GRF and trunk angle terms were included simultaneously, the peak vertical contact forces at heelstrike were further reduced or stayed the same: 1.17, 1.19, and 1.13 BW (Figure 4-2, 4-4, and 4-6). For normal human walking, the average experimental values have been measured to be 1.10 ± 0.08 BW (Chao et al., 1983). The model exhibited relatively larger trunk angles (up to minus 7.8 degrees) without the trunk angle term included as an additional optimality criteria, but with the inclusion of the trunk angle term, the trunk excursion was confined to ± 1 degree band (Figure 4-2, 4-4, and 4-6).

Average muscle utilization over a stride increased by including the trunk angle and vertical GRF terms. For example, average muscle utilization over a stride increased from 6.3% to 7.9%, 15.0% to 18.2%, and 5.2% to 8.4% for simulations created using muscle activation, metabolic energy expenditure, and mechanical energy expenditure effort terms, respectively. For muscle activation effort term simulations, GAS action was late when compared to the experimental data. Also, VAS, RF, and HFL muscles were not activated at the initial contact. On the other hand, with the inclusion of the vertical GRF term, TA activation was increased at the heelstrike up to similar amplitudes measured in human experiments (Figure 4-3, 4-5, and 4-7). For the metabolic energy expenditure effort term simulations, knee muscles HAM, VAS, RF were not activated throughout the stride (Figure 4-7). Additionally, similar to the muscle

activation effort term simulations, TA activation at the heelstrike was increased in metabolic energy expenditure effort term simulations with the inclusion of the vertical GRF term.

The model underestimated metabolic energy expenditure in metabolic energy expenditure simulations (Figure 4-8). The model consumed metabolic energy at a rate of 4.46-4.83, 3.37-3.83, and 7.82-8.63 W/kg for simulations created using muscle activation, metabolic energy expenditure, and mechanical energy expenditure effort terms, respectively. (Figure 4-8); while oxygen consumption experiments indicated that humans' energy consumption rate for level walking at 1.306 m/s was 4.7 W/kg (Burdett et al., 1983).

4.4 Discussion

The hybrid approach was successful in terms of creating predictive dynamic simulations of periodic full normal walking cycles with various optimality criteria. The simulations did not track experimentally obtained gait data, but rather predicted joint angles, joint velocities, muscle activations, muscle fiber lengths, muscle controls, and stride time in an optimal control framework. Furthermore, the simulations did not have any explicit dependency on human experimental data for the estimation of initial states or the initial guess for the muscle control histories. The muscle activation effort term simulations converged to feasible and optimal solutions in approximately one hour, but the other simulations used more computation time. Different optimality criteria produced distinct gait cycles in terms of muscle utilization, peak vertical ground reaction forces, stride length and frequency, and average metabolic energy expenditure rate. The additional optimality criteria based on trunk angle and vertical GRF yielded simulations with less trunk excursion over a stride and peak vertical contact forces at the heelstrike.

The novelty of this simulation study was two-fold. First, to our knowledge, the present study is the first hybrid approach in terms of implementing a feedforward control with reflexes to obtain initial guess data and test abilities of the mathematical model along with an optimal control with direct multiple shooting to synthesize human walking without using any experimental human gait data explicitly. In previous predictive simulations, experimental gait data was used to specify initial states (e.g., Anderson and Pandy, 2001), and to estimate initial guess for states and controls (e.g., Ackermann and van den Bogert, 2010). Second, we introduced new terms as optimality measures, namely, trunk angle and vertical GRF to improve model's ability in terms of reproducing salient features of normal human walking. Previous authors have typically used efforts terms alone, such as cost of transport (Anderson and Pandy, 2001), metabolic energy expenditures (Ren et al., 2007), and muscle activation integrals (Ackermann and van den Bogert, 2010).

Inclusion of a GRF term in the objective function in the present work reduced the spikes in GRF that have been reported for previous predictive simulations. In general, predictive simulations of walking produce spikes in the ground reaction forces. As evident from the current study and previous studies (Anderson and Pandy, 2001; Ren et al. 2007; and Ackermann and van den Bogert, 2010), optimal control approach in predictive simulations did not yield smooth GRF trajectories with an objective function consisting of only effort terms. Ren et al., 2007 suggested that lack of smooth GRF trajectories probably arose from model simplifications such as lack of a pelvis segment. However, even when the pelvis segment was modeled by Anderson and Pandy (2001), similar spikes were present. The results of the present study suggest that this condition does not arise from a lack of model complexity, but rather from poor muscle control as weight is accepted at the beginning of stance phase. The relatively simple bipedal model used in this study

equipped with reflex loops was able to produce GRF trajectories that closely resembled experimental GRF traces. In optimal control simulations, the foot contacted with the ground with larger horizontal velocities, yet reached zero velocity quicker when compared with the values from human experiments (Winter, 1992). As also mentioned above, there was lack of adequate and timely activation of muscle groups. For instance, in the HAM muscle, which could control contact velocity prior heel contact (Winter, 1992), activity was relatively late and small in the predictive simulations of walking (also in Anderson and Pandy, 2001; Ackermann and van den Bogert, 2010). Furthermore, while average toe clearance was 1.29 cm in human subjects (Winter, 1992), the model 'brushed' the ground in the simulations (also in Anderson and Pandy, 2001). These imply that optimal controller does not aim to produce a safe trajectory of the foot (Winter, 1992), but rather favor a trajectory that would minimize effort. In summation, our results showed that GRF terms helped to prevent unrealistically high GRFs and to alleviate spikes by using such strategies as a more active stance preparation by increasing TA activation before and after contact with the ground.

Metabolic energy expenditure effort term simulations did not produce the most realistic gait in terms of metabolic energy expenditure. Specifically, metabolic energy expenditure simulations underestimated the average metabolic energy expenditure rate (simulation values, 3.37-3.83 W/kg vs. experimental value, 4.7 W/kg (Burdett et al., 1983)), but the values for the muscle activation simulations were closer to the experimental value (4.46-4.83 W/kg). Similarly, mechanical energy expenditure simulations underestimated average metabolic energy expenditure rate (simulation values, 0.57-0.93 W/kg vs. experimental value, 1.09 W/kg (Umberger and Martin, 2007)), whereas muscle activation (1.59-2.62 W/kg) and metabolic energy expenditure simulations (1.32-1.90 W/kg) overestimated the metabolic energy

expenditure rate. While our simulations underestimated the optimality measure it minimized, some other predictive simulations made overestimations; for instance, Anderson and Pandy (2001) and Ren et al. (2007) estimated average metabolic and mechanical energy expenditure as 6.6 W/kg and 2.80 W/kg respectively. These results indicated that minimizing an optimality measure does not necessarily lead to realistic gaits for that particular measure, and that some other measures may perform better. The possible explanations for those observed underestimations were that the model did not use larger muscles such as VAS and HAM at all in the metabolic energy expenditure simulations, because their usage would be costly in the objective function, and cocontraction of agonist and antagonist muscles would be inefficient in terms of producing joint motion yet would have stabilizing effect on joints.

In the present study, direct multiple shooting produced predictive walking simulations efficiently. Anderson and Pandy (2001) implemented direct single shooting, and solution of their optimization required 10,000 hours yet was never able to satisfy the periodicity constraints. It should be noted, however, that the authors used a 3D model with 54 muscles and their optimization problem was solved using processors available in 2001. The simulation times for Ackermann and van den Bogert (2010) and Ren et al. (2007) were comparable to ours, but they used approaches that do not require integration of state equations. In those integration-free approaches, the error between discretization nodes should be estimated by re-solving the optimization problem with a finer mesh which may increase the computation time dramatically; otherwise, the influence of discretization error of the state trajectories on the objective function value will be unclear. In our simulations, with the parallelization of the independent integration intervals, the overall execution time for forward integration was decreased by nearly four-fold with a four-core processor. The trend of increasing the number of independent central processing

units (cores) in a single computing component (die or chip) is expected to continue in the coming years (Sutter, 2005). Thus it would be possible to create more complex models and still solve similar problems in an acceptable time period. Unlike muscle activation effort term simulations, the mechanical and metabolic energy effort term simulations took longer to converge. The reason was probably that the gradient of the objective function suffered from the errors in numerical integration process of the objective functions described in Equation 4.5 and 4.7. That indicates computational times depend on the behavior of the optimality criteria to some extent.

There were several limitations of the study to consider. We cannot know that a global optimum was found but the objective function values of the effort terms following convergence were comparable to or even lower than the experimentally measured effort in humans. Also, the model included not all but major lower extremity muscles. The choice of which muscles were included depended on previous successful modeling studies of human locomotion (e.g., Geyer and Herr, 2010; Wang et al., 2012; Ackermann and van den Bogert, 2010). The excluded muscles were not prime movers, but might have had secondary effects. In the muscle activation simulations, we used sum of the squared muscle activation integrals scaled with muscle volumes, yet there were other studies implemented unitary weights and various exponents (e.g., Ackermann and van den Bogert, 2010). We chose such exponent and weight combinations to emulate ‘effort’, since higher exponents with unitary weights were considered as ‘fatigue’ cost functions (Ackermann and van den Bogert, 2010). The selection of the exponent for the vertical GRF term was also an open question; therefore, we tried powers of two, four, six, eight, and ten. We selected the power of four because this choice resulted in better agreement with the experimental data (Chao et al., 1983) in terms of similarity of peak values.

In conclusion, the computer model and simulation framework used in this study enabled efficient synthesis of normal biped walking; however, using only effort terms such as metabolic and mechanical energy expenditure did not reproduce several important features of human walking. Our findings indicated that criteria other than effort need to be included if a truly realistic predictive simulation is the goal. We proposed two new terms for the objective function, minimizing trunk excursion and vertical GRF over a stride cycle. Including these terms helped to alleviate some undesired behaviors, but those terms were generally considered as the outputs of the motor behavior. Thus, future research might focus getting better results in predictive simulations by incorporating additional terms such as comfort, safety, and disturbance rejection that have the potential to reproduce desired behavior without explicitly incorporating output variables. Predictive simulations have great potential to be used in addressing theoretical questions about gait, as well as for use in clinical applications. Producing faster simulations with better realism would increase the value and applicability of predictive simulation approach.

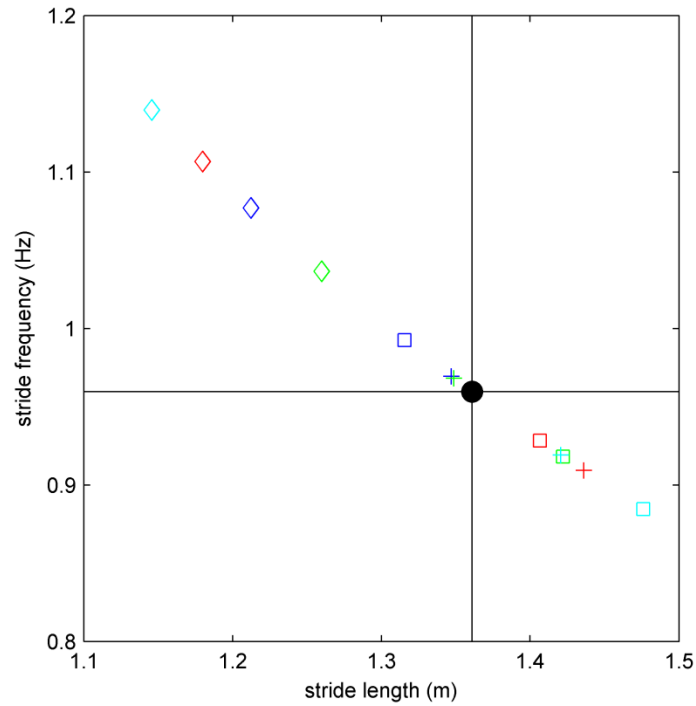


Figure 4-1 The stride length (SL) and stride frequency (SF) values observed in the walking simulations. The diamond, plus sign, and square markers indicated muscle activation, mechanical energy expenditure, and metabolic energy expenditure simulations respectively. Cyan, red, blue, and green colors were used for weighting factors (1,0,0), (1,0,1), (1,1,0), and (1,1,1) respectively. The black lines with the filled circular marker showed average experimental values for SL and SF derived from Chao et al., 1983.

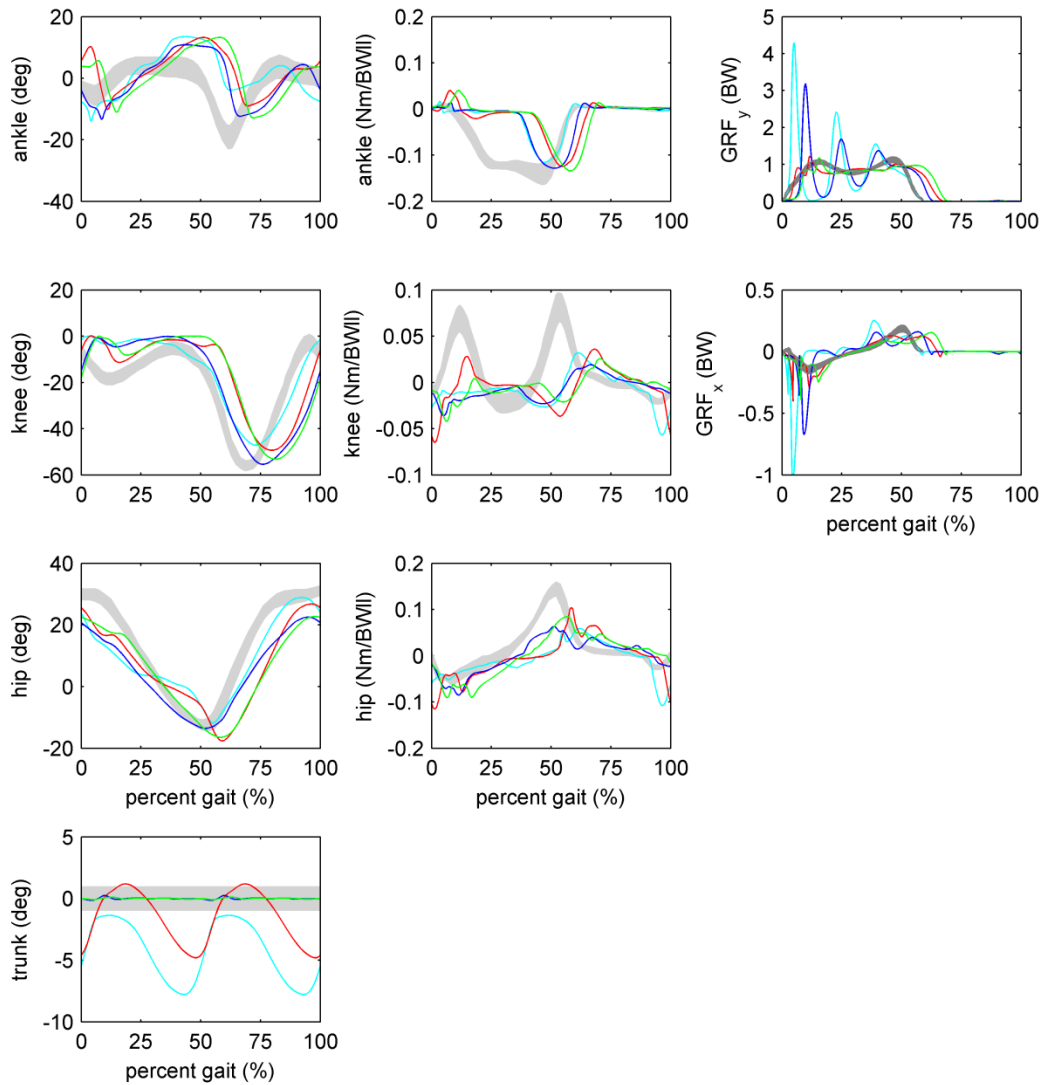


Figure 4-2 The joint angles, joint moments, and GRFs of the muscle activation simulations for one full walking cycle from left foot heel strike to left foot heel strike. Cyan, red, blue, and green colors were used for weighting factors (1,0,0), (1,0,1), (1,1,0), and (1,1,1) respectively. The shaded gray areas in the ankle, knee, and hip angles and moments were reproduced from Kadaba et al., 1989; which are enclosed by one plus and minus standard deviations' of a representative subjects' nine trials (three cycles x three days). According to the sign convention, plantarflexion, knee flexion, and hip extension were negative. The shaded gray area in the trunk angle enclosed by ± 1 degree (Winter, 1995). The shaded gray areas in GRFs were reproduced from Chao et al., 1983; which are enclosed by one plus and minus standard deviations' of the general pattern of 26 normal subjects.

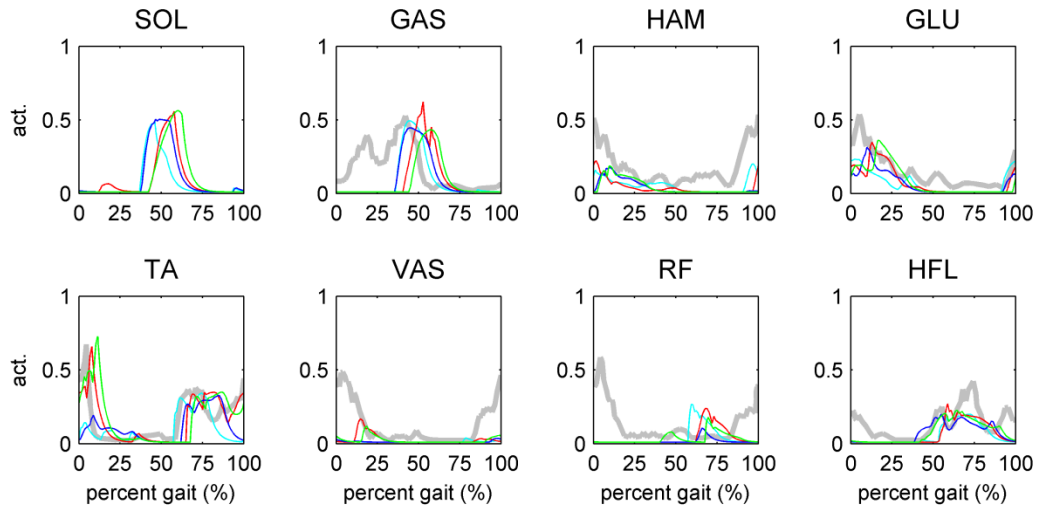


Figure 4-3 The muscle activations for one full walking cycle from left foot heel strike to left foot heel strike for the muscle activation simulations. Cyan, red, blue, and green colors were used for weighting factors (1,0,0), (1,0,1), (1,1,0), and (1,1,1) respectively. The gray lines were reproduced from Kadaba et al., 1989; and represent the mean value of EMG envelopes of a representative subjects' nine trials (three cycles x three days).

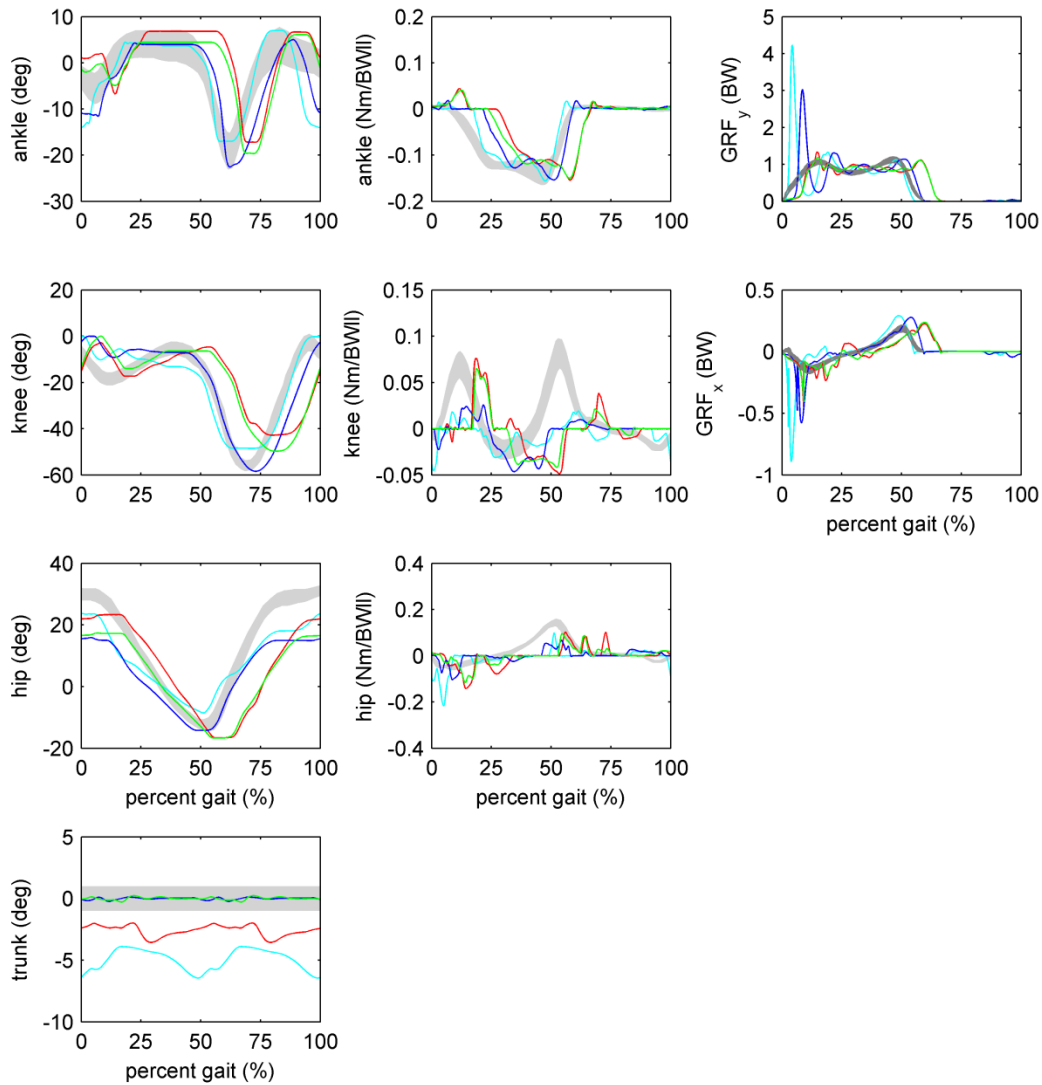


Figure 4-4 The joint angles, joint moments, and GRFs of the mechanical energy expenditure simulations for one full walking cycle from left foot heel strike to left foot heel strike. Cyan, red, blue, and green colors were used for weighting factors (1,0,0), (1,0,1), (1,1,0), and (1,1,1) respectively. The shaded gray areas in the ankle, knee, and hip angles and moments were reproduced from Kadaba et al., 1989; which are enclosed by one plus and minus standard deviations' of a representative subjects' nine trials (three cycles x three days). According to the sign convention, plantarflexion, knee flexion, and hip extension were negative. The shaded gray area in the trunk angle enclosed by ± 1 degree (Winter, 1995). The shaded gray areas in GRFs were reproduced from Chao et al., 1983; which are enclosed by one plus and minus standard deviations' of the general pattern of 26 normal subjects.

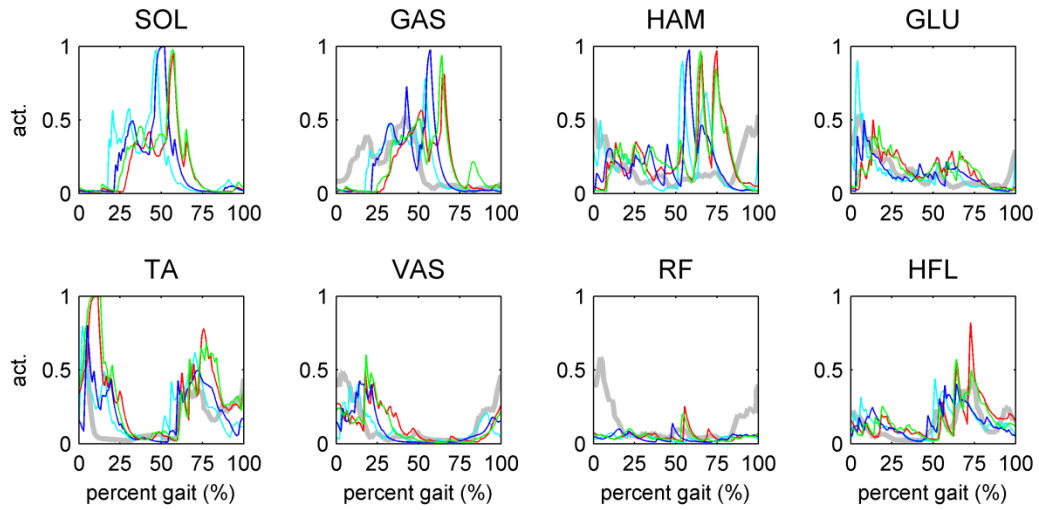


Figure 4-5 The muscle activations for one full walking cycle from left foot heel strike to left foot heel strike for the mechanical energy expenditure simulations. Cyan, red, blue, and green colors were used for weighting factors (1,0,0), (1,0,1), (1,1,0), and (1,1,1) respectively. The gray lines were reproduced from Kadaba et al., 1989; and represent the mean value of EMG envelopes of a representative subjects' nine trials (three cycles x three days).

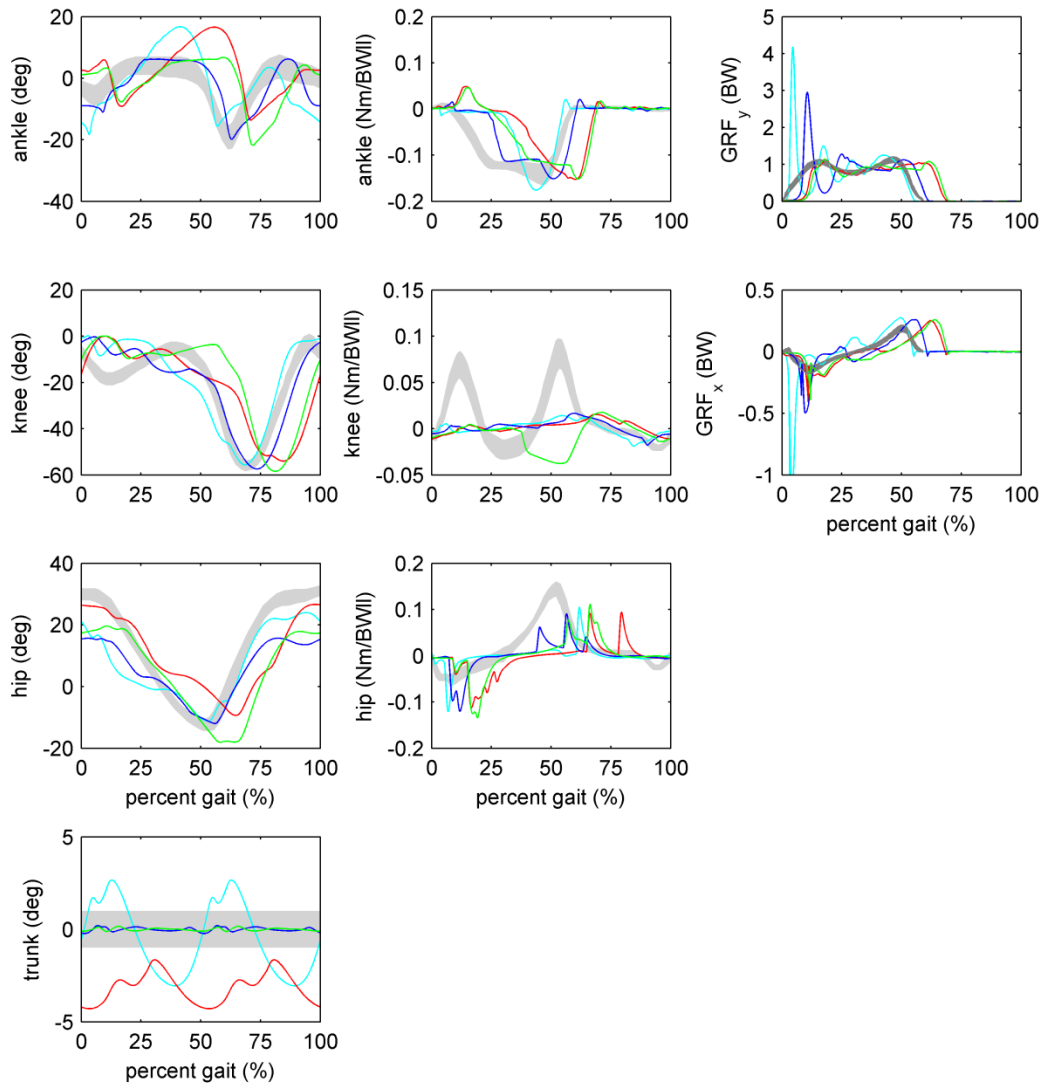


Figure 4-6 The joint angles, joint moments, and GRFs of the metabolic energy expenditure simulations for one full walking cycle from left foot heel strike to left foot heel strike. Cyan, red, blue, and green colors were used for weighting factors (1,0,0), (1,0,1), (1,1,0), and (1,1,1) respectively. The shaded gray areas in the ankle, knee, and hip angles and moments were reproduced from Kadaba et al., 1989; which are enclosed by one plus and minus standard deviations' of a representative subjects' nine trials (three cycles x three days). According to the sign convention, plantarflexion, knee flexion, and hip extension were negative. The shaded gray area in the trunk angle enclosed by ± 1 degree (Winter, 1995). The shaded gray areas in GRFs were reproduced from Chao et al., 1983; which are enclosed by one plus and minus standard deviations' of the general pattern of 26 normal subjects.

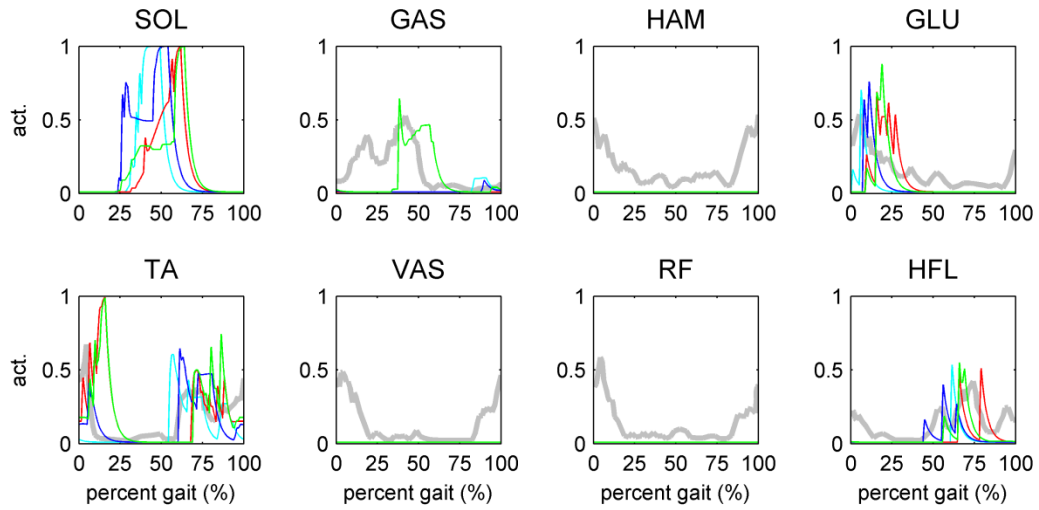


Figure 4-7 The muscle activations for one full walking cycle from left foot heel strike to left foot heel strike for the metabolic energy expenditure simulations. Cyan, red, blue, and green colors were used for weighting factors (1,0,0), (1,0,1), (1,1,0), and (1,1,1) respectively. The gray lines were reproduced from Kadaba et al., 1989; and represent the mean value of EMG envelopes of a representative subjects' nine trials (three cycles x three days).

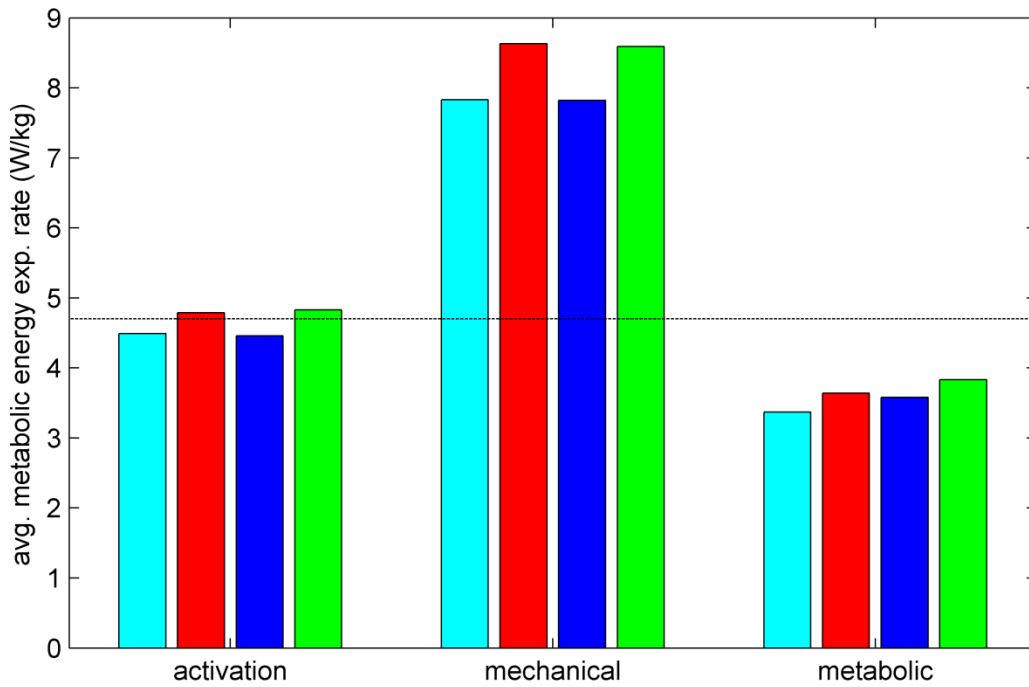


Figure 4-8 Average metabolic energy expenditure rate for muscle activation, mechanical energy expenditure, and metabolic energy expenditure simulations. Cyan, red, blue, and green colors were used for weighting factors (1,0,0), (1,0,1), (1,1,0), and (1,1,1) respectively. The black horizontal dashed line indicated the experimental value, 4.7 W/kg (Burdett et al., 1983)

Chapter 5

Sensitivity of maximum simulated sprinting speed to plantarflexor muscle parameters

5.1 Introduction

Dynamic simulations of human movement may be used to predict changes in performance due to perturbations when the motion simulated is predicted through minimization of optimality criteria subject to constraints. In contrast, simulations that reproduce experimentally measured motions and forces lack this capability (Pandy, 2001), although they do have the capability to describe musculoskeletal function. The latter “tracking” approach cannot be used to predict how changes in musculoskeletal architecture affect task performance because the performance of the task does not change. The effects of altered musculoskeletal architecture are of interest because musculoskeletal structure determines locomotor performance to a great extent. In particular, there is increasing evidence that musculoskeletal architecture affects sprinting ability in complex ways (e.g., Mero et al., 1981; Abe et al., 2000; Lee and Piazza 2009).

Predictive dynamic simulations of locomotion have been used to test ‘what if’ hypotheses related to locomotion, estimate novel gaits, and study the sensitivity of performance to variation in musculoskeletal parameters. For example, using a maximum height vertical jump simulation, van Soest et al. (1993) predicted that converting gastrocnemius into a mono-articular muscle would decrease jumping performance. Sellers and Manning (2007) estimated maximum running speeds of dinosaurs, and their sensitivity analysis demonstrated that increasing mass and maximum contraction velocity of muscles would increase top speed. Recently, Miller et al. (2012a) studied the sensitivity of maximum sprinting speed to parameters describing the muscle

force–velocity property and found that maximum shortening velocity was the parameter with the most influence on maximum speed.

There are other predictive dynamic simulation studies of sprinting in the literature. Lee and Piazza (2009) simulated push-off phase of sprinting with a simple linked segment model driven by plantarflexor and toe flexor muscles, and found that the model generated greater forward impulse with longer toe and shorter plantarflexor moment arm. Schultz and Mombaur (2010) simulated running at an average speed of 10 m/s, the approximate maximum speed of elite sprinters, with a torque-driven three-dimensional model to investigate the internal forces and joint moments required for such a motion. Baxter et al. (2012) developed a simple foot model to simulate toe pushing with maximal plantarflexor muscle effort and investigate the effect of forefoot to rearfoot ratio (i.e., gear ratio) on force and work output, and demonstrated that larger gear ratios generated higher contact force and plantarflexor work. In a recent study, Celik and Piazza (2013) simulated a 20 m sprint race from rest with a modified spring-loaded inverted pendulum biped model with torque and force actuators on the hips and telescoping legs. Although the model was very simple, it exhibited a number of features characteristic of human sprinters, such as forward trunk lean at the start, straightening of the trunk during acceleration, and a dive at the finish.

There is plenty of evidence that musculoskeletal structure of plantarflexor muscles of sprinters differs from non-sprinters, but the specific influence of these differences on sprinting ability is not always clear. Mero et al. (1981) showed that running velocity is correlated positively and significantly with the percentage of fast twitch fibers, stride rate, speed strength, and maximal isometric force. In a histochemical study (Costill et al., 1976), sprinters had the highest fast to slow twitch fiber ratio among various track athletes including distance runners and

long-high jumpers, and also untrained adults. Owing to the force-velocity property of muscle fibers, a muscle with higher fast to slow twitch fiber ratio would produce more force for a given shortening velocity (e.g., Miller et al., 2012a). The data obtained through ultrasound imaging showed that sprinters have stiffer Achilles' tendons than distance runners and adults not active in sports (Arampatzis et al., 2007). A stiffer Achilles' tendons would tolerate higher mechanical loading on the stance phase of sprinting where plantarflexors reaches peak muscle forces. In addition to having stiffer tendons and higher proportion of fast twitch muscle fibers, sprinters have also longer plantarflexor fascicle lengths than non-sprinters (e.g., Lee and Piazza 2009, Abe et al., 2000 and 2001). Longer plantarflexor muscle fascicles might also be expected to enhance force generation in the stance phase of sprinting due to the force-length property of muscle fibers, because longer fibers would operate in more favorable ranges(i.e., nearer to isometric) on the force-length curve. By using ultrasound and MRI, it has been revealed that sprinters have shorter Achilles tendon moment arms (Lee and Piazza 2009; Baxter et al., 2012). The effect of this property is rather complex, since shorter moment arms would attenuate joint moment generation around ankle due by reducing mechanical advantage, but the lost leverage might be compensated for by enhanced force generation. Such compensation has been hypothesized to occur because plantarflexor muscles with a shorter moment arm would shorten less and slower for a given joint rotation, and thus generate more force than in case of a longer moment arm (e.g., Nagano and Komura, 2003). In another ultrasound imaging study, sprinters have been found to have thicker plantarflexor muscles than controls which would enable the sprinters to reach higher peak forces when they exert maximum effort during competition (Kubo et al., 2011). The authors also discovered a positive association between thickness of medial side of knee extensors and sprinting performance. Kumagai et al. (2000) also investigated the

relationship between performance and structure and showed that fascicle length correlated with sprinting performance. Karamanidis et al. (2011), however, did not find correlations between musculoskeletal architecture parameters and the performance of elite sprinters.

The purposes of this study were: (i) to create predictive dynamic simulations of maximum speed bipedal sprinting with a muscle-driven planar model; and (ii) to examine the sensitivity of maximum sprinting speed to the following plantarflexor muscle parameters: maximum isometric force, optimal fiber length, tendon stiffness, and moment arm. The effects of perturbations to musculoskeletal structure of the foot and ankle on sprinting performance were investigated by applying isolated changes to structural parameters in the computer model. The results of the nominal sprint simulation were compared to the experimental data to evaluate the realism of the simulation. We hypothesized that increasing maximum isometric force, increasing optimal fiber length, increasing tendon stiffness; or decreasing moment arm of plantarflexor muscles would enhance maximum sprinting speed.

5.2 Methods

5.2.1 Musculoskeletal biped model

The musculoskeletal biped model (Figure B-1 in Appendix B) was a 9-degree-of-freedom planar linkage composed of seven body segments (trunk, thighs, shanks, and feet) with revolute joints at the ankle, knee, and hip and a planar joint between the trunk and the ground. The motions of the model were driven by sixteen Hill-type musculotendon (MT) actuators (eight for each leg): soleus (SOL), tibialis anterior (TA), gastrocnemius (GAS), vasti (VAS), hamstrings (HAM), rectus femoris (RF), glutei (GLU), and hip flexors (HFL). The biped model and its parameters were based on models previously used in successful simulations of locomotion, specifically those described by Ackermann and van den Bogert (2010) and Geyer and Herr (2010).

Each MT actuator model had two states (fiber length and activation), and consisted of an active contractile element (CE) and a series elastic element (SEE) with a parallel elastic element (HPE) that engages when muscle fiber length exceeds its optimal fiber length, and a parallel buffer elastic element (LPE) engages to prevent shrinkage of the active contractile element when tendon is completely slack (HPE and LPE abbreviations were originated from Geyer and Herr, 2010).

$$F_{mt} = F_{see} = F_{ce} + F_{hpe} - F_{lpe} \quad (5.1)$$

The CE actively generated force depending on muscle activation (a), muscle fiber length (l_m), muscle contraction velocity (v_m), and maximum isometric force (F_{max})

$$F_{ce} = aF_{max}f_l(\bar{l}_m)f_v(\bar{v}_m) \quad (5.2)$$

where functions f_l and f_v encode muscle force-length and muscle force-contraction velocity properties respectively, \bar{l}_m was the muscle fiber length scaled by optimal fiber length (l_{opt}), and \bar{v}_m was the muscle contraction velocity scaled by maximum contraction velocity.

Each MT actuator force output was multiplied by its corresponding moment arm around the joint(s) it spans to calculate its contribution to active joint moments. Passive joint moments, which represent the mechanical effects of other tissues than muscles, were then added to obtain total joint torques. The equations defining passive joint moments and their parameters are provided in the Appendix B.

The MT actuator models were adapted from those described by Geyer and Herr (2010). RF actuators were added (Wang et al., 2012) to account for the role of this muscle in regulating knee flexion (Piazza and Delp, 1996). The equation governing muscle activation and deactivation dynamics were changed with another model (He et al., 1991), since Geyer and Herr

(2010) used a model with only one time constant, yet generally models with two different time constants for muscle activation and deactivation have been used in dynamic simulation.

The state variables for the model were as follows: nine generalized position variables (\mathbf{p}) including ankle, knee, and hip angles for the right and left leg, the horizontal (x_h), vertical (y_h) positions of the hip, and the angular position of the trunk (θ_t); nine generalized speed variables (\mathbf{v}), which were time derivatives of generalized position variables; 16 muscle fiber length variables (\mathbf{l}_m); and 16 muscle activation variables (\mathbf{a}). The state vector (\mathbf{q}) thus had 50 entries in total:

$$\mathbf{q} = [\mathbf{p}, \mathbf{v}, \mathbf{l}_m, \mathbf{a}] \quad (5.3)$$

The dynamics of the system were described in implicit form by using SD/FAST software which has routines to return the derivatives of the state variables (Equations 5.4-5.7) and integrate the first order differential equations of the system forward in time with a Runge-Kutta fourth order explicit integrator subject to 16 muscle controls (\mathbf{u}):

$$\dot{\mathbf{p}} = \mathbf{v} \quad (5.4)$$

$$\dot{\mathbf{v}} = \mathbf{M}^{-1}(\mathbf{p})\mathbf{f}(\mathbf{p}, \mathbf{v}, \mathbf{l}_m, \mathbf{a}) \quad (5.5)$$

$$\dot{\mathbf{l}}_m = \mathbf{g}(\mathbf{p}, \mathbf{l}_m, \mathbf{a}) \quad (5.6)$$

$$\dot{\mathbf{a}} = \mathbf{h}(\mathbf{a}, \mathbf{u}) \quad (5.7)$$

where \mathbf{M} is the mass matrix, \mathbf{f} and \mathbf{g} are implicit functions, and explicit form of \mathbf{h} is given in the Appendix B.

5.2.2 Foot-ground contact model

A compliant contact model with nonlinear damping was used to simulate foot-ground contact (Marhefka et al., 1999; van den Bogert et al., 2009). According to this model, the ground applies

point forces to contact points on ball of the foot and the heel that depend on ground penetration of contact points and the penetration velocity of the contact points with respect to the ground. To avoid the vertical tensile forces that would occur when the foot is pulled from the ground very quickly, a velocity based contact separation term was added. Additionally, to eliminate discontinuity in contact force and therefore enhance convergence in numerical optimization, a linear spring and damper was engaged between the contact points when the foot approached the ground. The vertical component of the point force (normal to the horizontal contact surface) was formulated as

$$GRF_y = \begin{cases} -k_1 y_{cp} (1 - b \dot{y}_{cp}) & \text{if } y_{cp} \geq 0 \\ (-k_1 y_{cp} - k_2 y_{cp}^3) (1 - b \dot{y}_{cp}) & \text{if } y_{cp} < 0 \ \& \ \dot{y}_{cp} \leq 1/b \\ 0 & \text{if } y_{cp} < 0 \ \& \ \dot{y}_{cp} > 1/b \end{cases} \quad (5.8)$$

where y_{cp} and \dot{y}_{cp} stands for the vertical position and velocity of the contact point respectively, k_1 and k_2 are the stiffness constants, and b is the damping constant.

The frictional force tangential to the contact surface was modeled with a quasi-Coulomb friction model incorporating a hyperbolic tangent factor to approximate the force discontinuity at small velocities, in order to ensure differentiability. The horizontal component of the contact force was given by

$$GRF_x = -\mu GRF_y \tanh(c \dot{x}_{cp}) \quad (5.9)$$

where \dot{x}_{cp} is the horizontal velocity of the contact point, μ is the friction coefficient, and c is the parameter that controls the shape of hyperbolic tangent function. The coefficients in Equations 5.8 and 5.9 and coordinates of the contact points are given in Appendix B.

5.2.3 Optimal control problem formulation

The optimal control problem was formulated to search for the set of optimization parameters that maximized the average horizontal speed of the hip over a stride from the initial time $t=0$ to the final time $t=t_f$

$$\max_{\mathbf{r}} \quad (x_h(t = t_f) - x_h(t = 0)) / t_f \quad (5.10)$$

subject to the constraints derived from the system dynamics, and simple upper (\mathbf{r}^U) and lower bounds (\mathbf{r}^L) on the state variables, muscle controls, and the final time

$$\mathbf{r}^L \leq \mathbf{r} \leq \mathbf{r}^U \quad (5.11)$$

where the optimization variables (\mathbf{r}) are

$$\mathbf{r} = [\mathbf{q}(t), \mathbf{u}(t), t_f] \quad (5.12)$$

and periodicity constraints on all of the initial and final states, with the exception of the first state variable, the horizontal position of the hip (x_h)

$$\mathbf{q}^k(t = 0) - \mathbf{q}^k(t = t_f) = 0, \quad k = 2 \dots 50 \quad (5.13)$$

5.2.4 Discretization of the optimal control problem

The direct multiple shooting method was used to formulate the optimal control problem (Diehl et al., 2006; Betts, 2010). The first step in this implementation was the discretization of the infinite dimensional optimal control problem into a new form with a finite number of variables at n -many nodes. Thus, the total simulation time was divided into m short integration intervals ($m=n-1$) between subsequent discretization nodes each of which has a set of initial states ($\hat{\mathbf{q}}$) and constant muscle controls ($\hat{\mathbf{u}}$). The nonlinear continuity violations are defined as the differences between the terminal values for the states at the end of each integration interval ($\tilde{\mathbf{q}}_j$) and the initial values for the next interval ($\hat{\mathbf{q}}_{j+1}$) (Figure B-2 in Appendix B). These step transformed the

original problem into a general nonlinear programming (NLP) problem in which the solution vector s is searched for in order to minimize the scalar objective function (Equation 5.14) subject to linear constraints (Equation 5.17), nonlinear continuity violations (Equation 5.15), and simple bounds (Equation 5.16). With these definitions, the NLP problem takes the following form

$$\max_{\hat{s}} \quad \frac{1}{n} \sum_{i=1}^n \hat{x}_{h_i} \quad (5.14)$$

$$\hat{q}_{j+1}^k - \tilde{q}_j^k = 0, \quad j = 1 \dots m, \quad k = 1:50 \quad (5.15)$$

$$\hat{s}^L \leq \hat{s} = [\hat{q}_i^k; \hat{u}_i^z, t_f] \leq \hat{s}^U, \quad i = 1 \dots n, \quad k = 1:50, \quad z = 1:16 \quad (5.16)$$

$$\hat{q}_1^k - \hat{q}_n^k = 0, \quad k = 2:50 \quad (5.17)$$

where \hat{x}_h stands for the horizontal velocity of the hip.

5.2.5 Initial guess for the first iteration

The optimization problem requires a good initial guess for state variables and muscle controls at each discretization node; this guess was obtained in three steps. First, state and control trajectories of a complete one full walking cycle was obtained by using a muscle reflex controller previously described by Geyer and Herr (2010). Second, an initial guess vector was made up by re-sampling walking motion trajectories at n -many node. Third, a periodic running cycle was synthesized at a speed of 3.15 m/s (with a stride length of 2.27 m and a stride frequency of 1.38 Hz; Cavanagh and Kram, 1989) by minimizing sum of the squared muscle activation integrals and using the initial guess obtained in the second step. Then, initial guess of the sprint simulations was that periodic running cycle. The very first iteration in this optimization was neither feasible nor optimal, but was integrable, and the iteration process proceeded until a feasible and optimal point was located. The feasibility and optimality tolerances were set to 1e-5

and $1e-3$ respectively. The nominal maximum speed sprinting simulation solution was used as the initial guess for the sensitivity simulations.

5.2.6 Solution of the NLP Problem

The NLP problems described above were solved using numerical optimization, specifically with SNOPT (Gill et al., 2005), an efficient sequential quadratic programming method provided in the TOMLAB (TOMLAB Optimization, Seattle, WA) optimization environment. The objective function of the sprint simulation was linear, thus permitting an analytical gradient vector to be provided to the solver to improve computation times and accuracy of the gradient. The Jacobian of the nonlinear equality constraints was obtained by an external sparse finite difference method built into the TOMLAB optimization environment that takes advantage of the sparsity of the Jacobian. Exploiting the sparsity of the Jacobian dramatically reduced computation times since multiple independent columns of the NLP variables (\hat{s}) in the Jacobian were perturbed simultaneously. Bilateral symmetry was imposed, permitting simulation of a single step rather than an entire stride. The periodicity constraints were modelled as linear constraints. All state variables, muscle controls, and the final time had appropriate upper and lower bounds for both scaling and enforcing some biological and design limits. For the generalized position variables, physiological and geometrical joint limits were imposed. While some bounds on position, muscle activation, and control variables were active, the bounds on generalized speed variables, muscle fiber lengths, and the final time were never active, and were used only for scaling purposes. The numerical values of the upper and lower bounds are given in the Appendix B. The muscle activations and excitations were bounded between 0.01 and 1. Fifty discretization nodes ($n=50$) were used for each state variable and muscle control. The developers of SNOPT stated that it is best suited for problems with a moderate number of optimization variables (~ 2000). Increasing

the number of discretization points further would decrease efficiency of SNOPT, while decreasing would increase accumulation of nonlinearity at the discretization nodes. With the addition of the final time (t_f), there were 3301 NLP variables. For the nominal simulation, the solution of the NLP problem generally took less than hour on an Intel Xeon E53442 CPU with four parallel processing units, but some perturbed simulations took longer to converge because the computation times for integration were affected by the changes to the musculoskeletal parameters.

5.2.7 Sensitivity analysis simulations

Four parameters governing the forces generated by the plantarflexors SOL and GAS (maximum isometric force, optimal fiber length, tendon stiffness, and plantarflexor moment arm) were perturbed to examine their influence on maximum sprinting speed. Parameters for SOL and GAS were perturbed together rather than independently in each case. The magnitudes of the perturbations were determined using the coefficients of variation for each parameter previously measured in adults who were not active in competitive sports (moment arm and fiber length: Lee et al., 2009; maximum isometric force: Albracht et al., 2008; tendon stiffness: Arampatzis et al., 2007). In each case, the coefficient of variation (CoV) was used to set the magnitude of the perturbation (p_{perturb}) from the model's nominal (p_{nominal}) values.

$$p_{\text{perturb}} = \text{CoV} \cdot p_{\text{nominal}} \quad (5.18)$$

Each parameter (p) was perturbed four times: -2 SD, -1 SD, +1 SD, and +2 SD.

$$p = p_{\text{nominal}} + i \cdot p_{\text{perturb}}, \quad i = -2, -1, 1, 2 \quad (5.19)$$

5.3 Results

Following optimization, the speed of the model's running was increased from 3.15 m/s to 6.10 m/s. The model ran faster by increasing both the stride length and the stride frequency, from 2.27 m to 2.78 m and from 1.38 Hz to 2.78 Hz, respectively. The solver spent 34 minutes in the optimization process (69 major iterations). The kinematics and kinetics output variables such as joint angles and joint moments, ground reaction forces (GRFs), and muscle activation patterns from the nominal maximum speed sprinting simulation agreed well with corresponding experimental measurements (Miller et al., 2012a and Dorn et al., 2012) (Figures 5-1 and 5-2). The joint angles followed similar extension/flexion patterns with some timing shift and discrepancies in magnitudes. As an example of the differences between the model and the experimental results, the model's peak knee flexion angle in the swing phase was 25 degrees lower than the measured experimental values within $\pm 2SD$ range (63.5 vs 88.5 - 151.0 degrees knee flexion). The model's joint moments in the nominal simulation mostly followed trends observed in the experimental data (Figure 5-1). The main difference was the relatively higher magnitude flexion moments on ankle, knee, and hip with approximate peaks as 0.5, 2.8, and 6.6 N-m/kg on the late swing phase (75 - 100 percent gait cycle). For the GRFs (Figure 5-1), there was a similar timing shift as experienced in the joint extension/flexion cycles, and the ground contact of each foot was shorter for the model (27.9 vs 43.1 percent of the gait cycle). The model also produced vertical contact force with a higher peak value (3.96 vs 3.51 BW). While the model's muscle activations compared favorably to experimentally measured EMG envelopes (Figure 5-2), there were some substantial differences; for example, the model's VAS muscle was not active in the swing phase, and the RF muscle was not active in the stance and late swing phases.

The model's ankle joint played a major role in the propulsive phase of support in which the body accelerated in forward direction while the most positive work was done on the system (59.49 J) (Figure 5-3). In this phase, the peak ankle power (17.93 W/kg) was higher than knee (5.23 W/kg) and hip (12.77 W/kg). The joint powers were also similar to experimentally obtained data (Dorn et al., 2012) (Figure 5-3). The model's power absorption/generation patterns followed similar trends as the experimental lines with some discrepancy.

The results of the sensitivity simulations indicated that maximum sprinting speed is most sensitive to maximum isometric force capacity (Figure 5-4). The top speed increased with positive perturbations (+1 SD and +2 SD), and decreased with negative perturbations (-1 SD and -2 SD) of four plantarflexor muscle parameters analyzed in this study. The changes on the top speed in either direction were the greatest with the perturbations on maximum isometric force (+10.7% for +2SD and -14.2% for -2SD), yet the smallest with the perturbations on tendon stiffness (+1.28% for +2SD and -2.13% for -2SD). As the locomotion speed is the product of stride frequency and stride length, to be able to run faster, either stride frequency or stride length, or both of them must be modulated positively. When compared to the nominal simulation (Figure 5-4), the model modulated stride length (maximum +14.0% to minimum -14.7%) more than stride frequency (minimum -2.9% to maximum +1.8%) in response to the parameter perturbations.

While stride time did not change substantially (minimum -1.8% to maximum 2.9%) over the sensitivity simulations, the changes in contact time (minimum -13.1% to maximum 26.7%) and swing time (maximum +9.1% to minimum -10.9%) were not negligible (Figure 5-5). Generally, shorter contact times and longer swing times were observed as the model ran faster. Swing time in the simulation seemed to be directly related to effective impulse (Figure 5-5). For

example, the increase was 9.1% vs. 11.4%, and the decrease was 10.9% vs. 11.9% for the +2 SD and -2 SD perturbations of the maximum isometric force over the nominal simulation for the swing time and effective impulse respectively.

In the sensitivity simulations, faster maximum sprinting speeds were accompanied by greater ground forces (Figure 5-6). In general, the biggest changes in kinematic variables happened to be on the maximum isometric force perturbation simulations, for example, the peak ankle power changed 54.2% with a +2 SD perturbation and decreased 50.9% with a -2 SD perturbation (Figure 5-6). For the work done in the propulsive phase, the reduction in GRF (e.g., 19.8% for -2 SD) was higher in magnitude for negative perturbations of the fiber length than the gain (e.g., 9.1% for +2SD) with positive perturbations (Figure 5-6). On the contrary, the loss in GRF (e.g., 4.2% for -2SD) was lower in magnitude for negative perturbations of the moment arm than the gain (e.g., 6.8% for +2SD) with positive perturbations on the work done in the propulsive phase (Figure 5-6).

5.4 Discussion

The simulation of maximum-speed sprinting described in this paper is the first to use an optimal controls approach without any explicit “tracking” or other dependency on experimentally measured human motion. Neither the initial states nor the initial guess for the history of muscle controls were derived from experimentally obtained motion, force, or EMG data. The simulation was guided by a simple objective function, maximizing average horizontal speed over a stride, yet was still able to replicate many features associated with human sprinters, namely, spatiotemporal variables, joint mechanics, GRFs, and muscle activation patterns (Figures 5-1, 5-2, and 5-3). The sensitivity analysis using the simulation showed that the model increased maximum sprinting velocity when maximum isometric force, optimal fiber length, tendon

stiffness, and moment arm of plantarflexor muscles were increased (Figure 5-4). Higher maximum sprinting velocities were accompanied by longer swing times and larger average ground forces (Figure 5-5 and 5-6).

The present work differs from previous attempts to simulate maximum-speed sprinting using optimal controls in several important respects. Miller et al. (2012 a, b) also developed a simulation of maximum-speed periodic sprinting using a planar model, but the authors used a single shooting approach. As in the present study, the objective function had a term that represented sprinting speed but Miller et al. also included terms that penalized differences between the initial and final segment angular positions and velocities, as well as the sum of the squared passive joint moment integrals. While a periodicity constraint was used, this constraint was not satisfied to the same degree that it was in the present simulation. For example, authors reported such periodicity violations as 2.5 deg. for the joint angles, and 15.9 deg/s for joint angular velocities; on the other hand, we set feasibility tolerance on the periodicity constraints as $1e-6$. Van den Bogert et al. (2009) implemented direct collocation (DC) to simulate maximum speed sprinting with some aid of experimental human gait data. In our study, we used direct multiple shooting without any explicit dependency on experimental motion data. While DC has been successfully used in many optimal control problems, the question of proper discretization error control is not addressed in many studies (Diehl et al., 2006). Unlike DC, direct multiple shooting method does not require control of discretization error and re-gridding which would in turn require addition of new discretization points to the grid. Schultz and Mombaur (2010) simulated sprinting as a two-phase problem using direct multiple shooting in which a weighted sum of torque magnitudes and torque variations were minimized for a prescribed velocity. As suggested by the objective function, the three-dimensional model was not a muscle-driven model

but rather was a torque driven model. The complex objective function used in that study would be difficult to justify, but the objective function we used in our simulations was a natural and unambiguous choice. Therefore, our study was the first study that used direct multiple shooting method to generate predictive dynamic simulations of maximum speed sprinting with a muscle driven model and an unambiguous objective function and without using any measured human motion data.

Some previous authors have simulated sprinting by tracking measured motions and applying measured ground reaction forces. When such an approach has been used, the simulated motions and forces can be made to match to a high degree what is observed in the experiment (Pandy, 2001). These tracking simulations have been used to analyze muscle contributions to forward propulsion and support. With such a tracking simulation, it has been shown that plantarflexor muscles are the greatest contributors to propulsion and support in the stance phase of running, while the contribution of the arms are minimal, as they generate less than 1% of the peak mass center acceleration (Hamner et al., 2010). We also found that most positive work was done on the system in the propulsive phase of support when peak ankle power was greater than knee and hip (Figure 5-3). Tracking simulations might also be useful to investigate the causes of injuries. For example, in another tracking based simulation, the mechanics of hamstring muscles were studied, thus, possible causes of hamstring injuries in sprinting were tried to be identified (Schache et al., 2012). In summation, although tracking approaches are generally more numerically tractable and recreate the experimentally recorded motion with high fidelity, they reduces predictive power of the dynamic simulation approach and are not capable of predicting how perturbations in musculoskeletal architecture affect function and performance (Pandy, 2001).

As in previous reports we found the musculoskeletal model architecture parameters to influence the performance of motor tasks. In our study, we found that maximum sprinting speed is most sensitive (10.7% for +2SD) to maximum isometric force parameters among perturbed plantarflexor muscle parameters. In a predictive simulation of maximum vertical jump, it was found that jumping performance was increased when the maximum isometric force of knee extensor or all muscles were increased from the nominal value provided that muscle controls were re-optimized for perturbed parameters (Bobbert et al., 1994). We also found that maximum sprinting speed was sensitive to muscle optimal fiber length (4.5% for +2SD) and moment arm (3.6% for +2SD). Experimentally collected data from sprinters showed that sprinters have longer plantarflexor muscle fascicle length (Abe et al., 2000 and 2001), and longer fascicle lengths are positively correlated with 100-m sprint performance (Kumagai et al., 2000). In a sprinting simulation, van den Bogert et al. (2009) observed a speed increase of 2.6% by increasing the moment arm of the GLU muscle. In an experimental study, subjects with longer moment arms jumped higher (van Werkhoven and Piazza, 2013). Lastly, in the current study, the influence of tendon stiffness on top speed found to be minimal (1.3% for +2SD). Arampatzis et al. (2007) and Kubo et al. (2011) illustrated that sprinters have stiffer Achilles' tendons, but they did not find a positive relationship between stiffness of Achilles' tendons and sprinting performance.

The model increased stride length rather than stride frequency and generated larger average ground forces to be able to run faster (Figure 5-4 and 5-6). Dorn et al. (2012) obtained gait data from nine subjects who were experienced runners, and performed analysis using a pseudo-inverse induced acceleration analysis on a generic musculoskeletal model implemented in OpenSim (Delp et al., 2007). Their experimental data suggested that human sprinters modulate stride length to get faster for speeds up to 7 m/s which is higher than the maximum sprint speed

(6.75 m/s) obtained in our simulations. By using the computer model, Dorn et al. estimated that the plantarflexor muscles contribute most significantly to vertical ground forces and hence increase stride length. Weyand et al. (2000) measured kinematic and kinetic variables of 33 subjects running on a treadmill at varying speeds, and suggested that human sprinters achieve faster top running speeds with greater vertical ground forces not more rapid leg movements. Similar to those experimental findings, the model also attained larger stride lengths and average ground forces with increasing top running speeds (Figure 5-4 and 5-6). Therefore, it could be inferred that the model got faster by exploiting mechanisms similar to those observed to be used by human sprinters.

Our sensitivity analysis revealed that higher speeds were possible when the plantarflexor moment arm was greatest, a result that seems to contrast with experimental measurements of sprinter foot and ankle structure (Lee and Piazza, 2009; Baxter et al., 2012). In other words, unlike the experimental finding that indicates sprinters have smaller plantarflexor moment arms, the model with larger moment arms did perform better on maximum speed sprinting. A shorter moment arm would compromise joint moment generation due to shorter mechanical advantage. On the other hand, for a given joint rotation, a muscle with a shorter moment arm and longer fiber would operate in more favorable ranges of muscle force-length and force-velocity curves in terms of force production (e.g., Nagano and Komura, 2003; Lee and Piazza, 2009; Baxter et al., 2012). Therefore, the gain on force generation may compensate or exceed the disadvantage on moment arm. The sprinting mechanics on the acceleration and maximum velocity phases are different (e.g., van Ingen Schenau et al., 1994; Majumdar and Robergs, 2011). Therefore, better performance on one phase of sprinting may not reflect on overall 100-m or 200-m performance. Also, there is recent evidence that supports our finding about moment arms, as Baxter and Piazza

(2014) reported that plantarflexors with longer moment arms generate larger joint moments around ankle in isometric and isokinetic conditions which would help to achieve higher maximum sprinting speeds (Alexander, 1989). In summation, sprinters have shorter moment arms (Lee and Piazza, 2009; Baxter et al., 2012), but our simulation results suggested that larger moment arms favor higher top speeds in maximum speed bipedal sprinting. For other three parameters we studied, the results were in line with the previous experimental findings. For example, as we hypothesized, incrementing maximum isometric force increased top sprint speed (Figure 5-4). It has been shown that animal running speed any particular speed is nearly directly proportional to the force exerted by its muscles (Taylor et al., 1980); and, as described in Equation 5.2, the muscle force is directly proportional to the maximum isometric force parameter. Longer optimal fiber lengths enabled higher top sprint speeds (Figure 5-4) by providing that plantarflexor muscles operate favorable regions in force–length and force–velocity curves in terms of force production (McMahon, 1984). Lastly, the influence of tendon stiffness on performance was minimal (Figure 5-4). It is true that sprinters have stiffer Achilles' tendons, but this additional stiffness may be a result of repetitive higher loadings, rather than a determinant of performance (Arampatzis et al., 2007).

There were several limitations of the study to consider. We cannot know that a global optimum was found. We did not suffer from significant local minimum problems because SNOPT has some advantages over some other optimization algorithms as it has routines to control global convergence rigorously. Out of plane motions of joints such as pelvis motions are important in sprinting, especially at the start, but a planar model without such motions was used in the study. Another limitation related to the model is that it failed to include many lower extremity muscles. Muscle selection was based on the muscles chosen for inclusion in previous

simulations of human locomotion (e.g., Geyer and Herr, 2010; Wang et al., 2012; Ackermann and van den Bogert et al., 2010). The muscle parameters were not derived from data collected from human sprinters, but from the reports in the literature based on measurements made in human cadavers. The muscle force–velocity, excitation–activation, and force–length properties and their characteristic parameters such as maximum shortening velocity were suggested as limiting factors on maximum sprinting speed (Miller et al., 2012 a, b), yet we did not include sensitivity of maximum sprinting speed to the parameters of those properties. The maximum knee flexion value was lower than those observed on human sprinters, perhaps because the model used the minimum knee flexion necessary for ground clearance, which is something human sprinters might not risk at such high running speeds. Another reason may be that contact between the ground and the distal end of the toes was not modeled; the distance between two contact points of the model was 21 cm while the distance from heel to toe is much larger, approximately 26.9 ± 2.0 cm (Lee and Piazza, 2009).

In conclusion, the computer model used in this study showed how variations in architecture of plantarflexors affect maximum speed bipedal sprinting performance. Positive increments of each parameter analyzed in the study (maximum isometric force, optimal fiber length, tendon stiffness, and moment arm) positively influenced maximum speed bipedal sprinting performance. The model employed mechanisms similar to those observed in human sprinters to attain higher speeds. Future studies may simulate both acceleration and maximum speed sprinting phases simultaneously which would allow to predict influence of musculoskeletal architecture to overall sprint performance. Our model and simulation framework could be used to simulate other gaits such as normal walking, steady state running, and walking with prosthesis with minor modifications.

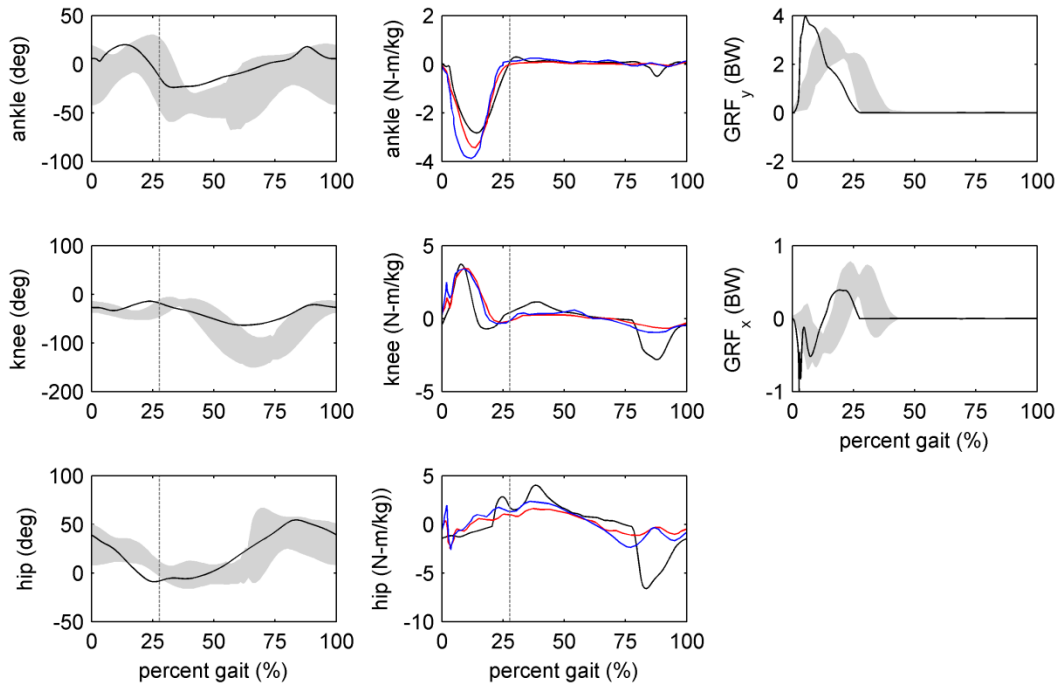


Figure 5-1 The joint angles, joint moments, and GRFs for one full sprinting cycle from left foot heel strike to left foot heel strike for the maximum speed sprinting simulation with nominal parameter values. The shaded gray areas in the joint angles and GRFs plots were reproduced from Miller et al., 2012; which are enclosed by two plus and minus between twelve women subjects' standard deviations around the mean (mean speed 6.42 ± 0.61 m/s). The blue and red lines in the joint moment plots were reproduced from Schache et al., 2011; and represent mean joint moments of eight subjects running at 5.02 m/s (red) and 6.97 m/s (blue). The dashed vertical gray lines indicate the time of toe-off.

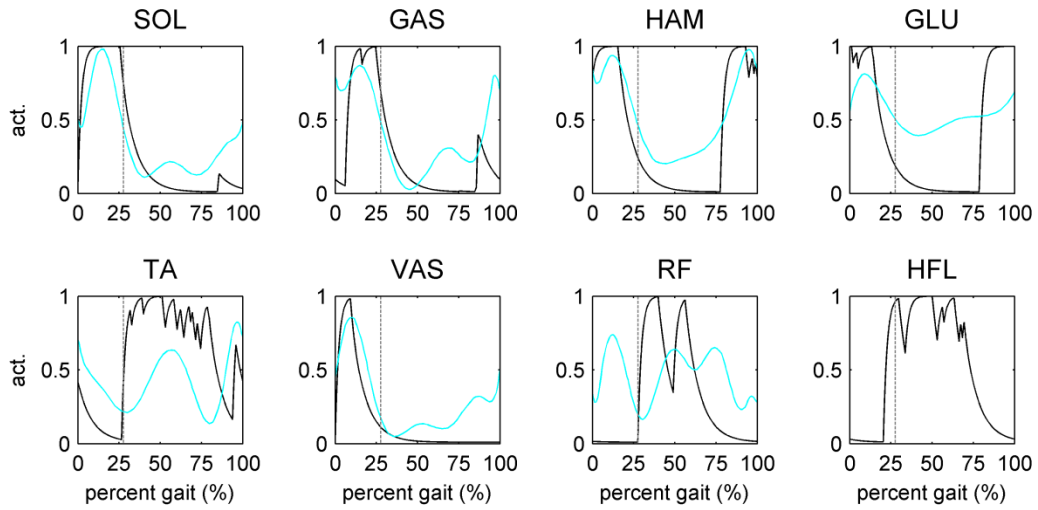


Figure 5-2 The muscle activations for one full sprint cycle from left foot heel strike to left foot heel strike for the maximum speed sprinting simulation with nominal parameter values. The cyan lines were reproduced from Miller et al., 2012; and represent EMG linear envelopes. The dashed vertical gray lines indicate the time of toe-off.

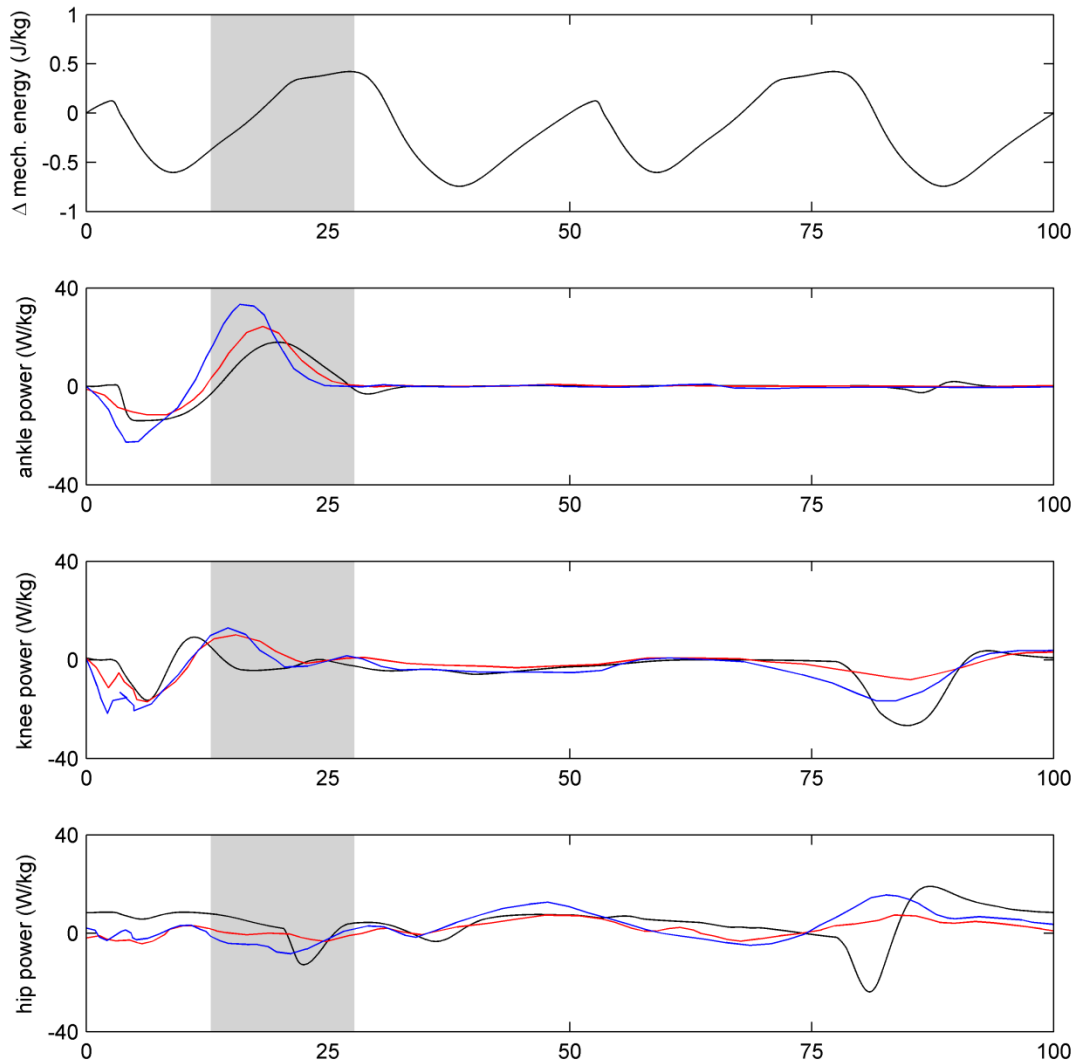


Figure 5-3 The changes in the mechanical energy and the joint powers of ankle, knee, and hip for one full sprint cycle from left foot heel strike to left foot heel strike for the maximum speed sprinting simulation with nominal parameter values. The shaded gray area is enclosed by the start and the end of the propulsive phase of support. The blue and red lines in the joint power plots were reproduced from Schache et al., 2011; and represent mean joint power of eight subjects running at 5.02 m/s (red) and 6.97 m/s (blue).

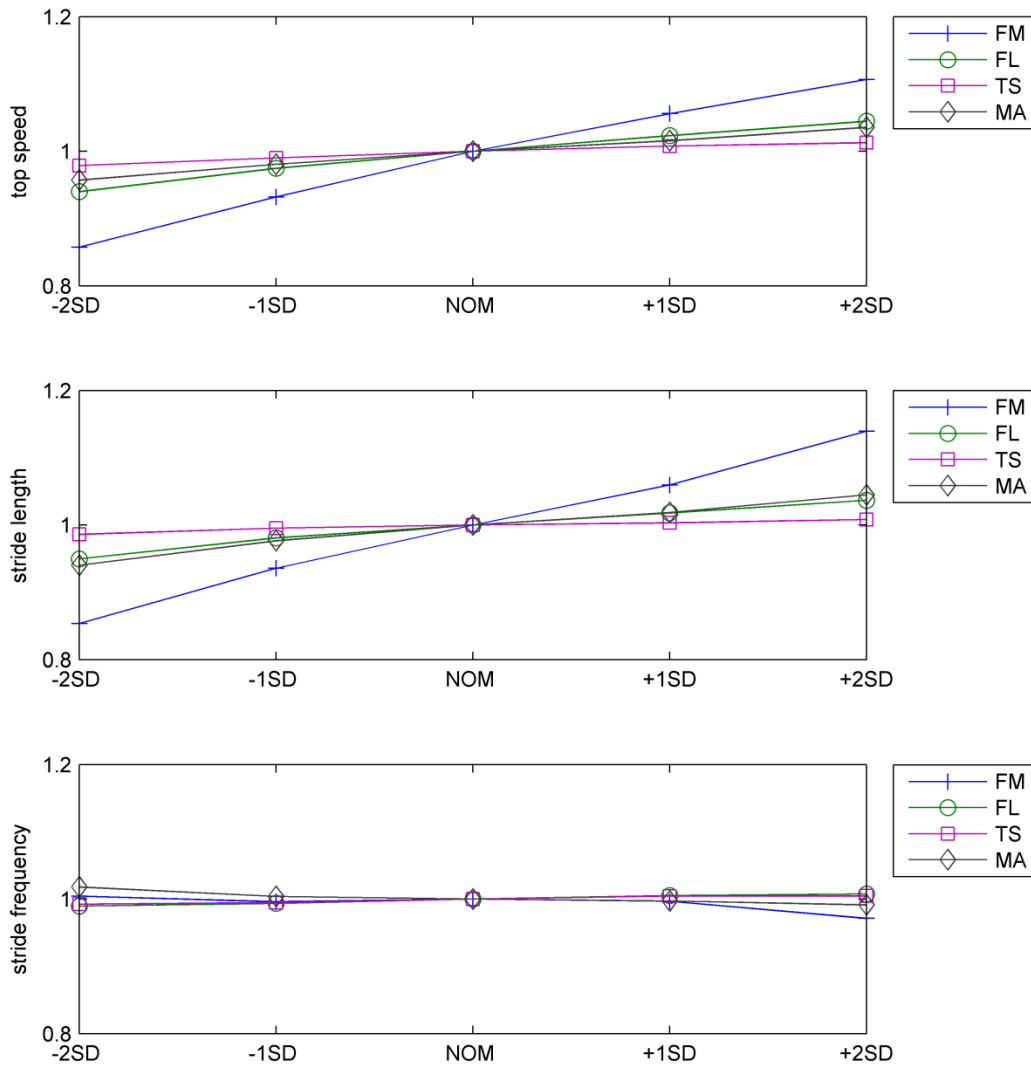


Figure 5-4 The alterations in top sprint speed, stride length, and stride frequency for -2 SD, -1 SD, +1 SD, and +2 SD perturbations of plantarflexor muscles parameters, namely, maximum isometric force (FM), optimal fiber length (FL), tendon stiffness (TS), and moment arm (MA) normalized with values from the maximum speed sprinting simulation with nominal parameter values (NOM).

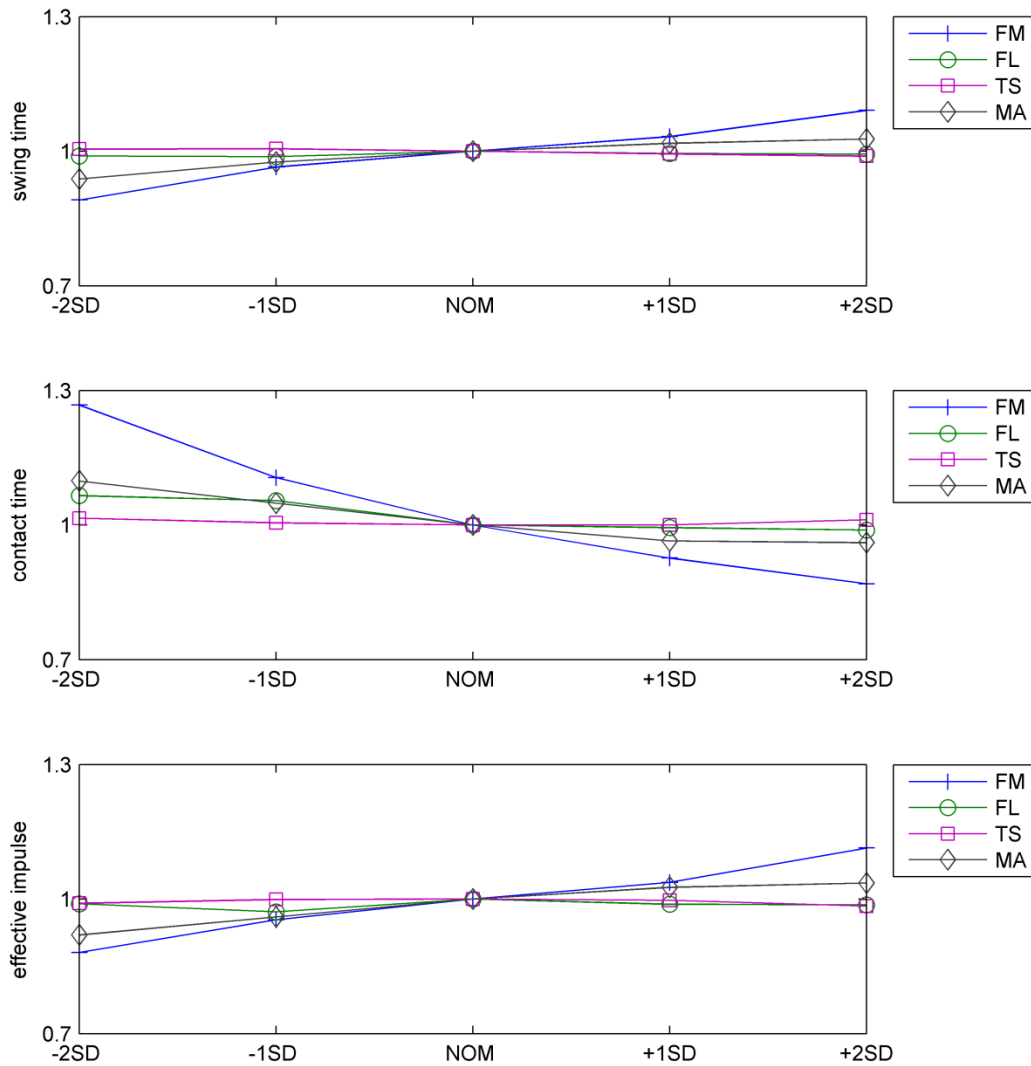


Figure 5-5 The alterations in swing time, contact time, and effective impulse of GRF_y for -2 SD, -1 SD, +1 SD, and +2 SD perturbations of plantarflexor muscles parameters, namely, maximum isometric force (FM), optimal fiber length (FL), tendon stiffness (TS), and moment arm (MA) normalized with values from the maximum speed sprinting simulation with nominal parameter values (NOM).

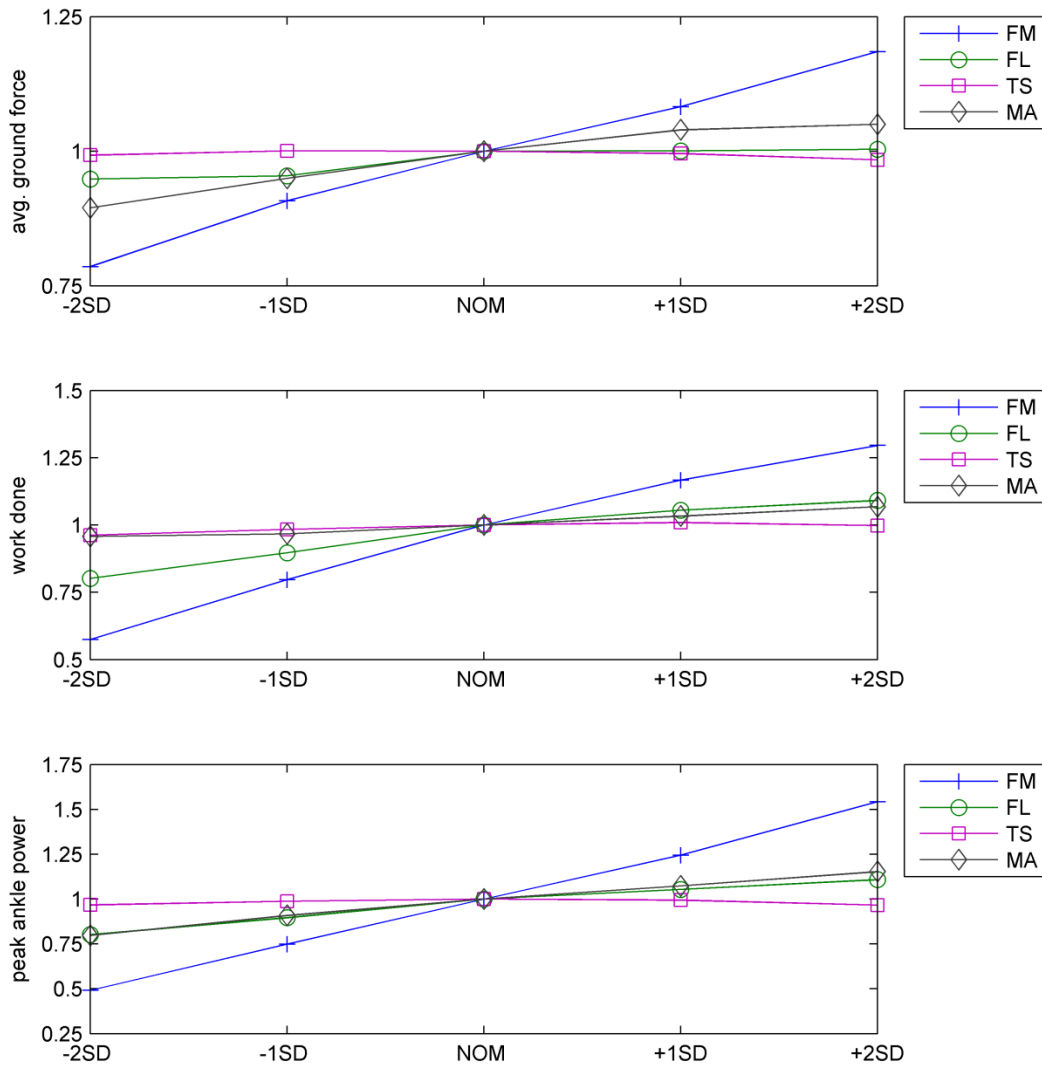


Figure 5-6 The alterations in average ground force of GRF_y , work done in the propulsive phase of support, and peak ankle power for -2 SD, -1 SD, +1 SD, and +2 SD perturbations of plantarflexor muscles parameters, namely, maximum isometric force (FM), optimal fiber length (FL), tendon stiffness (TS), and moment arm (MA) normalized with values from the maximum speed sprinting simulation with nominal parameter values (NOM).

Chapter 6

Sensitivity of maximum simulated sprinting speed to the maximum force-generating capacity of individual muscles

6.1 Introduction

Human sprinting performance depends on rapid acceleration up to maximum speed at the start of a race and the ability to maintain that maximum speed until the finish line is crossed (van Ingen Schenau et al., 1994; Majumdar and Robergs, 2011). The ability to accelerate and maintain top speed is generally understood to be influenced in large part by skillful neuromuscular control and having favorable musculoskeletal architecture (e.g., Mero et al., 1992; Bret et al., 2002; Majumdar and Robergs, 2011). While physical characteristics and technique vary considerably among athletes (e.g., Majumdar and Robergs, 2011), there are often traits in common among athletes who play the same sport. For instance, human sprinters are known to have higher proportion of fast-twitch muscle fibers (e.g., Costill et al., 1976; Mero et al., 1981), longer fascicle lengths and smaller pennation angles for the leg muscles (e.g., Abe et al., 2001; Lee and Piazza, 2009), stiffer Achilles' tendons (e.g., Arampatzis et al., 2007; Kubo et al., 2011), smaller plantarflexor moment arms (e.g., Lee and Piazza, 2009; Baxter et al., 2011), and larger leg muscles (e.g., Maughan et al., 1983; Abe et al., 2000; Kubo et al., 2011).

Previous experimental studies have compared the leg muscles of sprinters to those of non-sprinters to show that the sizes of certain muscles are greater in sprinters. Maughan et al. (1983) found the knee extensor muscle cross sectional areas of sprinters to be larger than those of distance runners and untrained subjects. Abe et al. (2000) reported that the thickness of the knee extensors and plantarflexors were greater among sprinters than for distance runners and

untrained subjects. Kubo et al. (2011) showed that plantarflexor and medial side knee extensor muscle thickness was larger for sprinters when compared to non-sprinters. Furthermore, a significant correlation between 100m sprint time and muscle thickness at the medial side of knee extensor was estimated in the same study. Surprisingly, there is not any research study that compared hip flexor muscle size between sprinters and non-sprinters, but in a training study (Deane et al., 2005), it was claimed that subjects who followed a hip flexor resistance-training program improved hip flexion torque capacity and time to complete 40-yard dash.

Muscle size is often expressed using the muscle's physiological cross sectional area (PCSA) (Powell et al., 1984), which is the area of the largest cross section of a muscle perpendicular to its fibers. In musculoskeletal models that incorporate Hill-type musculotendon actuators, measures of PCSA are often used to specify maximum isometric force F_{max} , an important force-generating property of each actuator. The parameter F_{max} is typically obtained by multiplying PCSA by a muscle-independent specific tension, which has a median value of 25 N/cm² for mammalian muscle (Zatsiorsky and Prilutsky, 2012). As its name suggests, maximum isometric force is the force muscle can generate under isometric contraction conditions with maximum activation.

While larger leg muscles are known to contribute to the generation of larger joint moments (Blazevich et al., 2009; Baxter and Piazza, 2014) that in turn reduce 100 m sprint time (Alexander, 1989), the manner in which strengthening individual muscle would affect maximum sprinting velocity is not clear. It is difficult to imagine how it would be possible to study the relationship between individual muscle strength and sprinting ability with an *in vivo* experiment because sprinting ability is output of a very complex neuromuscular control and musculoskeletal architecture. Computer simulation, however, has the potential to answer this question. For

instance, Hamner et al. (2010) employed muscle-induced acceleration analysis to assess individual muscle contributions to braking, propulsion, and support of the body during steady-state running at 3.96 m/s. The authors found that ankle plantarflexors make the greatest contribution to propulsion and support during the propulsive phase of support, while the quadriceps muscle group was the largest contributor to braking in the braking phase of support.

The purpose of the present study was to use a computer simulation of maximum-speed bipedal sprinting to examine the effects of isolated perturbations to maximum isometric force for each muscle included in the model. We hypothesized that perturbations to maximum isometric force capacity of larger muscles VAS and SOL would contribute most to maximum sprinting speed.

6.2 Methods

We used a planar biped model actuated by eight major Hill-type muscle groups as soleus (SOL), tibialis anterior (TA), gastrocnemius (GAS), vasti (VAS), hamstrings (HAM), rectus femoris (RF), glutei (GLU), and hip flexors (HFL) on each leg. The model had nine degree-of-freedom (dof): right and left ankle, knee, and hip angles; the x- and y-positions of the hip; and the trunk angle. Seven body segments made up the model: the trunk and the right and left thighs, shanks, and feet which were articulated with revolute joints on ankle, knee, and hip and a planar joint between hip and ground. Each muscle had two states, fiber length and activation, and a control. In addition to muscle states, there were nine position and nine velocity states for each dof aforementioned. Therefore, the model had 50 state variables and 16 controls in total.

The musculotendon (MT) actuator force (F_{mt}) was equal to force on series elastic element (F_{see}) and sum of forces on active contractile element (F_{ce}), parallel elastic element (F_{hpe}), and parallel buffer elastic element (F_{lpe}).

$$F_{mt} = F_{see} = F_{ce} + F_{hpe} - F_{lpe} \quad (6.1)$$

The joint moments (M_j) were calculated by multiplying MT actuator force with its corresponding moment arm (r) around the joint(s) it spans and adding passive joint moments ($M_{passive}$), which represent the mechanical effects of other tissues than muscles

$$M_j = F_{mtu} \cdot r + M_{passive,j}, \quad j = 1:6 \quad (6.2)$$

The equations to define passive joint moments and their parameters are provided in the Appendix B. The active contractile element (CE) force generation was depended on muscle activation (a), muscle fiber length (l_m), muscle contraction velocity (v_m), and maximum isometric force (F_{max})

$$F_{ce} = aF_{max}f_l(\bar{l}_m)f_v(\bar{v}_m) \quad (6.3)$$

where f_l and f_v were muscle force-length and muscle force-contraction velocity functions respectively. \bar{l}_m was the muscle fiber length scaled with respect to the optimal fiber length (l_{opt}) and \bar{v}_m was the muscle contraction velocity scaled with respect to maximum contraction velocity.

We used a compliant contact model with nonlinear damping to model foot-ground contact (Marhefka et al., 1999; van den Bogert et al., 2009). According to this model, the ground applies point forces in the vertical direction to contact points on ball of the foot and the heel that depend on ground penetration of contact points and the penetration velocity of the contact points with respect to the ground.

$$GRF_y = \begin{cases} -k_1 y_{cp} (1 - b \dot{y}_{cp}) & \text{if } y_{cp} \geq 0 \\ (-k_1 y_{cp} - k_2 y_{cp}^3)(1 - b \dot{y}_{cp}) & \text{if } y_{cp} < 0 \text{ \& } \dot{y}_{cp} \leq 1/b \\ 0 & \text{if } y_{cp} < 0 \text{ \& } \dot{y}_{cp} > 1/b \end{cases} \quad (6.4)$$

where y_{cp} and \dot{y}_{cp} stands for the vertical position and velocity of the contact point respectively, k_1 and k_2 are the stiffness constants, and b is the damping constant. A quasi-Coulomb friction model

incorporating a hyperbolic tangent factor to approximate the force discontinuity at small velocities was used to model the frictional force tangential to the contact surface.

$$GRF_x = -\mu GRF_y \tanh(c\dot{x}_{cp}) \quad (6.5)$$

where \dot{x}_{cp} is the horizontal velocity of the contact point, μ is the friction coefficient, and c is the parameter that controls the shape of hyperbolic tangent function. The constants in Equations 6.4 and 6.5 and coordinates of the contact points are given in Appendix B.

The maximum speed sprinting simulations were obtained through numerical optimization. To formulate the optimization problem, the direct multiple shooting method (Diehl et al., 2006; Betts, 2010) was used. Each continuous state trajectory was discretized at n -many discrete nodes, and constant muscle controls were used between those discrete nodes. Then, the system dynamics equations were integrated not in a single shot but in multiple shots, where each discrete state value at discretization node was used as an initial state in m -many integration intervals ($n = m - 1$). Setting the continuity violations at the discretization nodes equal to zero formed nonlinear constraints, defined as the difference between the terminal values for the states at the end of each integration interval and the initial values for the next interval (Figure B-2 in Appendix B). Bilateral symmetry was assumed, so that only one periodic step of walking was simulated, and the periodicity constraints were implemented as linear equality constraints. Every state and control variable had an appropriate upper and lower bound derived from muscle or joint physiology, and model geometry.

The objective function of the optimizations was the maximization of the average horizontal velocity of the hip over a stride. That objective function was minimized subject to constraints and bounds defined above. The optimization problem was solved using the SNOPT (Gill et al., 2005) numerical optimization toolbox, which is an efficient method for trajectory

optimization problems provided in the TOMLAB (TOMLAB Optimization, Seattle, WA) optimization environment. As the nominal maximum speed sprinting simulation, the solution obtained in the Chapter 5 was used. Sensitivity simulations were obtained by re-optimizing all state and control variables after isolated perturbations of maximum isometric force capacity of each muscle. Positive and negative perturbations of plus and minus 20 percent of maximum isometric force were used. Further details of the methods and musculoskeletal model can be found on Chapter 5 and Appendix B.

6.3 Results

The results of the sensitivity simulations indicated that maximum sprinting speed was most sensitive to changes in the maximum isometric force in the SOL and HFL musculotendon actuators (Figure 6-1). Generally, increases in maximum isometric force for individual muscles led to increases in the maximum sprinting velocity, but these changes in velocity varied depending on which muscle was strengthened (0.35 % to 3.73%). Conversely, reductions in maximum isometric force cause decreases in the maximum sprinting velocity (-0.43% to -3.92%). The smallest contributions to sprinting speed came from increases to RF, VAS, and TA (Figure 6-1). Reductions in the force-generating capacity of individual muscles produced decreases in speed that mirrored the increases in speed produced by those same muscles when maximum isometric force was increased (Figure 6-1).

Among those simulations in which muscle strength was increased, the model ran faster in general by increasing stride length (SL) and stride frequency (SF). While positive perturbations increased SL (0.56% to 3.36%) except RF, the greatest increases were observed on VAS and SOL muscles (Figure 6-2). Like SL, SF was increased with positive perturbations (0.29% to 2.68%) except VAS and TA, and the largest increments happened on HFL and HAM muscles

(Figure 6-3). Negative perturbations produced similar patterns in the negative direction (Figure 6-4 and 6-5).

The change in maximum sprinting speed was also characterized in terms of the velocity change per newton of change in maximum isometric force capacity (Figure 6-6). Because each muscle actuator had a different maximum isometric force, perturbing these values by 20% meant that each actuator's maximum isometric force was perturbed by a different absolute value. When examined in this manner, HFL and GAS showed the biggest increases in speed for a given increase in force, whereas VAS showed the smallest increase (Figure 6-6).

6.4 Discussion

The plantarflexors and hip flexors were found to be the most important contributors to maximum sprinting speed (Figure 6-1 and 6-6). Increases in the force-generating capacity of those muscles were accompanied by characteristic changes in SL and SF that produced increased sprinting speed. We hypothesized that perturbations to maximum isometric force capacity of larger muscles VAS and SOL would contribute to maximum sprinting speed most; however, VAS was one of the smallest contributors to maximum sprinting speed. This study was the first simulation study that examined sensitivity of maximum sprinting speed to the isolated perturbations of maximum isometric force of all major leg muscle groups and explored the functional roles of muscles in sprinting with such an approach.

The model exploited mechanisms similar to those observed in human sprinters to achieve higher speeds. It has been hypothesized in the literature that there exist two mechanisms to increase running velocity (Dorn et al., 2012). The first mechanism was an ankle strategy, that is, plantarflexors increase SL mainly by generating larger ground forces at the stance phase. It could be suggested that the model employed a similar mechanism as it modulated SL by 2.97%, but SF

by only 0.29%; and average ground force was arisen to 1.87 BW from 1.80 BW (3.89% increase) in the positive SOL perturbation simulation. However, the change in SL and SF was very similar for the positive GAS perturbation simulation (0.93% for SL, and 1.00% for SF). Moreover, model experienced a larger speed increment in the SOL perturbation than GAS, probably owing to the fact that SOL is a bigger muscle in our simulations (maximum isometric force values: 4000 N for SOL, and 1500 N for GAS). Yet, GAS was more efficient in terms of increasing sprinting speed when normalized with the magnitude of the perturbation (Figure 6-6). The second mechanism was that hip muscles increase SF mainly by generating larger forces at the swing phase. The simulation results indicated a similar tendency, as the average increment in SF for four hip muscle groups was 1.72% whereas the average increment in SL was 0.45%. The hip muscles except RF took advantage of larger isometric force capacity by reaching full-activation.

Contrary to the experimental finding that suggests there is a positive correlation between 100 m sprint time and muscle thickness at the medial side of knee extensors (Kubo et al., 2011); in our simulations, VAS performed poor in terms of incrementing maximum sprinting velocity (Figure 6-6). Interestingly, the model demonstrated the biggest increase (3.36%) in SL in the positive VAS perturbation simulation; but speed gain was relatively small (0.79%) since that increment was accompanied with a 2.48% decrement in SF. The locomotion velocity is the product of SL and SF, so that running velocity is increased by taking longer strides at higher rates (e.g., Weyand et al., 2000). However, SL and SF are not independent variables; on the contrary, SL and SF are shown to be inversely proportional during sprinting (Hunter et al., 2004). Thus, to be able increase maximum sprinting velocity, either SL or SF would be incremented without a similar decrement on the other one. VAS muscle group did not take advantage of a larger isometric force capacity as it never reached full activation in any instance

of the stride cycle. Actually, only knee extensor muscles VAS and RF muscle groups did not reach maximum activation in the simulations and they were the ones produced least speed increase with TA. It was also important to note that VAS had the largest isometric force capacity (6000 N), but, RF and TA were the smallest (1000 N and 800 N) respectively. However, these results cannot suggest that VAS muscle is not important in sprinting. As mentioned before, Kubo et al. (2011) reported a positive correlation between 100 m sprint time and muscle thickness at the medial side of knee extensors. One possible explanation to that was isometric force capacity of VAS muscle group might be important in the other phases of sprinting such as start and acceleration. It is known that demand on musculature is different in different phases of sprinting (e.g., van Ingen Schenau et al., 1994; Majumdar and Robergs, 2011). In addition, performance gain from knee extensors may be possible when increase in knee extensor strength is accompanied by increases in the other muscle groups.

The contributions of individual muscle groups to maximum sprinting speed were similar in some respects to the muscle-induced accelerations during running that were computed by Hamner et al. (2010) using a similar model. Hamner et al. (2010) analyzed muscle contributions to propulsion and support during running using induced acceleration analysis, and found that quadriceps (RF and VAS muscle groups) were the largest contributors to braking and support during the braking phase of support, while plantarflexors were the greatest contributors to propulsion and support in the propulsive phase of support. Those implications might be useful to explain why VAS, the strongest muscle in the model, was not able to increase maximum sprinting velocity to the same extent that SOL or HFL did. VAS controls knee flexion in the stance phase, but has been found to be active for knee extension only at very high sprinting velocities (Mann and Hagy, 1980; and Dorn et al., 2012). Thus, there is a possible link between

the poor performance of VAS in terms of increasing maximum sprinting velocity and its function perhaps being for braking and stabilizing rather than propulsion. On the other hand, it would not be possible to estimate hip flexors' strong performance from the analysis of Hamner et al. (2010), as hip flexors were activated in the swing phase of sprinting, yet their analysis was limited to the stance phase of running. They pointed out that hip flexor iliopsoas muscle only accelerated the mass center downward at the late stance.

The results of this study have implications for the development of resistance training programs for increasing sprint performance. Our results suggest that focusing on quadriceps alone may not be an effective strategy for enhancing maximum sprinting speed. To increase maximum sprinting speed, the hip flexors and plantarflexors should be strengthened. Our results also indicated that our model and simulation framework can be used to simulate muscle weakness as well. It could be particularly important to make assessments on muscle groups which have most potential to limit mobility in elderly population. The same techniques developed in this study could be used to understand how elderly walking speed among those with movement disorders is limited by muscle weakness.

There were several limitations of the study to consider. It is not certain that the solutions were global optima; however, it is reassuring that the positive changes mirrored the negative changes. The model included only major muscle groups whose functions were more important in the sagittal plane motions. The muscle parameters were not derived from data collected from human sprinters, but from the reports in the literature based on measurements made in human cadavers. It is clear from Chapter 5 and previous simulation studies of sprinting (e.g., Miller et al., 2012) that other muscle parameters are also critical for determining maximum sprinting speed, but we did not include them in this particular study.

In conclusion, the computational model used in this study showed how variations in maximum isometric force capacity of muscles affect maximum speed bipedal sprinting performance. Increases in maximum isometric force caused the maximum speed of bipedal sprinting to increase, and simulated muscle weakness limited maximum speed of sprinting. The maximum sprinting speed was most and least sensitive to HFL and VAS muscle groups' maximum isometric force capacity. The model employed mechanisms similar to those observed in human sprinters to reach higher speeds. Future studies may extend Hamner et al.'s (2010) study by including swing phase of running which would allow a better assessment of muscle function in running; so that, a better comparison would be possible with our findings. Also simulation of a full sprint race, including the acceleration from rest at the start, may lead to a better evaluation of the relationship between muscle isometric force capacity and overall sprint performance. Finally, our model and simulation framework is not specific to maximum speed sprinting, and could be adapted to simulate other bipedal gaits to study the influence of muscle strengthening and weakness.

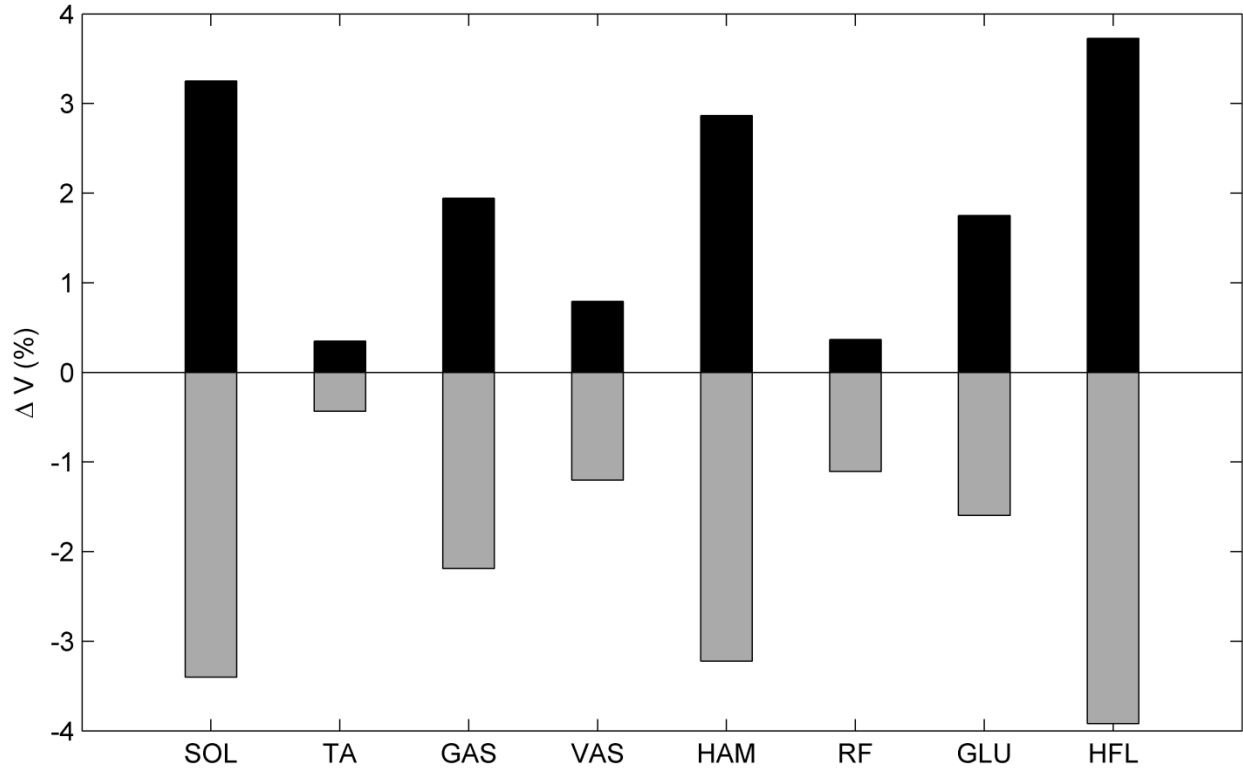


Figure 6-1 Percent change in maximum sprinting velocity over the nominal simulation for isolated positive (black bar) and negative (gray bar) perturbations of each muscle group.

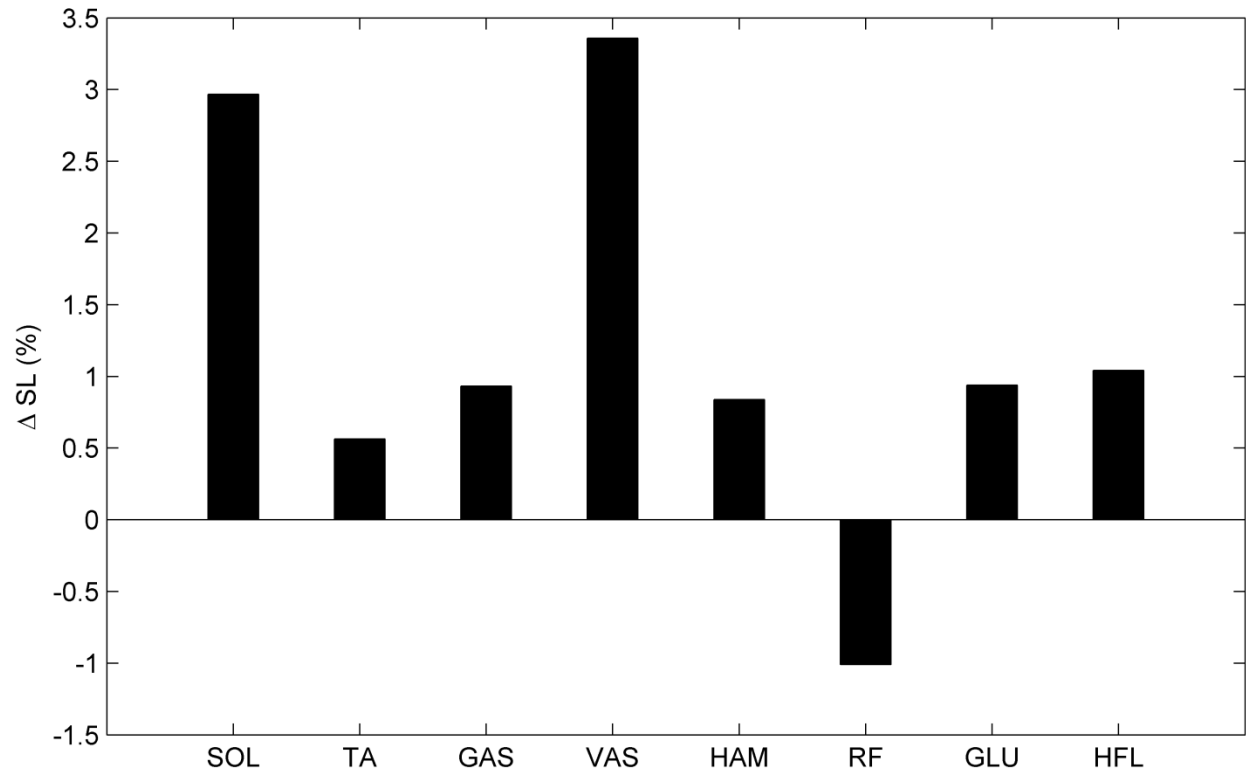


Figure 6-2 Percent change in stride length (SL) over the nominal simulation for isolated positive perturbation of each muscle group.

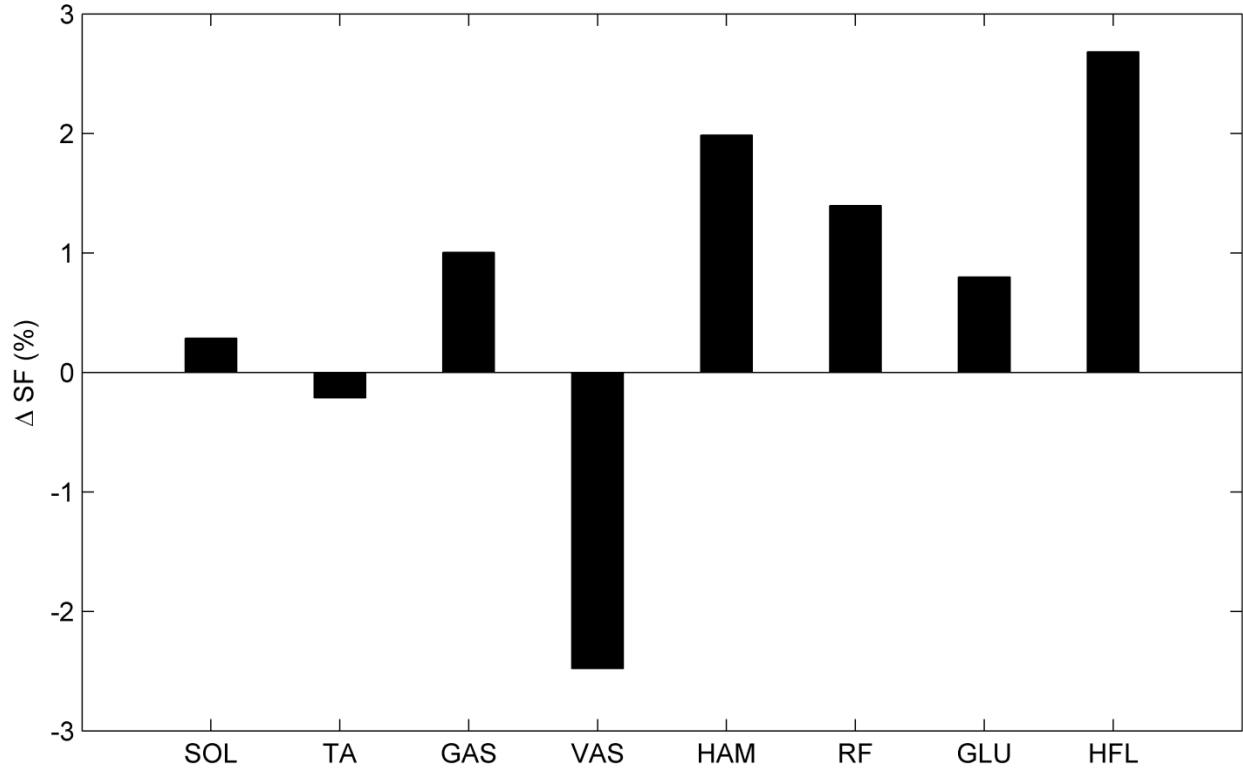


Figure 6-3 Percent change in stride frequency (SF) over the nominal simulation for isolated positive perturbation of each muscle group.

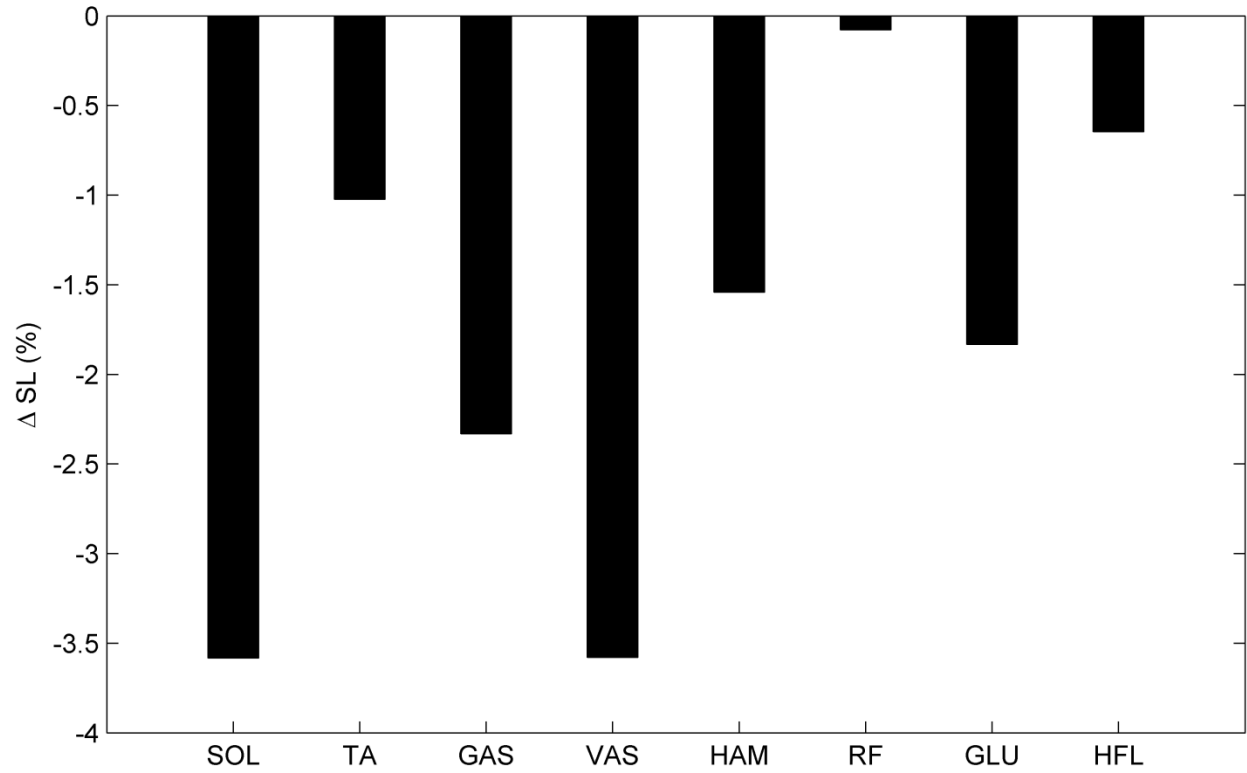


Figure 6-4 Percent change in stride length (SL) over the nominal simulation for isolated negative perturbation of each muscle group.

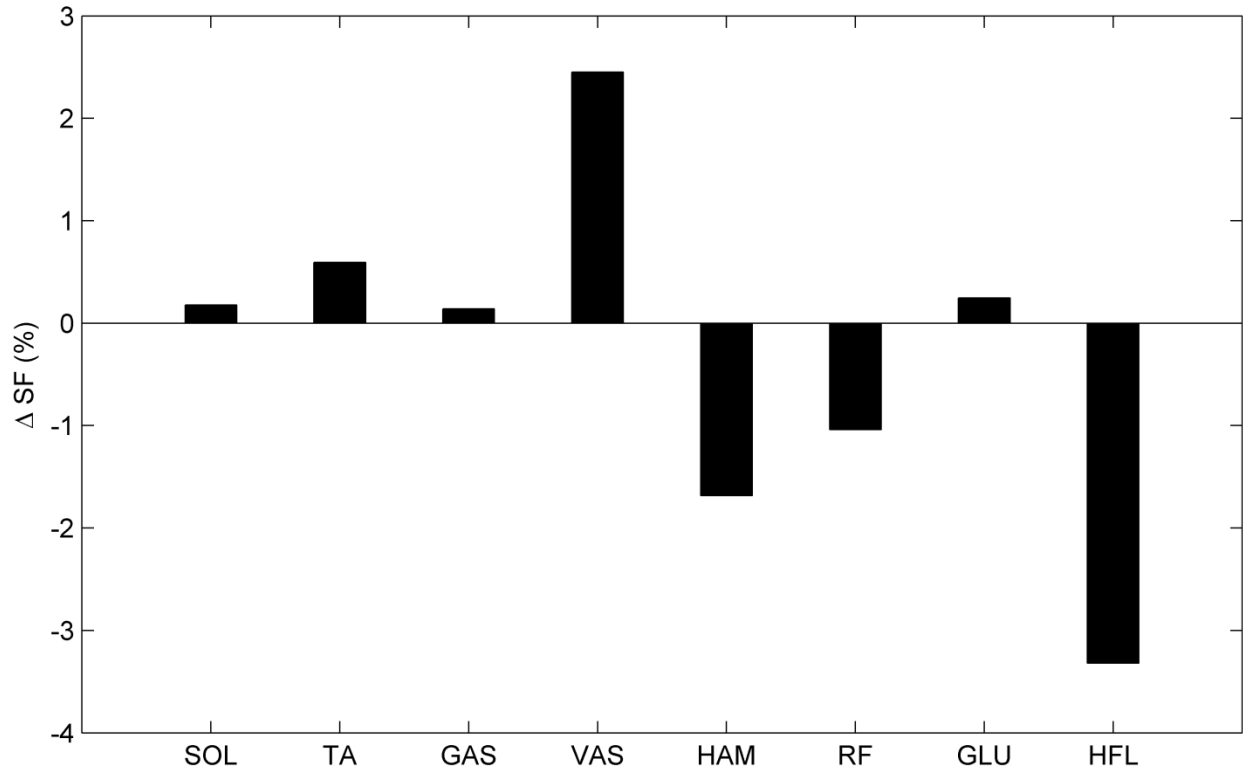


Figure 6-5 Percent change in stride frequency (SF) over the nominal simulation for isolated negative perturbation of each muscle group.

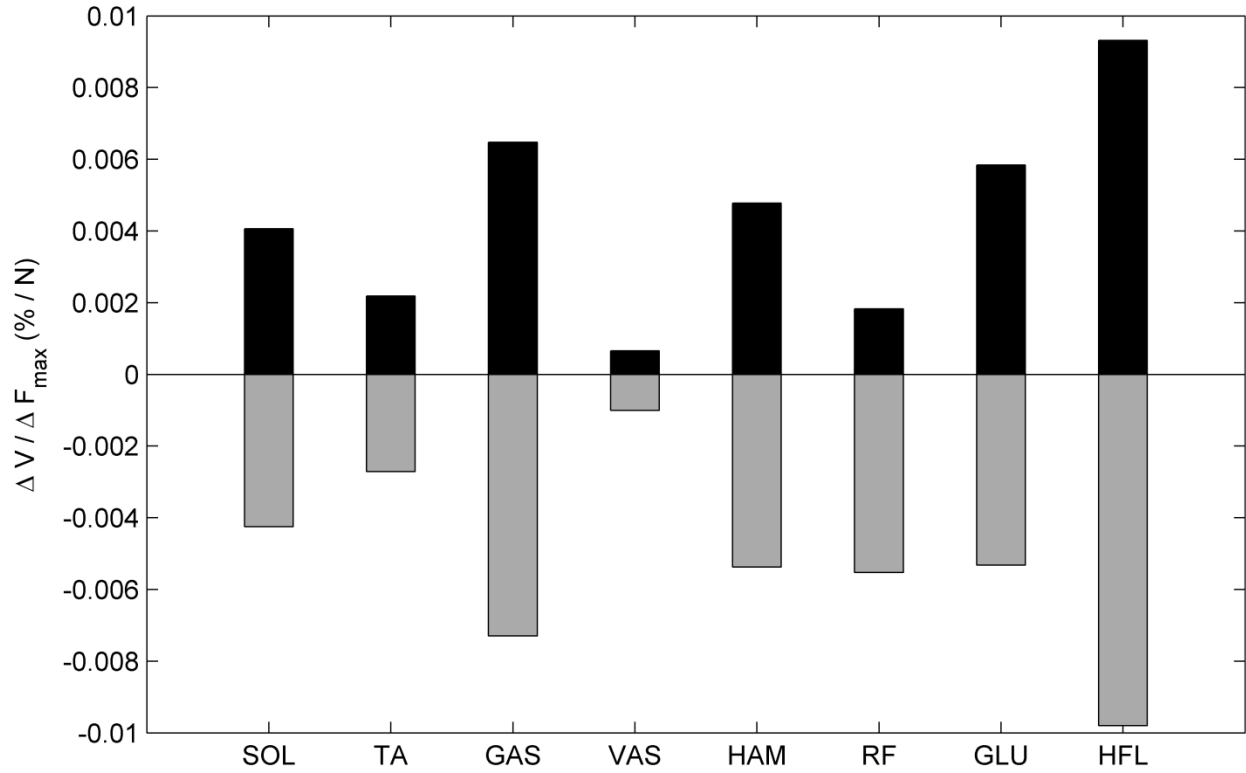


Figure 6-6 Percent change in maximum sprinting velocity scaled with the magnitude of the perturbation over the nominal simulation for isolated positive (black bar) and negative (gray bar) perturbations of each muscle group.

Chapter 7

Discussion

7.1 Summary

The purpose of this dissertation was to apply a model-based optimal controls approach to create novel simulations of bipedal gaits. These simulations were then used to evaluate new optimality criteria for predictive dynamic simulations of normal walking and investigate how variations in musculoskeletal architecture influence maximum-speed bipedal sprinting performance. Each of these simulations employed “multiple shooting” in the formulation of the optimal controls problem, which allowed for more robust solutions than what would have been possible using more conventional techniques.

The goal of our first study was to create a novel simulation of aperiodic sprinting. For that purpose, we developed a computer model of a modified bipedal spring-loaded inverted pendulum (SLIP) driven by torque actuators at the hip and force actuators acting on the model’s retracting legs. The objective of the simulation was to traverse a pre-specified distance from rest in minimum time. We formulated the optimization problem using the direct multiple shooting method (Betts, 2010), and the resulting nonlinear programming problem was solved iteratively using a sequential quadratic programming method, SNOPT (Gill, Murray, and Saunders, 2005), which is an efficient algorithm to solve trajectory optimization problems. The starting point for the optimizer was an initial guess simulation that was a slow alternating-gait jogging simulation developed using proportional-derivative feedback to control trunk attitude, swing leg angle, and leg retraction and extension (Raibert, 1986). Several gait features demonstrated in the optimized sprint simulation correspond to behaviors of human sprinters: forward trunk lean at the start;

straightening of the trunk during acceleration; and a dive at the finish. Although the minimized objective function was simple, the model replicated several complex behaviors such as modulation of the foot contact and executing a forward dive at the finish line. None of these observed behaviors were imposed explicitly by constraints but rather were discovered by the optimizer.

The goal of our second study was to create predictive dynamics simulations of normal bipedal walking with a planar musculoskeletal model and evaluate various optimality criteria. We developed a new hybrid approach, that is, initial guess to the optimizations were generated using a feedforward control that relied on muscle reflex loops (Geyer and Herr, 2010), and then with optimal controls we created predictive simulations. Unlike previous predictive dynamics simulations of normal bipedal walking with muscle-driven models (Anderson and Pandy, 2001; Ackermann and van den Bogert, 2010), our simulation did not depend on any experimental data explicitly. Our simulation results indicated that different effort terms derived from muscle activation, mechanical energy expenditure, and metabolic energy expenditure converge to different gait cycles in terms of EMG activity, metabolic energy expenditure, stride length and frequency. As observed in the previous predictive simulations of normal walking (Anderson and Pandy, 2001; Ren, Jones, and Howard, 2007; and Ackermann and van den Bogert, 2010), predictive simulations only driven by effort terms cause spikes in ground reaction force (GRF) and excessive trunk excursion. We included additional terms as vertical GRF and trunk angle to test their effect on simulation outcomes. The simulation results suggested that including those terms helped to lessen spikes in GRFs and confine trunk excursion to a narrow band as observed on normal human walking. The hybrid approach we develop to create the simulations showed potential to be an efficient method to generate predictive simulations in general.

The goal of our third study was to create predictive dynamics simulations of maximum speed sprinting with a planar musculoskeletal model and investigate how variations in musculoskeletal architecture parameters of plantarflexors, namely, maximum isometric force, optimal fiber length, tendon stiffness, and moment arm influence maximum speed bipedal sprinting performance. The simulation framework and model were successful to reproduce salient features of human sprinting in maximum speed phase in terms of joint angles, joint moments, GRFs, and EMG activity with the nominal parameters. Our results suggested that positive perturbations to each parameter analyzed in the study positively influence maximum speed bipedal sprinting performance. Experimental studies compared morphology of sprinters and non-sprinters showed that sprinters have bigger leg muscles (e.g., Kubo et al., 2011), longer fascicle length (e.g., Abe et al., 2000), stiffer Achilles' tendons (e.g., Arampatzis et al., 2007), and smaller plantarflexor moment arms (e.g., Baxter et al., 2012). Therefore, our results were in line with the experimental findings for maximum isometric force, optimal fiber length, and tendon stiffness. On the other hand, unlike the experimental finding that indicates sprinters have smaller plantarflexor moment arms, the model with larger moment arms did perform better on maximum speed sprinting. Yet, performing better on maximum sprinting phase of sprinting may not reflect on overall 100 m or 200 m performance. Lee and Piazza (2009) simulated push-off phase of sprinting before reaching maximum speed phase and showed that having smaller plantarflexor moment arm favorable at that phase. Thus, smaller plantarflexor moment arms may be still advantageous for sprinters, because first strides are the ones that differentiate an elite sprint performance from a merely good one (Hunter et al., 2005).

The goal of our fourth study was to explore how variations in maximum isometric force capacity of muscles affect maximum speed bipedal sprinting performance. While we

hypothesised that larger muscle group as soleus and vasti would increment maximum sprinting speed most, hip flexors demonstrated the most potential to increase top speed. The model employed mechanisms similar to those observed in human sprinters to achieve higher speeds; that is, hip flexors and plantarflexors primarily modulated stride frequency and length respectively (Dorn et al., 2012). Surprisingly, vasti performed poor in terms of incrementing maximum sprinting velocity. It was suggested that quadriceps (rectus femoris and vasti muscle groups) were the largest contributor to braking and support during the braking phase of support in running (Hamner et al., 2010). Vasti muscle groups' braking and stabilizing function may be the reason that even being the strongest muscle in the simulations could not able to increase maximum sprinting velocity in the order of soleus or hip flexors. This idea should be further investigated.

7.2 Limitations and future work

Our simulations converged to feasible and optimal solutions but we could not be certain that the solutions found were global optima. While there is no direct or analytical way to test whether solutions are global, we did perturb the initial guess or solutions by adding some uniformly distributed random noise, and then re-optimized. In each case, the re-optimized solutions were nearly identical to the original solutions. In many cases we were able to compare the simulation results to the experimental measurements of walking and sprinting from reports in the literature and in general there was good agreement between simulation and experiment. It is anticipated that further studies will be focused on developing new approaches to formulating the optimization problem, perhaps for example using evolutionary algorithms to solve the optimization problem. Generating solutions using different solvers will allow solutions from the

various approaches to be compared so that the most appropriate solution methods can be identified.

We created aperiodic bipedal sprinting simulations with a torque and force-driven spring-loaded inverted pendulum model (Chapter 3). We tried to extend that simulation by creating an aperiodic muscle-driven model with ankle and knee joints. Unfortunately, this effort was not successful; we could not find solutions that altered the number of steps taken by the model from the number used in the initial guess sprint. One future alternative that may be more successful is to employ a feedback or feedforward control that would reproduce bipedal sprinting followed by optimal tuning of the parameters defining the controller.

We used a planar musculoskeletal model driven by eight muscles on each leg to create maximum speed sprinting simulations. This simple model would be improved by addition of a pelvis segment which would enable simulation of out-of-plane motions. Another way in which the model's complexity could be enhanced is the addition of more muscles, especially those important to out-of-plane motions. In addition, the model had only two possible contact points on each foot, at the ball of the foot and heel. Adding a toe segment and another contact point would add to the realism of the push-off that occurs in late stance phase of both walking and running gaits. It is also known that elastic energy storage is critical for steady-state running so it may be useful to include additional elements to the foot segment to represent energy storage in the spring ligament and plantar fascia to better estimate energy expenditure in running. Finally, we did not model the effects of air friction on the body; this drag force has been calculated to be approximately 6.7 N for running at 6.1 m/s (McIlveen, 2002).

To develop the musculoskeletal model, we used data compiled from measurements made in human cadavers. There are of course differences between young athletic living subjects and

cadavers from donors who are often much older, and experimental data suggest that there are stereotypical differences in musculoskeletal architecture between sprinters and non-sprinters. A more appropriate set of model parameters for the sprinter models might be obtained by collecting experimental medical image data from sprinters. Finally, we studied the influence of variation in a particular set of musculoskeletal architecture parameters upon maximum sprinting speed. Other parameters, however, have the potential to affect maximum sprinting speed to some extent, and future studies may expand the current set of parameters to investigate that relationship.

We created normal bipedal walking simulations with various optimality criteria. As effort terms alone were not successful to reproduce all salient features of human walking, we proposed two new criteria: trunk angle and vertical GRF. They helped to lessen some undesired behaviors but those terms would generally be considered to be the outputs of the motor behavior. In this respect, controlling these variables is somewhat like performing a simulation in which experimental movements or forces are “tracked”. Therefore, future research might evaluate different criteria such as comfort, safety, and disturbance rejection that have possible potential to help reproduce desired behavior without using such output variables. In addition, the simulations described in this thesis did not include a complete evaluation of all possible exponents and weighting factors combinations; future research may evaluate a more exhaustively complete set of such parameters.

In our fourth study, we studied how variation in the maximum isometric force capacity of muscles affects maximum speed bipedal sprinting performance. Based on the simulation results, we made some inferences about muscle function during maximum speed sprinting phase. Muscle-induced acceleration analysis has been used by previous researchers to assess muscle function similarly during walking and running. The current results could be compared directly

with the results of muscle-induced acceleration analysis if the latter were performed using the same simulation results.

7.3 Conclusion

This dissertation presents the first example of an aperiodic sprinting simulation from rest.

Another important novel modeling achievement is the hybrid approach we used to create normal bipedal walking simulations. With those simulations, we demonstrated that optimality criteria based on effort alone may fall short when it comes to reproducing some important features of normal human walking. Additional optimality criteria such as vertical GRF and trunk angle, however, helped to reduce some undesired behaviors in predictive walking simulations. The results of maximum speed sprinting simulations suggested that sprinting performance would be enhanced by increasing maximum isometric force, optimal fiber length, tendon stiffness, and moment arm for the plantarflexors. When plantarflexor properties were augmented in these ways, the musculoskeletal model employed mechanisms similar to those observed in human sprinters to attain higher speeds. It is hoped that in the future the models and simulation frameworks described in this thesis will be used to create predictive simulations of other bipedal gaits.

Appendix A

Simple biped properties and parameters

The upper triangle of the symmetric mass matrix \mathbf{M} (Equation 3.3) is given by

$$\mathbf{M} = \begin{bmatrix} m_{body} & 0 & m_f \sin \theta_R & m_f \sin \theta_L & (m_f l_R + m_{leg} z_{leg}) \cos \theta_R & (m_f l_L + m_{leg} z_{leg}) \cos \theta_L & -m_t z_t \cos \theta_t \\ & m_{body} & -m_f \cos \theta_R & -m_f \cos \theta_L & (m_f l_R + m_{leg} z_{leg}) \sin \theta_R & (m_f l_L + m_{leg} z_{leg}) \sin \theta_L & -m_t z_t \sin \theta_t \\ & & m_f & 0 & 0 & 0 & 0 \\ & & & m_f & 0 & 0 & 0 \\ & & & & m_{leg} z_{leg}^2 + m_f l_R^2 + I_{leg} & 0 & 0 \\ & & & & & m_{leg} z_{leg}^2 + m_f l_L^2 + I_{leg} & 0 \\ & & & & & & m_t z_t^2 + I_t \end{bmatrix}$$

where

$$m_{body} = m_t + 2m_{leg} + 2m_f$$

The elements of \mathbf{f} , the right hand-side of Equation 3.3, are given by:

$$\begin{aligned} \mathbf{f}_1 &= -2m_f \cos \theta_R \dot{\theta}_R \dot{l}_R - 2m_f \cos \theta_L \dot{\theta}_L \dot{l}_L + (m_f l_R + m_{leg} z_{leg}) \sin \theta_R \dot{\theta}_R^2 + \dots \\ & (m_f l_L + m_{leg} z_{leg}) \sin \theta_L \dot{\theta}_L^2 - m_t z_t \sin \theta_t \dot{\theta}_t^2 - GRF_{xR} - GRF_{xL} \\ \mathbf{f}_2 &= -2m_f \sin \theta_R \dot{\theta}_R \dot{l}_R - 2m_f \sin \theta_L \dot{\theta}_L \dot{l}_L - (m_f l_R + m_{leg} z_{leg}) \cos \theta_R \dot{\theta}_R^2 - \dots \\ & (m_f l_L + m_{leg} z_{leg}) \cos \theta_L \dot{\theta}_L^2 + m_t z_t \cos \theta_t \dot{\theta}_t^2 + GRF_{yR} + GRF_{yL} + m_{body} g \\ \mathbf{f}_3 &= m_f l_R \dot{\theta}_R^2 + m_f g \cos \theta_R - k_{leg} (l_R - l_0) - b_{leg} \dot{l}_R + F_R - GRF_{xR} \sin \theta_R - GRF_{yR} \cos \theta_R \\ \mathbf{f}_4 &= m_f l_L \dot{\theta}_L^2 + m_f g \cos \theta_L - k_{leg} (l_L - l_0) - b_{leg} \dot{l}_L + F_L - GRF_{xL} \sin \theta_L - GRF_{yL} \cos \theta_L \\ \mathbf{f}_5 &= -2m_f l_R \dot{\theta}_R \dot{l}_R - (m_f l_R + m_{leg} z_{leg}) g \sin \theta_R - GRF_{xR} l_R \cos \theta_R + GRF_{yR} l_R \sin \theta_R + T_R \\ \mathbf{f}_6 &= -2m_f l_L \dot{\theta}_L \dot{l}_L - (m_f l_L + m_{leg} z_{leg}) g \sin \theta_L - GRF_{xL} l_L \cos \theta_L + GRF_{yL} l_L \sin \theta_L + T_L \\ \mathbf{f}_7 &= m_t g z_t \sin \theta_t - T_R - T_L \end{aligned}$$

Values for constants appearing in the above expressions are:

Masses:

$$m_{body} = 11.98 \text{ kg}, m_t = 0.6594 \cdot m_{body}, m_{leg} = 0.1569 \cdot m_{body}, m_f = 0.0134 \cdot m_{body}$$

Lengths:

$$l_0 = 1.00 \text{ m}, z_t = 0.34 \cdot l_0 \text{ m}, z_{\text{leg}} = 0.38 \cdot l_0 \text{ m}$$

Moments of inertia:

$$I_t = 0.1110 \cdot m_{\text{body}} \cdot l_0^2 \text{ kg} \cdot \text{m}^2, I_{\text{leg}} = 0.0326 \cdot m_{\text{body}} \cdot l_0^2 \text{ kg} \cdot \text{m}^2$$

Leg stiffness and damping:

$$k_{\text{leg}} = 10^3 \text{ N/m}, b_{\text{leg}} = 10^2 \text{ N/m}$$

Foot-floor contact model parameters:

$$a = 5 \times 10^7 \text{ N/m}^3, b = 0.75 \text{ s/m}, c = 50 \text{ s/m}, \mu = 0.6, s = 0.05$$

The lower (LB) and upper (UB) bounds on the actuators and generalized coordinate variables

(the order was as in Equations 3.1 and 3.2; first the controls, then the coordinates):

$$\mathbf{LB} = [-140 \quad -140 \quad -400 \quad -400 \quad -0.5 \quad 0.7 \quad 0.7 \quad 0.7 \quad -\pi/2 \quad -\pi/2 \quad -\pi/2]^T$$

$$\mathbf{UB} = [140 \quad 140 \quad 400 \quad 400 \quad 21 \quad 1.3 \quad 1.3 \quad 1.3 \quad \pi/2 \quad \pi/2 \quad \pi/2]^T$$

Appendix B

Musculoskeletal biped properties and parameters

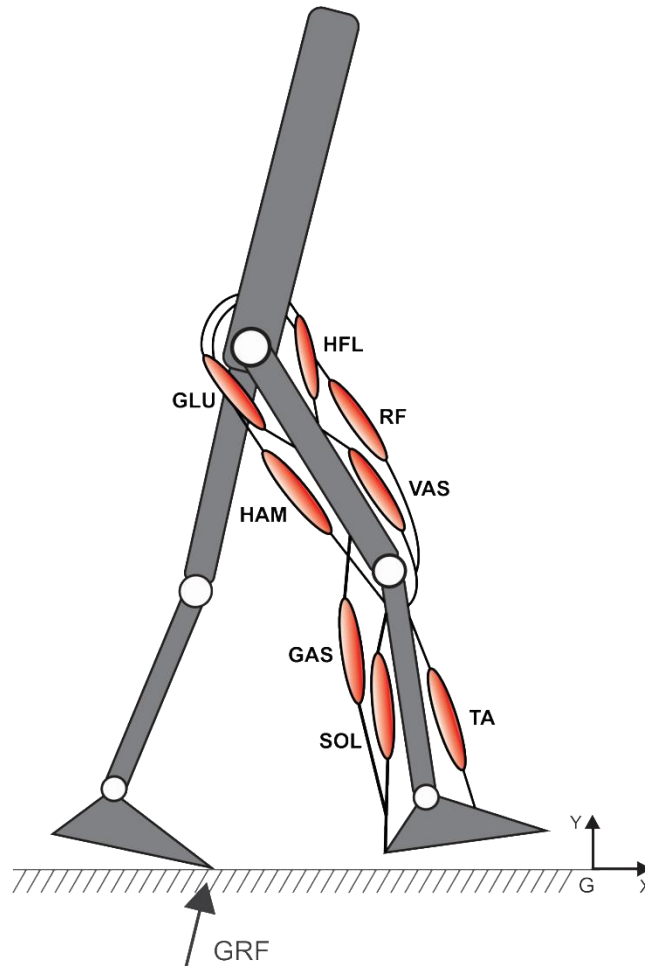
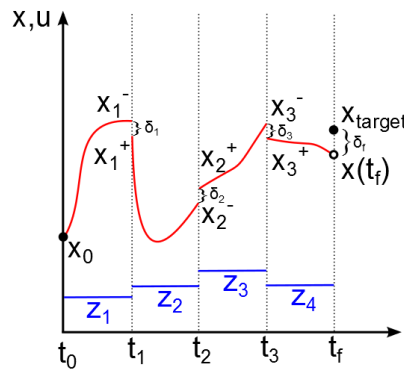
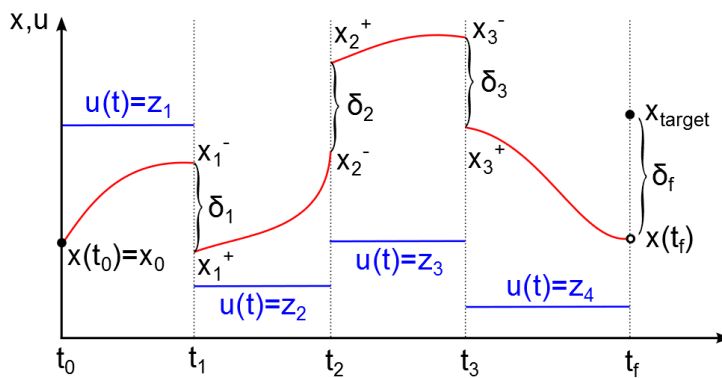
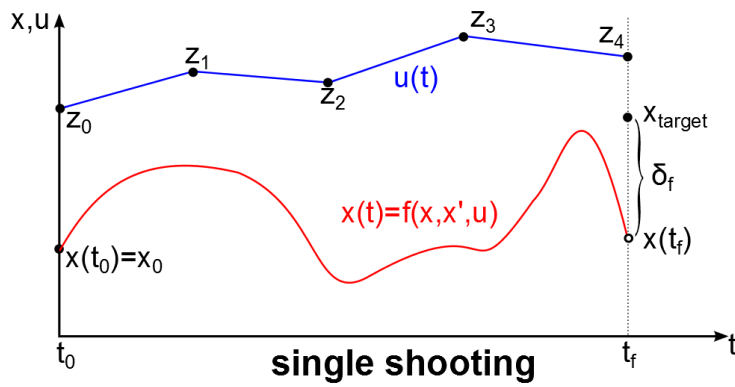


Figure B-1. The musculoskeletal bipedal model. The planar model was actuated by eight major Hill-type muscle groups on each leg: soleus (SOL), tibialis anterior (TA), gastrocnemius (GAS), vasti (VAS), hamstrings (HAM), rectus femoris (RF), glutei (GLU), and hip flexors (HFL). The model had nine degrees-of-freedom: right and left ankle, knee, and hip angles; the x- and y-positions of the hip; and the trunk angle. Seven body segments made up the model: the trunk and the right and left thighs, shanks, and feet which were articulated with revolute joints at the ankle, knee, and hip and a planar joint between hip and ground.



multiple shooting

$$\begin{aligned} &\min t_f \\ &\text{subject to} \\ &\forall \delta < \varepsilon \end{aligned}$$

Figure B-2. Illustration of optimization problem formulation using direct single shooting (*top*) and direct multiple shooting (*middle and bottom*). Multiple shooting entails minimization of an objective function (time in this case) subject to constraints corresponding to interinterval continuity.

The force on the MT actuator (F_{mt}) is given by

$$F_{mt} = F_{see} = F_{ce} + F_{hpe} - F_{lpe}$$

where F_{see} is the force on the series elastic element

$$F_{see} = \begin{cases} (\varepsilon / \varepsilon_{ref})^2 & \text{if } \varepsilon > 0 \\ 0 & \text{if } \varepsilon \leq 0 \end{cases}$$

where $\varepsilon_{ref} = 0.04$ is the reference strain, and ε is the normalized tendon strain

$$\varepsilon = \frac{l_{mt} - l_m}{l_{slack}} - 1$$

F_{hpe} is the force on the parallel elastic element

$$F_{hpe} = \begin{cases} F_{max} \left(\frac{\bar{l}_m - 1}{w} \right)^2 & \text{if } \bar{l}_m > 1 \\ 0 & \text{if } \bar{l}_m \leq 1 \end{cases}$$

where F_{max} is the maximum isometric force, and w is the width of the bell-shaped force-length function.

F_{lpe} is the force on the parallel buffer elastic element

$$F_{lpe} = \begin{cases} F_{max} \left(\frac{\bar{l}_m - (1-w)}{w/2} \right)^2 & \text{if } \bar{l}_m - (1-w) < 0 \\ 0 & \text{if } \bar{l}_m - (1-w) \geq 0 \end{cases}$$

F_{ce} is the force on the active contractile element

$$F_{ce} = a F_{max} f_l(\bar{l}_m) f_v(\bar{v}_m)$$

where a is the muscle activation, f_l and f_v are force-length and muscle force-contraction velocity functions respectively

$$f_l(\bar{l}_m) = \exp\left(c \left| \frac{\bar{l}_m - 1}{w} \right|^3\right)$$

$$f_v(\bar{v}_m) = \begin{cases} \frac{1 - \bar{v}_m}{1 + K\bar{v}_m} & \text{if } \bar{v}_m < 0 \\ N + (N - 1) \frac{1 + \bar{v}_m}{7.56K\bar{v}_m - 1} & \text{if } \bar{v}_m \geq 0 \end{cases}$$

where \bar{l}_m is the muscle fiber length scaled by optimal fiber length (l_{opt}), \bar{v}_m is the muscle contraction velocity scaled by maximum contraction velocity (v_{max}), $K = 5$ is the shape factor, $c = 0.05$ is the residual force factor, $N = 1.5$ is the eccentric force enhancement.

The governing equation of muscle excitation-activation dynamics is given by (He et al., 1991)

$$\dot{a} = (u - a)(u/t_{act} + (1 - u)/t_{deact})$$

where $t_{act} = 0.01$ s and $t_{deact} = 0.04$ s are muscle activation and deactivation time constants, and u is muscle excitation or control.

The passive joint moments are described as

$$M_{passive} = \begin{cases} -k_3\theta - b_2\theta + k_4(\theta_{min} - \theta)^2 & \text{if } \theta_{min} > \theta \\ -k_3\theta - b_2\theta & \text{if } \theta_{max} > \theta > \theta_{min} \\ -k_3\theta - b_2\theta - k_4(\theta - \theta_{max})^2 & \text{if } \theta > \theta_{max} \end{cases}$$

where θ_{min} and θ_{max} define the range of joint angles (adapted from Norkin and White, 1995).

Table B-1. Joint angle ranges

	θ_{min} (deg)	θ_{max} (deg)
Ankle	-25	45
Knee	-155	5
Hip	-105	35

To calculate muscle moment arms and MT lengths, first joint angles (h :hip, k :knee, a :ankle) are converted into degrees after adding corresponding constants

$$\varphi_h = (\theta_h + \pi) \cdot (180 / \pi)$$

$$\varphi_k = (\theta_k + \pi) \cdot (180 / \pi)$$

$$\varphi_a = (\theta_a + \pi/2) \cdot (180 / \pi)$$

The muscle moment arms are modelled with the following equations:

For hip muscles

$$r_m = r_0$$

For knee muscles

$$r_m = r_0 \cos(\varphi_k - \varphi_{\max})$$

For ankle muscles

$$r_m = r_0 \cos(\varphi_a - \varphi_{\max})$$

where r_0 is the moment arm value at φ_{\max} (Table B-2).

The changes in the MT lengths are modelled with the following equations:

For hip muscles

$$\Delta l_{mt} = \rho r_0 (\varphi_h - \varphi_{ref})$$

For knee muscles

$$\Delta l_{mt} = \rho r_0 [\sin(\varphi_k - \varphi_{\max}) - \sin(\varphi_{ref} - \varphi_{\max})]$$

For ankle muscles

$$\Delta l_{mt} = \rho r_0 [\sin(\varphi_a - \varphi_{\max}) - \sin(\varphi_{ref} - \varphi_{\max})]$$

where ρ accounts for pennation angle, φ_{ref} is the joint angle at which $l_{mt} = l_{opt} + l_{slack}$ where l_{slack} is the tendon slack length (Table B-3).

Table B-2. MT attachment parameters

	Ankle			Knee				Hip			
	SOL	TA	GAS	GAS	VAS	HAM	RF	HAM	RF	GLU	HFL
r_0 (cm)	5	4	5	5	6	5	6	8	10	10	10
φ_{\max} (deg)	20	80	110	140	165	180	165	-	-	-	-
φ_{ref} (deg)	80	110	80	165	125	180	125	155	180	150	180
ρ	0.5	0.7	0.7	0.7	0.7	0.7	0.7	0.7	0.7	0.5	0.5

Table B-3. Individual MT parameters

	SOL	TA	GAS	VAS	HAM	RF	GLU	HFL
F_{max} (N)	4000	800	1500	6000	3000	1000	1500	2000
v_{max} (l_{opt}/s)	12	12	12	12	12	12	12	12
l_{opt} (cm)	4	6	5	8	10	8	11	11
l_{slack} (cm)	26	24	40	23	31	30	13	10

Table B-4 presents model segment parameters (mass, length, inertia).

Table B-4. Model segment parameters

	mass (kg)	length (cm)	inertia (kg/m^2)
Trunk	50.8500	84.62	3.1777
Thigh	7.5000	44.10	0.1522
Shank	3.4875	44.28	0.0624
Foot	1.0875	7.00	0.0184

In the optimization problems (Chapter 4, 5, and 6), the lower and upper bounds for velocity states are -25 and +25. The lower and upper bounds for muscle fiber lengths are $0.25 \cdot l_{opt}$ and $1.35 \cdot l_{opt}$. The lower and upper bounds for x and y position, trunk angle; and ankle, knee, and hip angles of left and right legs are

$$\mathbf{LB} = [-0.1, 0.85, -120 \cdot d2r, -20 \cdot d2r, -150 \cdot d2r, -100 \cdot d2r, -20 \cdot d2r, -150 \cdot d2r, -100 \cdot d2r]^T$$

$$\mathbf{UB} = [2 \cdot s_{l,i}, 1.0, 120 \cdot d2r, 40 \cdot d2r, 0, 30 \cdot d2r, 40 \cdot d2r, 0, 30 \cdot d2r]^T$$

where $d2r = \pi/180$ is a constant, and $s_{l,i}$ is the step length of gait in the initial guess simulation.

The foot-ground contact model parameters are

$$k_1 = 1 \text{ N}^{-1}; k_2 = 5e7 \text{ Nm}^{-3}; b = 1 \text{ sm}^{-1}; \mu = 1; c = 50$$

The contact point coordinates (Winter, 2005; Ackermann and van den Bogert, 2010) in the muscle-driven sprinting simulations with respect to the ankle (in centimeters)

$$\text{Heel: } X = -0.06, Y = -0.07; \text{ Ball of the foot: } X = 0.15, Y = -0.07$$

The contact point coordinates in the walking simulation with respect to the ankle (in centimeters)

$$X = -0.06 + 0.021 \cdot i, i = 0 \dots 10; Y = -0.07$$

References

- Abdallah, Muhammad E., and Kenneth J. Waldron. 2008. "The Mechanics of Biped Running and a Stable Control Strategy." *Robotica* 27 (05): 789. doi:10.1017/S0263574708005134.
- Abe, Takashi, Senshi Fukashiro, Yasuhiro Harada, and Kazuhisa Kawamoto. 2001. "Relationship Between Sprint Performance and Muscle Fascicle Length in Female Sprinters." *Journal of Physiological Anthropology and Applied Human Science* 20 (2): 141–47.
- Abe, Takashi, Kenya Kumagai, and William F Brechue. 2000. "Fascicle Length of Leg Muscles Is Greater in Sprinters than Distance Runners." *Medicine and Science in Sports and Exercise* 32 (6): 1125–29.
- Ackermann, Marko, and Antonie J. van den Bogert. 2010. "Optimality Principles for Model-Based Prediction of Human Gait." *Journal of Biomechanics* 43 (6): 1055–60. doi:10.1016/j.jbiomech.2009.12.012.
- Ackermann, Marko, and Antonie J. van den Bogert. 2012. "Predictive Simulation of Gait at Low Gravity Reveals Skipping as the Preferred Locomotion Strategy." *Journal of Biomechanics* 45 (7): 1293–98. doi:10.1016/j.jbiomech.2012.01.029.
- Albracht, K., A. Arampatzis, and V. Baltzopoulos. 2008. "Assessment of Muscle Volume and Physiological Cross-Sectional Area of the Human Triceps Surae Muscle in Vivo." *Journal of Biomechanics* 41 (10): 2211–18. doi:10.1016/j.jbiomech.2008.04.020.
- Albro, J.V., G.A. Sohl, J.E. Bobrow, and F.C. Park. 2000. "On the Computation of Optimal High-Dives." In *Robotics and Automation, 2000. Proceedings. ICRA '00. IEEE International Conference on*, 4:3958–63.
- Alexander, M.J. 1989. "The Relationship between Muscle Strength and Sprint Kinematics in Elite Sprinters." *Canadian Journal of Sport Sciences= Journal Canadien Des Sciences Du Sport* 14 (3): 148–57.
- Alexander, R. McN. 1980. "Optimum Walking Techniques for Quadrupeds and Bipeds." *Journal of Zoology* 192 (1): 97–117. doi:10.1111/j.1469-7998.1980.tb04222.x.
- Alexander, R.M.N. 1992. "A Model of Bipedal Locomotion on Compliant Legs." *Philosophical Transactions of the Royal Society of London. Series B: Biological Sciences* 338 (1284): 189–98.
- Anderson, Frank C., and Marcus G. Pandy. 2001a. "Dynamic Optimization of Human Walking." *Journal of Biomechanical Engineering* 123 (5): 381. doi:10.1115/1.1392310.
- Anderson, Frank C., and Marcus G. Pandy. 2001b. "Static and Dynamic Optimization Solutions for Gait Are Practically Equivalent." *Journal of Biomechanics* 34 (2): 153–61. doi:10.1016/S0021-9290(00)00155-X.
- Anderson, Frank C., and Marcus G. Pandy. 2003. "Individual Muscle Contributions to Support in Normal Walking." *Gait & Posture* 17 (2): 159–69. doi:10.1016/S0966-6362(02)00073-5.
- Arampatzis, Adamantios, Kiros Karamanidis, Gaspar Morey-Klapsing, Gianpiero De Monte, and Savvas Stafilidis. 2007. "Mechanical Properties of the Triceps Surae Tendon and Aponeurosis in Relation to Intensity of Sport Activity." *Journal of Biomechanics* 40 (9): 1946–52. doi:10.1016/j.jbiomech.2006.09.005.
- Baumann, W. 1976. "Kinematic and Dynamic Characteristics of the Sprint Start." *Biomechanics V Vol. B*, 194–99.
- Baxter, J. R., T. A. Novack, H. Van Werkhoven, D. R. Pennell, and S. J. Piazza. 2012. "Ankle

- Joint Mechanics and Foot Proportions Differ between Human Sprinters and Non-Sprinters.” *Proceedings of the Royal Society B: Biological Sciences* 279 (1735): 2018–24. doi:10.1098/rspb.2011.2358.
- Baxter, Josh R., and Stephen J. Piazza. 2014. “Plantar Flexor Moment Arm and Muscle Volume Predict Torque-Generating Capacity in Young Men.” *Journal of Applied Physiology* 116 (5): 538–44. doi:10.1152/jappphysiol.01140.2013.
- Betts, John T. 2010. *Practical Methods for Optimal Control and Estimation Using Nonlinear Programming*. Philadelphia: Society for Industrial and Applied Mathematics.
- Betts, John T. 1998. “Survey of Numerical Methods for Trajectory Optimization.” *Journal of Guidance, Control, and Dynamics* 21 (2): 193–207. doi:10.2514/2.4231.
- Blazevich, Anthony J., David R. Coleman, Sara Horne, and Dale Cannavan. 2009. “Anatomical Predictors of Maximum Isometric and Concentric Knee Extensor Moment.” *European Journal of Applied Physiology* 105 (6): 869–78. doi:10.1007/s00421-008-0972-7.
- Blickhan, R. 1989. “The Spring-Mass Model for Running and Hopping.” *Journal of Biomechanics* 22 (11): 1217–27.
- Bobbert, Maarten F, and Arthur J Van Soest. 1994. “Effects of Muscle Strengthening on Vertical Jump Height: A Simulation Study.” *Medicine and Science in Sports and Exercise* 26 (8): 1012–20.
- Bodine, S. C., R. R. Roy, D. A. Meadows, R. F. Zernicke, R. D. Sacks, M. Fournier, and V. R. Edgerton. 1982. “Architectural, Histochemical, and Contractile Characteristics of a Unique Biarticular Muscle: The Cat Semitendinosus.” *Journal of Neurophysiology* 48 (1): 192–201.
- Bret, C, A Rahmani, AB Dufour, L Messonnier, and JR Lacour. 2002. “Leg Strength and Stiffness as Ability Factors in 100 M Sprint Running.” *The Journal of Sports Medicine and Physical Fitness* 42 (3): 274–81.
- Burdett, Ray G., Gary S. Skrinar, and Sheldon R. Simon. 1983. “Comparison of Mechanical Work and Metabolic Energy Consumption during Normal Gait.” *Journal of Orthopaedic Research* 1 (1): 63–72. doi:10.1002/jor.1100010109.
- Carrier, David R., Norman C. Heglund, and Kathleen D. Earls. 1994. “Variable Gearing During Locomotion in the Human Musculoskeletal System.” *Science, New Series*, 265 (5172): 651–53.
- Cavanagh, Peter R., and Rodger Kram. 1989. “Stride Length in Distance Running: Velocity, Body Dimensions, and Added Mass Effects.” *Medicine and Science in Sports and Exercise* 21 (4): 467–79.
- Celik, Huseyin, and Stephen J. Piazza. 2013. “Simulation of Aperiodic Bipedal Sprinting.” *Journal of Biomechanical Engineering* 135 (8): 081008–081008. doi:10.1115/1.4024577.
- Chao, E. Y., R. K. Laughman, E. Schneider, and R. N. Stauffer. 1983. “Normative Data of Knee Joint Motion and Ground Reaction Forces in Adult Level Walking.” *Journal of Biomechanics* 16 (3): 219–33. doi:10.1016/0021-9290(83)90129-X.
- Cheng, H., C. Yu, and K. Cheng. 2009. “Computer Simulation of the Optimal Vaulting Motion during the Horse (table) Contact Phase.” In *ISBS-Conference Proceedings Archive*. Vol. 1.
- Chow, C.K., and D.H. Jacobson. 1971. “Studies of Human Locomotion via Optimal Programming.” *Mathematical Biosciences* 10 (3–4): 239–306. doi:10.1016/0025-5564(71)90062-9.
- Čoh, Milan, Bojan Jošt, Branko Škof, Katja Tomažin, and Aleš Dolenc. 1998. “Kinematic and

- Kinetic Parameters of the Sprint Start and Start Acceleration Model of Top Sprinters.” *Gymnica* 28: 33–42.
- Collins, J. J., and M. W. Whittle. 1989. “Impulsive Forces during Walking and Their Clinical Implications.” *Clinical Biomechanics* 4 (3): 179–87. doi:10.1016/0268-0033(89)90023-5.
- Collins, S., Andy Ruina, R. Tedrake, and Martijn Wisse. 2005. “Efficient Bipedal Robots Based on Passive-Dynamic Walkers.” *Science* 307 (5712): 1082–85. doi:10.1126/science.1107799.
- Collins, Steven H., Martijn Wisse, and Andy Ruina. 2001. “A Three-Dimensional Passive-Dynamic Walking Robot with Two Legs and Knees.” *The International Journal of Robotics Research* 20 (7): 607–15. doi:10.1177/02783640122067561.
- Costill, DL, J Daniels, W Evans, W Fink, G Krahenbuhl, and B Saltin. 1976. “Skeletal Muscle Enzymes and Fiber Composition in Male and Female Track Athletes.” *Journal of Applied Physiology* 40 (2): 149–54.
- Crowninshield, Roy D., and Richard A. Brand. 1981. “A Physiologically Based Criterion of Muscle Force Prediction in Locomotion.” *Journal of Biomechanics* 14 (11): 793–801. doi:10.1016/0021-9290(81)90035-X.
- Davy, D. T., and M. L. Audu. 1987. “A Dynamic Optimization Technique for Predicting Muscle Forces in the Swing Phase of Gait.” *Journal of Biomechanics* 20 (2): 187–201. doi:10.1016/0021-9290(87)90310-1.
- Deane, Russell S, John W Chow, Mark D Tillman, and Kim A Fournier. 2005. “Effects of Hip Flexor Training on Sprint, Shuttle Run, and Vertical Jump Performance.” *The Journal of Strength & Conditioning Research* 19 (3): 615–21.
- Delp, S.L., F.C. Anderson, AS. Arnold, P. Loan, A Habib, C.T. John, E. Guendelman, and D.G. Thelen. 2007. “OpenSim: Open-Source Software to Create and Analyze Dynamic Simulations of Movement.” *IEEE Transactions on Biomedical Engineering* 54 (11): 1940–50. doi:10.1109/TBME.2007.901024.
- Diehl, M., H.G. Bock, H. Diedam, and P.-B. Wieber. 2006. “Fast Direct Multiple Shooting Algorithms for Optimal Robot Control.” In , edited by Moritz Diehl and Katja Mombaur, 340:65–93. Lecture Notes in Control and Information Sciences. Springer Berlin / Heidelberg. http://dx.doi.org/10.1007/978-3-540-36119-0_4.
- Dorn, Tim W., Anthony G. Schache, and Marcus G. Pandy. 2012. “Muscular Strategy Shift in Human Running: Dependence of Running Speed on Hip and Ankle Muscle Performance.” *The Journal of Experimental Biology* 215 (11): 1944–56. doi:10.1242/jeb.064527.
- Eriksen, H. K., J. R. Kristiansen, O. Langangen, and I. K. Wehus. 2009. “Velocity Dispersions in a Cluster of Stars: How Fast Could Usain Bolt Have Run?” *American Journal of Physics* 77 (3): 224. doi:10.1119/1.3033168.
- Garcia, M., A. Chatterjee, A. Ruina, and M. Coleman. 1998. “The Simplest Walking Model: Stability, Complexity, and Scaling.” *Journal of Biomechanical Engineering* 120 (2): 281–88.
- Geyer, Hartmut, and Hugh Herr. 2010. “A Muscle-Reflex Model That Encodes Principles of Legged Mechanics Produces Human Walking Dynamics and Muscle Activities.” *IEEE Transactions on Neural Systems and Rehabilitation Engineering* 18 (3): 263–73. doi:10.1109/TNSRE.2010.2047592.
- Gilchrist, L.A., and David A. Winter. 1997. “A Multisegment Computer Simulation of Normal Human Gait.” *IEEE Transactions on Rehabilitation Engineering* 5 (4): 290–99.

- doi:10.1109/86.650281.
- Gill, Philip E., Walter Murray, and Michael A. Saunders. 2005. "SNOPT: An SQP Algorithm for Large-Scale Constrained Optimization." *SIAM Review* 47 (1): 99–131. doi:10.1137/S0036144504446096.
- Glitsch, U., and W. Baumann. 1997. "The Three-Dimensional Determination of Internal Loads in the Lower Extremity." *Journal of Biomechanics* 30 (11–12): 1123–31. doi:10.1016/S0021-9290(97)00089-4.
- Gomes, Mario, and Andy Ruina. 2011. "Walking Model with No Energy Cost." *Physical Review E* 83 (3): 032901. doi:10.1103/PhysRevE.83.032901.
- Gubina, Ferdinand, Hooshang Hemami, and R.B. Mcghee. 1974. "On the Dynamic Stability of Biped Locomotion." *IEEE Transactions on Biomedical Engineering* BME-21 (2): 102–8. doi:10.1109/TBME.1974.324294.
- Hamner, Samuel R., and Scott L. Delp. 2013. "Muscle Contributions to Fore-Aft and Vertical Body Mass Center Accelerations over a Range of Running Speeds." *Journal of Biomechanics* 46 (4): 780–87. doi:10.1016/j.jbiomech.2012.11.024.
- Hamner, Samuel R., Ajay Seth, and Scott L. Delp. 2010. "Muscle Contributions to Propulsion and Support during Running." *Journal of Biomechanics* 43 (14): 2709–16. doi:10.1016/j.jbiomech.2010.06.025.
- Harland, M. J., and J. R. Steele. 1997. "Biomechanics of the Sprint Start." *Sports Medicine* 23 (1): 11–20.
- Hast, Michael W., and Stephen J. Piazza. 2013. "Dual-Joint Modeling for Estimation of Total Knee Replacement Contact Forces During Locomotion." *Journal of Biomechanical Engineering* 135 (2): 021013–021013. doi:10.1115/1.4023320.
- Hay, James G. 1994. *The Biomechanics of Sports Techniques*. Englewood Cliffs, N.J.: Prentice-Hall.
- He, Jiping, W.S. Levine, and G.E. Loeb. 1991. "Feedback Gains for Correcting Small Perturbations to Standing Posture." *IEEE Transactions on Automatic Control* 36 (3): 322–32. doi:10.1109/9.73565.
- Hildebrand, Milton. 1960. "How Animals Run." *Scientific American* 202: 148–57.
- Hildebrand, Milton, and G. E Goslow. 2001. *Analysis of Vertebrate Structure*. New York: J. Wiley.
- Hudson, Penny E., Sandra A. Corr, Rachel C. Payne-Davis, Sinead N. Clancy, Emily Lane, and Alan M. Wilson. 2011a. "Functional Anatomy of the Cheetah (*Acinonyx Jubatus*) Forelimb." *Journal of Anatomy* 218 (4): 375–85. doi:10.1111/j.1469-7580.2011.01344.x.
- Hudson, Penny E., Sandra A. Corr, Rachel C. Payne-Davis, Sinead N. Clancy, Emily Lane, and Alan M. Wilson. 2011b. "Functional Anatomy of the Cheetah (*Acinonyx Jubatus*) Hindlimb." *Journal of Anatomy* 218 (4): 363–74. doi:10.1111/j.1469-7580.2010.01310.x.
- Hunter, J. P., R. N Marshall, and P. J McNair. 2005. "Relationships between Ground Reaction Force Impulse and Kinematics of Sprint-Running Acceleration." *Journal of Applied Biomechanics* 21 (1): 31–43.
- Hunter, J. P., R. N. Marshall, and P. J McNair. 2004. "Interaction of Step Length and Step Rate during Sprint Running." *Medicine & Science in Sports & Exercise February 2004* 36 (2): 261–71.
- Huxley, Andrew F. 1957. "Muscle Structure and Theories of Contraction." *Progress in Biophysics and Biophysical Chemistry* 7: 255–318.
- Kadaba, M. P., H. K. Ramakrishnan, M. E. Wootten, J. Gainey, G. Gorton, and G. V. B.

- Cochran. 1989. "Repeatability of Kinematic, Kinetic, and Electromyographic Data in Normal Adult Gait." *Journal of Orthopaedic Research* 7 (6): 849–60. doi:10.1002/jor.1100070611.
- Karamanidis, Kiros, Kirsten Albracht, Bjoern Braunstein, Maria Moreno Catala, Jan-Peter Goldmann, and Gert-Peter Brüggemann. 2011. "Lower Leg Musculoskeletal Geometry and Sprint Performance." *Gait & Posture* 34 (1): 138–41. doi:10.1016/j.gaitpost.2011.03.009.
- Kubo, Kanehisa, Kawakami, and Fukunaga. 2000. "Elasticity of Tendon Structures of the Lower Limbs in Sprinters." *Acta Physiologica Scandinavica* 168 (2): 327–35. doi:10.1046/j.1365-201x.2000.00653.x.
- Kubo, Keitaro, Toshihiro Ikebukuro, Hideaki Yata, Minoru Tomita, and Masaji Okada. 2011. "Morphological and Mechanical Properties of Muscle and Tendon in Highly Trained Sprinters." *Journal of Applied Biomechanics* 27 (4): 336–44.
- Kumagai, Kenya, Takashi Abe, William F Brechue, Tomoo Ryushi, Susumu Takano, and Masuhiko Mizuno. 2000. "Sprint Performance Is Related to Muscle Fascicle Length in Male 100-M Sprinters." *Journal of Applied Physiology* 88 (3): 811–16.
- Kuo, Arthur D. 2001. "Energetics of Actively Powered Locomotion Using the Simplest Walking Model." *Journal of Biomechanical Engineering* 124 (1): 113–20. doi:10.1115/1.1427703.
- Lee, S. S.M, and S. J Piazza. 2009. "Built for Speed: Musculoskeletal Structure and Sprinting Ability." *Journal of Experimental Biology* 212 (22): 3700–3707.
- Lieber, Richard L., and Jan Fridén. 2000. "Functional and Clinical Significance of Skeletal Muscle Architecture." *Muscle & Nerve* 23 (11): 1647–66. doi:10.1002/1097-4598(200011)23:11<1647::AID-MUS1>3.0.CO;2-M.
- Majumdar, Aditi, and Robert Robergs. 2011. "The Science of Speed: Determinants of Performance in the 100 M Sprint." *International Journal of Sports Science and Coaching* 6 (3): 479–94. doi:10.1260/1747-9541.6.3.479.
- Mann, Ralph. 2011. *The Mechanics of Sprinting and Hurdling*. S.l.: CreateSpace.
- Mann, Ralph, and Paul Sprague. 1980. "A Kinetic Analysis of the Ground Leg during Sprint Running." *Research Quarterly for Exercise and Sport* 51 (2): 334–48.
- Mann, Roger A., and John Hagy. 1980. "Biomechanics of Walking, Running, and Sprinting." *The American Journal of Sports Medicine* 8 (5): 345–50. doi:10.1177/036354658000800510.
- Marhefka, D.W., and D.E. Orin. 1999. "A Compliant Contact Model with Nonlinear Damping for Simulation of Robotic Systems." *Systems, Man and Cybernetics, Part A: Systems and Humans, IEEE Transactions on* 29 (6): 566–72.
- Maughan, R. J., Jennifer S. Watson, and J. Weir. 1983. "Relationships between Muscle Strength and Muscle Cross-Sectional Area in Male Sprinters and Endurance Runners." *European Journal of Applied Physiology and Occupational Physiology* 50 (3): 309–18. doi:10.1007/BF00423237.
- McGeer, T. 1990a. "Passive Dynamic Walking." *The International Journal of Robotics Research* 9 (2): 62–82. doi:10.1177/027836499000900206.
- McGeer, T. 1990b. "Passive Bipedal Running." *Proceedings of the Royal Society of London. B. Biological Sciences* 240 (1297): 107–34. doi:10.1098/rspb.1990.0030.
- McIlveen, J. F. R. 2002. "The Everyday Effects of Wind Drag on People." *Weather* 57 (11): 410–13. doi:10.1256/wea.29.02.
- McMahon, Thomas A. 1984. *Muscles, Reflexes, and Locomotion*. Princeton: Princeton

- University Press.
- Mero, A, PV Komi, and RJ Gregor. 1992. "Biomechanics of Sprint Running." *Sports Medicine* 13 (6): 376–92.
- Mero, A, P Luhtanen, JT Viitasalo, and PV Komi. 1981. "Relationships between the Maximal Running Velocity, Muscle Fiber Characteristics, Force Production and Force Relaxation of Sprinters." *Scand J Sports Sci* 3 (1): 16–22.
- Mero, A., and P. V Komi. 1990. "Reaction Time and Electromyographic Activity during a Sprint Start." *European Journal of Applied Physiology and Occupational Physiology* 61 (1): 73–80.
- Miller, Ross H., Brian R. Umberger, and Graham E. Caldwell. 2012b. "Limitations to Maximum Sprinting Speed Imposed by Muscle Mechanical Properties." *Journal of Biomechanics* 45 (6): 1092–97. doi:10.1016/j.jbiomech.2011.04.040.
- Miller, Ross H., Brian R. Umberger, and Graham E. Caldwell. 2012a. "Sensitivity of Maximum Sprinting Speed to Characteristic Parameters of the Muscle Force–velocity Relationship." *Journal of Biomechanics* 45 (8): 1406–13. doi:10.1016/j.jbiomech.2012.02.024.
- Miller, Ross H., Brian R. Umberger, Joseph Hamill, and Graham E. Caldwell. 2012c. "Evaluation of the Minimum Energy Hypothesis and Other Potential Optimality Criteria for Human Running." *Proceedings of the Royal Society B: Biological Sciences* 279 (1733): 1498–1505. doi:10.1098/rspb.2011.2015.
- Mochon, Simon, and Thomas A. McMahon. 1980. "Ballistic Walking." *Journal of Biomechanics* 13 (1): 49–57. doi:10.1016/0021-9290(80)90007-X.
- Nagano, Akinori, and Taku Komura. 2003. "Longer Moment Arm Results in Smaller Joint Moment Development, Power and Work Outputs in Fast Motions." *Journal of Biomechanics* 36 (11): 1675–81. doi:10.1016/S0021-9290(03)00171-4.
- Neptune, R. R., S. A. Kautz, and F. E. Zajac. 2001. "Contributions of the Individual Ankle Plantar Flexors to Support, Forward Progression and Swing Initiation during Walking." *Journal of Biomechanics* 34 (11): 1387–98. doi:10.1016/S0021-9290(01)00105-1.
- Neptune, R. R., I. C. Wright, and A. J. van den Bogert. 2000. "A Method for Numerical Simulation of Single Limb Ground Contact Events: Application to Heel-Toe Running." *Computer Methods in Biomechanics and Biomedical Engineering* 3 (4): 321–34. doi:10.1080/10255840008915275.
- Neptune, R. R., F. E. Zajac, and S. A. Kautz. 2004. "Muscle Force Redistributes Segmental Power for Body Progression during Walking." *Gait & Posture* 19 (2): 194–205. doi:10.1016/S0966-6362(03)00062-6.
- Norkin, Cynthia C. 2009. *Measurement of Joint Motion: A Guide to Goniometry*. 4th ed. Philadelphia: F.A. Davis.
- Onyshko, S., and D. A. Winter. 1980. "A Mathematical Model for the Dynamics of Human Locomotion." *Journal of Biomechanics* 13 (4): 361–68. doi:10.1016/0021-9290(80)90016-0.
- Pandy, M. G., B. A. Garner, and F. C. Anderson. 1995. "Optimal Control of Non-Ballistic Muscular Movements: A Constraint-Based Performance Criterion for Rising From a Chair." *Journal of Biomechanical Engineering* 117 (1): 15. doi:10.1115/1.2792265.
- Pandy, Marcus G. 2001. "Computer Modeling and Simulation of Human Movement." *Annual Review of Biomedical Engineering* 3 (1): 245–73. doi:10.1146/annurev.bioeng.3.1.245.
- Pandy, Marcus G., Felix E. Zajac, Eunsup Sim, and William S. Levine. 1990. "An Optimal Control Model for Maximum-Height Human Jumping." *Journal of Biomechanics* 23

- (12): 1185–98. doi:10.1016/0021-9290(90)90376-E.
- Pedotti, A., V.V. Krishnan, and L. Stark. 1978. “Optimization of Muscle-Force Sequencing in Human Locomotion.” *Mathematical Biosciences* 38 (1–2): 57–76. doi:10.1016/0025-5564(78)90018-4.
- Piazza, Stephen J., and Scott L. Delp. 1996. “The Influence of Muscles on Knee Flexion during the Swing Phase of Gait.” *Journal of Biomechanics* 29 (6): 723–33. doi:10.1016/0021-9290(95)00144-1.
- Powell, P. L., R. R. Roy, P. Kanim, M. A. Bello, and V. R. Edgerton. 1984. “Predictability of Skeletal Muscle Tension from Architectural Determinations in Guinea Pig Hindlimbs.” *Journal of Applied Physiology* 57 (6): 1715–21.
- Putnam, CA, GA Wood, and RN Marshall. 1987. “Simulations of the Recovery Action in Sprint Running.” In *1987 Biomechanics Symposium, New York, AMSE*.
- Raibert, Marc H. 1986. *Legged Robots That Balance*. Cambridge, Mass.: MIT Press.
- Ralston, H. J. 1976. “Energetics of Human Walking.” In *Neural Control of Locomotion*, edited by R. M. Herman, S. Grillner, P. S. G. Stein, and D. G. Stuart, 77–98. New York: Plenum Press.
- Rankin, Jeffery W., and Richard R. Neptune. 2008. “A Theoretical Analysis of an Optimal Chaining Shape to Maximize Crank Power during Isokinetic Pedaling.” *Journal of Biomechanics* 41 (7): 1494–1502. doi:10.1016/j.jbiomech.2008.02.015.
- Rassier, D. E., B. R. MacIntosh, and W. Herzog. 1999. “Length Dependence of Active Force Production in Skeletal Muscle.” *Journal of Applied Physiology* 86 (5): 1445–57.
- Ren, Lei, Richard K. Jones, and David Howard. 2007. “Predictive Modelling of Human Walking over a Complete Gait Cycle.” *Journal of Biomechanics* 40 (7): 1567–74. doi:10.1016/j.jbiomech.2006.07.017.
- Rogers, Joseph L, and USA Track & Field. 2000. *USA Track & Field Coaching Manual*. Champaign, IL: Human Kinetics.
- Sasaki, Kotaro, and Richard R. Neptune. 2006. “Differences in Muscle Function during Walking and Running at the Same Speed.” *Journal of Biomechanics* 39 (11): 2005–13. doi:10.1016/j.jbiomech.2005.06.019.
- Schache, Anthony G., Peter D. Blanch, Tim W. Dorn, Nicholas A. T. Brown, Doug Rosemond, and Marcus G. Pandy. 2011. “Effect of Running Speed on Lower Limb Joint Kinetics.” *Medicine & Science in Sports & Exercise* 43 (7): 1260–71. doi:10.1249/MSS.0b013e3182084929.
- Schache, Anthony G., Tim W. Dorn, Peter D. Blanch, Nicholas A. T. Brown, and Marcus G. Pandy. 2012. “Mechanics of the Human Hamstring Muscles during Sprinting.” *Medicine & Science in Sports & Exercise* 44 (4): 647–58. doi:10.1249/MSS.0b013e318236a3d2.
- Schultz, G, and K Mombaur. 2010. “Modeling and Optimal Control of Human-Like Running.” *IEEE/ASME Transactions on Mechatronics* 15 (5): 783–92. doi:10.1109/TMECH.2009.2035112.
- Seireg, A., and R. J. Arvikar. 1975. “The Prediction of Muscular Load Sharing and Joint Forces in the Lower Extremities during Walking.” *Journal of Biomechanics* 8 (2): 89–102. doi:10.1016/0021-9290(75)90089-5.
- Sellers, William Irvin, and Phillip Lars Manning. 2007. “Estimating Dinosaur Maximum Running Speeds Using Evolutionary Robotics.” *Proceedings of the Royal Society B: Biological Sciences* 274 (1626): 2711–16. doi:10.1098/rspb.2007.0846.
- Seyfarth, A., H. Geyer, and H. Herr. 2003. “Swing-Leg Retraction: A Simple Control Model for

- Stable Running.” *Journal of Experimental Biology* 206 (15): 2547–55.
- Shampine, Lawrence F, and M. K Gordon. 1975. *Computer Solution of Ordinary Differential Equations : The Initial Value Problem*. San Francisco: W.H. Freeman.
- Slawinski, J., A. Bonnefoy, G. Ontanon, J.M. Leveque, C. Miller, A. Riquet, L. Chèze, and R. Dumas. 2010. “Segment-Interaction in Sprint Start: Analysis of 3D Angular Velocity and Kinetic Energy in Elite Sprinters.” *Journal of Biomechanics* 43 (8): 1494–1502. doi:10.1016/j.jbiomech.2010.01.044.
- Srinivasan, Manoj, and Andy Ruina. 2006. “Computer Optimization of a Minimal Biped Model Discovers Walking and Running.” *Nature* 439 (7072): 72–75. doi:10.1038/nature04113.
- Sutter, Herb. 2005. “The Free Lunch Is over: A Fundamental Turn toward Concurrency in Software.” *Dr. Dobb’s Journal* 30 (3): 202–10.
- Taylor, C. Richard, Norman C. Heglund, Thomas A. McMAHON, and Todd R. Looney. 1980. “Energetic Cost of Generating Muscular Force During Running: A Comparison of Large and Small Animals.” *The Journal of Experimental Biology* 86 (1): 9–18.
- Thelen, Darryl G., and Frank C. Anderson. 2006. “Using Computed Muscle Control to Generate Forward Dynamic Simulations of Human Walking from Experimental Data.” *Journal of Biomechanics* 39 (6): 1107–15. doi:10.1016/j.jbiomech.2005.02.010.
- Thelen, Darryl G., Elizabeth S. Chumanov, Thomas M. Best, Stephen C. Swanson, and Bryan C. Heiderscheit. 2005. “Simulation of Biceps Femoris Musculotendon Mechanics during the Swing Phase of Sprinting.” *Medicine & Science in Sports & Exercise* 37 (11): 1931–38. doi:10.1249/01.mss.0000176674.42929.de.
- Todorov, Emanuel. 2004. “Optimality Principles in Sensorimotor Control.” *Nature Neuroscience* 7 (9): 907–15. doi:10.1038/nn1309.
- Townsend, M.A., and A. Seireg. 1972. “The Synthesis of Bipedal Locomotion.” *Journal of Biomechanics* 5 (1): 71–83. doi:10.1016/0021-9290(72)90020-6.
- Umberger, Brian R. 2010. “Stance and Swing Phase Costs in Human Walking.” *Journal of The Royal Society Interface* 7 (50): 1329–40. doi:10.1098/rsif.2010.0084.
- Umberger, Brian R., Karin G.M. Gerritsen, and Philip E. Martin. 2003. “A Model of Human Muscle Energy Expenditure.” *Computer Methods in Biomechanics and Biomedical Engineering* 6 (2): 99–111. doi:10.1080/1025584031000091678.
- Van den Bogert, Antonie J., and Marko Ackermann. 2009. “Direct Collocation for Simulation and Optimization of Movement.” In Cape Town, South Africa.
- Van Schenau, Gerrit Jan Ingen, Jos J de Koning, and Gert de Groot. 1994. “Optimisation of Sprinting Performance in Running, Cycling and Speed Skating.” *Sports Medicine* 17 (4): 259–75.
- Van Soest, A. J. Knoek, and L. J. Richard Casius. 2000. “Which Factors Determine the Optimal Pedaling Rate in Sprint Cycling?” *Medicine & Science in Sports & Exercise* 32 (11): 1927–34. doi:10.1097/00005768-200011000-00017.
- Van Soest, Arthur J., Arend L. Schwab, Maarten F. Bobbert, and Gerrit Jan van Ingen Schenau. 1993. “The Influence of the Biarticularity of the Gastrocnemius Muscle on Vertical-Jumping Achievement.” *Journal of Biomechanics* 26 (1): 1–8. doi:10.1016/0021-9290(93)90608-H.
- Van Werkhoven, Herman, and Stephen J. Piazza. 2013. “Single-Joint Jump Height Correlates with Heel Length and Toe Length.” In *Proceedings of ASB2013*. Omaha, NE.
- Vaughan, C.L. 1983. “Simulation of a Sprinter. Part I. Development of a Model.” *International Journal of Bio-Medical Computing* 14 (1): 65–74. doi:10.1016/0020-7101(83)90087-9.

- Wang, J. M, S. R Hamner, S. L Delp, and V. Koltun. 2012. "Optimizing Locomotion Controllers Using Biologically-Based Actuators and Objectives." *ACM Transactions on Graphics (TOG)* 31 (4): 25.
- Ward-Smith, A.J. 1985. "A Mathematical Theory of Running, Based on the First Law of Thermodynamics, and Its Application to the Performance of World-Class Athletes." *Journal of Biomechanics* 18 (5): 337–49. doi:10.1016/0021-9290(85)90289-1.
- Warner, Sharon Elaine, Phillip Pickering, Olga Panagiotopoulou, Thilo Pfau, Lei Ren, and John Richard Hutchinson. 2013. "Size-Related Changes in Foot Impact Mechanics in Hoofed Mammals." *PLoS ONE* 8 (1): e54784. doi:10.1371/journal.pone.0054784.
- Waters, Robert L., and Sara Mulroy. 1999. "The Energy Expenditure of Normal and Pathologic Gait." *Gait & Posture* 9 (3): 207–31. doi:10.1016/S0966-6362(99)00009-0.
- Weyand, Peter G., Deborah B. Sternlight, Matthew J. Bellizzi, and Seth Wright. 2000. "Faster Top Running Speeds Are Achieved with Greater Ground Forces Not More Rapid Leg Movements." *Journal of Applied Physiology* 89 (5): 1991–99.
- Whittle, Michael W. 1999. "Generation and Attenuation of Transient Impulsive Forces beneath the Foot: A Review." *Gait & Posture* 10 (3): 264–75. doi:10.1016/S0966-6362(99)00041-7.
- Winter, DA. 1995. "Human Balance and Posture Control during Standing and Walking." *Gait & Posture* 3 (4): 193–214. doi:10.1016/0966-6362(96)82849-9.
- Winter, David A. 1992. "Foot Trajectory in Human Gait: A Precise and Multifactorial Motor Control Task." *Physical Therapy* 72 (1): 45–53.
- Wisse, Martijn, Arend L Schwab, and Frans CT van der Helm. 2004. "Passive Dynamic Walking Model with Upper Body." *Robotica* 22 (06): 681–88.
- Xiang, Yujiang, Jasbir S. Arora, and Karim Abdel-Malek. 2011. "Optimization-Based Prediction of Asymmetric Human Gait." *Journal of Biomechanics* 44 (4): 683–93. doi:10.1016/j.jbiomech.2010.10.045.
- Yamaguchi, Gary T., and Felix E. Zajac. 1990. "Restoring Unassisted Natural Gait to Paraplegics via Functional Neuromuscular Stimulation: A Computer Simulation Study." *IEEE Transactions on Biomedical Engineering* 37 (9): 886–902. doi:10.1109/10.58599.
- Zajac, F E, and M E Gordon. 1989. "Determining Muscle's Force and Action in Multi-Articular Movement." *Exercise and Sport Sciences Reviews* 17: 187–230.
- Zajac, Felix E., Richard R. Neptune, and Steven A. Kautz. 2002. "Biomechanics and Muscle Coordination of Human Walking: Part I: Introduction to Concepts, Power Transfer, Dynamics and Simulations." *Gait & Posture* 16 (3): 215–32. doi:10.1016/S0966-6362(02)00068-1.
- Zajac, Felix E., Richard R. Neptune, and Steven A. Kautz. 2003. "Biomechanics and Muscle Coordination of Human Walking: Part II: Lessons from Dynamical Simulations and Clinical Implications." *Gait & Posture* 17 (1): 1–17. doi:10.1016/S0966-6362(02)00069-3.
- Zatsiorsky, Vladimir M. 2012. *Biomechanics of Skeletal Muscles*. Champaign, IL: Human Kinetics.

CURRICULUM VITAE

HUSEYIN CELIK

EDUCATION

- *The Pennsylvania State University (PSU), University Park, PA, US*
Ph.D. in Mechanical Engineering
Dissertation Advisor: Dr. Stephen J. Piazza
August 2009 – August 2014
- *Middle East Technical University (METU), Ankara, Turkey*
M.S. in Engineering Science
Thesis Advisor: Dr. Senih Gurses
January 2006 - September 2008
- *METU, Ankara, Turkey*
B.S. in Mechanical Engineering
September 2001 - June 2005

EMPLOYMENT

- **Graduate Assistant** at *PSU Biomechanics Lab, University Park, PA, US*
August 2009 – May 2014
- **Graduate Assistant** at *METU Biomechanics Lab, Ankara, Turkey*
August 2006 – August 2009

PEER-REVIEWED JOURNAL ARTICLES

- **Celik, H.**, & Piazza, S. J. (2013). Simulation of aperiodic bipedal sprinting. *ASME Journal of Biomechanical Engineering*, vol.135, pp. 081008-1 - 081008-8.
- Gurses, S. & **Celik, H.** (2013). Correlation dimension estimates of human postural sway. *Human Movement Science*, vol.32, pp.48-64.